Saarland University, Homburg
Medical Faculty (F2)
Theoretical Medicine and Biosciences
F2.5 Department of Biophysics
Prof. Dr. Markus Hoth
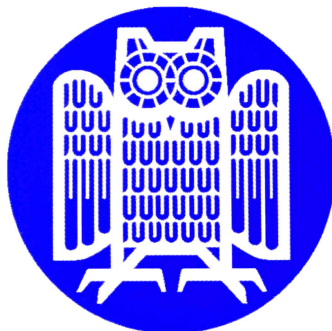
Über Kalziumsignale und Zytotoxizität menschlicher natürlicher Killerzellen

Calcium signaling and cytotoxicity of human natural killer cells

Dissertation zur Erlangung des Grades eines Doktors der Medizin

a doctoral thesis in medicine (Dr. med)

2017

by Sebastian Mang
*December 3, 1991, Saarbrücken

All experiments presented in this thesis were conducted at the biophysical as well as the physiological institute of Saarland University.

Alle experimentellen Arbeiten der vorliegenden Dissertation wurden am biophysikalischen und am physiologischen Institut der Universität des Saarlandes durchgeführt.

Referent: Prof. Dr. Markus Hoth
Ko-Referent:
Termin der Disputation:

Contents

List of Figures

Nomenclature

$[Ca^{2+}]$ .... Calcium concentration
$[Ca^{2+}]_{ext}$ ... Extracellular calcium concentration
$[Ca^{2+}]_{int}$ ... Intracellular calcium concentration
-AM .... -acetoxymethyl ester
AB .... Antibody
APC .... Antigen-presenting cell
apop .... Apoptosis
AR .... Apoptotic ratio
ATP .... Adenosine triphosphate
Ca^{2+} .... Calcium ion
Ca^{2+}_b .... Bound clcium ion
Ca^{2+}_f ...... Free calcium ion
CD .... Cluster of differentiation
CL .... Cytotoxic lymphocyte
CML .... Chronic myelogenous leukemia
CRAC ..... Calcium-release activated calcium current
ct .... Contact time
CTL .... Cytotoxic T-lymphocyte
DAG .... Diacyl-glycerole
DAMP ..... Damage-associated molecular pattern
DC .... Dentritic cell
DNA .... Deoxyribunucleic acid
EGF .... Epidermal growth factor
ER .... Endoplasmic reticulum
F2 .... Fura-2
FACS ...... Fluorescence-activated cell sorting
FasL .... Fas-ligand
FCS .... Fetal cattle serum
FRET ...... Förster resonance energy transfer
GFP .... Green fluorescent protein
IFN-γ ...... Interferon gamma
Ig .... Immunoglobulin
IL .... Interleukin
IP_3 .... Inositol trisphosphate
IP_3R .... IP_3 receptor
IS .... Immunological synapse
ITAM ...... Immunoreceptor tyrosine-based activation motif
ITIM .... Immunoreceptor tyrosine-based inhibitory motif
LAMP ..... Lysosome-associated membrane protein
mAB .... Monoclonal antibody
MAC .... Membrane attack complex
MCU .... Mitochondrial uniporter
MHC .... Major histocompatibility complex
MTOC ..... Microtubule organizing center
NK cell ..... Natural killer cell
NP-EGTA .. o-Nitrophenyl EGTA

PBMC ..... Peripheral blood mononuclear cell
PIP2 .... Phosphatidylinositol 4,5-bisphosphate
PLCγ ..... Phospholipase C gamma
PR .... Peak Fura-2 ratio
pt .... Peaking time
PTK .... Protein tyrosine kinase
RFP .... Red fluorescent protein
ROI .... Area of interest
RPMI ...... Roswell Park Memorial Institute
RR .... Resting Fura-2 ratio
rRFP .... relative RFP
SERCA .... Sarcoplasmic/endoplasmic reticulum calcium ATPase
SOCE ...... Store-operated calcium entry
TNF .... Tumor necrosis factor
TRAIL ..... TNF-related apoptosis-inducing ligand
TRP .... Transient receptor potential
U .... Unit
VAMP ..... Vesicle-associated membrane protein

Abstract

Calcium signaling is an essential component of immune cell function. Immunocompetent cells employ calcium ions as a second messenger to regulate proliferation, migration and maturation. In addition, intracellular calcium signals are necessary for cytotoxic lymphocytes (CLs) such as CD8$^+$ T-cells and natural killer cells (NK cells) to eliminate target cells. For several decades, the doctrine used to be that this elimination is mainly achieved by forcing a target cell into apoptosis. In recent years, several groups reported that there is at least one further way of target cell killing. Given the right circumstances, CLs are also able to kill by a direct lysis of the target cell's membrane, a process referred to as 'necrosis'.

Our research group, the Department of Biophysics at Saarland University, directed by Prof. Dr. Markus Hoth, investigates the Ca^{2+} dependence of signaling processes in immune cells. We found that calcium ion influx into killer cells is not only necessary for a successful attack on pathogens and tumor cells, but that extracellular calcium supply can influence a killer cell's global killing efficiency.

The aim of this doctoral thesis was to study influx kinetics of Ca^{2+} ions in active NK cells at a single-cell level using fluorescence microscopy. The conducted experiments led to two main conclusions:

I) Not only do NK cells employ both necrosis and apoptosis when killing certain target cells, but the *frequency distributions* of both killing types depend highly on the extracellular Ca^{2+} concentration ($[Ca^{2+}]_{ext}$). Low concentrations favor the occurrence of apoptosis, while an increase in $[Ca^{2+}]_{ext}$ shifts the balance towards necrotic killing. This shift occurs even after raising Ca^{2+} ion levels beyond the amount necessary for necrosis induction.

II) The *shape* of Ca^{2+} influx differs, regarding necrotic and apoptotic killing. Necrosis induction depends on high sustained rises in $[Ca^{2+}]_{int}$, while NK cells causing apoptosis tend to show low and oscillatory Ca^{2+} signals.

Further experiments were conducted in attempt to reveal the responsible molecular mechanisms. Artificially releasing high amounts of Ca^{2+} ions into the cytosol of killing NK cells, using a photolabile Ca^{2+} chelator, suggests that high cytosolic Ca^{2+} concentrations are necessary but not sufficient for necrosis induction by NK cells.

The presented results have contributed to shedding light on the Ca^{2+} dependence of NK cell function. In his doctoral thesis published in 2016, Christian Backes from our research group demonstrated that the balance of necrosis to apoptosis induced by NK cells greatly affects their total killing competence. The observation that global killing

efficiency of CD8$^+$ T-lymphocytes and NK cells depends on $[Ca^{2+}]_{ext}$ can now in parts be explained by the likelihood of necrotic and apoptotic killing processes shifting.

Although different Ca^{2+} influx patterns in active NK cells were previously described by other groups, no exact quantification of these signals has yet been provided. In addition to giving such a quantification, this thesis can provide evidence that these different signal types are clearly linked to distinct outcomes regarding NK cell cytotoxicity in vitro.

NK cells play a pivotal role in tumor surveillance and - in case of already developed cancer - keeping malignant cell clones in check. Apoptosis and lysis of target cells may both help achieve a shared aim but will differently affect the anti-tumor immune response. Hence, different Ca^{2+} signals in tumor-killing NK cells as well as their likelihood of inducing apoptosis or necrosis may also affect tumor development, progression as well as the efficacy of immune therapy and adoptive cell transfer. Many recent studies suggest that tumor cells benefit from necrosis by taking advantage of the resulting microenvironment. If we can deepen our understanding of how different calcium signal types in CLs come about, we could try to modulate killing behaviour to shape a more desirable cellular immune response to malignancies.

Zusammenfassung

Kalziumsignale spielen eine Schlüsselrolle in der Funktion unserer Immunabwehr. Immunzellen verwenden diese Signale, um komplexe Prozesse wie Proliferation, Migration und Reifung zu regulieren. Darüber hinaus benötigen Killerzellen wie CD8^{+}-T-Zellen und natürliche Killerzellen (NK-Zellen) hohe zytosolische Kalziumspiegel, um Zielzellen abzutöten. Die Doktrin der letzten Jahrzehnte war, dass dieses Abtöten im Wesentlichen auf einem einzigen Mechanismus basiert: der Aktivierung des programmierten Zelltodes, der Apoptose der Zielzelle. Seit einiger Zeit mehren sich jedoch die Hinweise, dass es noch mindestens einen weiteren Mechanismus gibt. Unter gewissen Voraussetzungen können Killerzellen ihre Opfer auch durch eine direkte Lyse der Zellmembran töten. Dieser Prozess wird gemeinhin als "Nekrose" bezeichnet.

Unter der Leitung von Prof. Dr. Markus Hoth erforscht unsere biophysikalische Arbeitsgruppe seit Jahren die Bedeutung von Kalziumsignalen für eine Vielzahl von Immunzellen. Wissenschaftler unserer Abteilung fanden heraus, dass ein Kalziumeinstrom in Killerzellen nicht nur notwendig für das Abtöten von Bakterien und Tumorzellen ist, sondern dass das extrazelluläre Kalziumionenangebot auch einen Einfluss auf die absolute Killingeffizienz ausübt.

Das Ziel der vorliegenden Doktorarbeit war, die Kinetik dieser Kalziumströme in aktiven NK-Zellen mittels Fluoreszenzmikroskopie auf Einzelzellebene zu erforschen. Die in diesem Rahmen durchgeführten Experimente lieferten zwei wichtige Erkenntnisse:

I) Zusätzlich zur Bestätigung, dass NK-Zellen sowohl Apoptose als auch Nekrose in geeigneten Zielzellen induzieren, stellte sich heraus, dass die statistische Verteilung beider Killingtypen stark vom extrazellulären Kalziumangebot abhängt. Niedrige Konzentrationen an Kalziumionen begünstigen das Auftreten von Apoptosen, während steigende Kalziumspiegel zu mehr und mehr Nekrosen führen. Dieser Einfluss zeigt sich auch noch bei extrazellulären Kalziumkonzentrationen, die weit über dem für Nekrose notwendigen Maß liegen.

II) NK-Zellen zeigen verschiedene Arten von Kalziumsignalen, je nachdem, welchen Typ Zytotoxizität (i.e. Nekrose oder Apoptose) sie in ihrer Zielzelle induzieren. Die Lyse der Zelle bedurfte dabei stets eines hohen und anhaltenden Einstroms von Kalziumionen, während Killerzellen, die Apoptose hervorriefen, niedrigere und oszillierende Kalziumströme zeigten.

Weitere Experimente zielten darauf ab, die molekularen Mechanismen für diese Unterschiede in den Signalen aufzudecken. Indem große Mengen an Kalziumionen mittels eines photolabilen Chelators künstlich in Killerzellen freigesetzt wurden, konnte gezeigt werden, dass hohe Kalziumeinströme zwar notwendig, aber sehr wahrscheinlich nicht hinreichend

für das nekrosebasierte Abtöten sind.

Die vorliegenden Ergebnisse haben dazu beigetragen, die Kalziumabhängigkeit der Funktion von NK-Zellen besser zu verstehen. In seiner 2016 publizierten Doktorarbeit konnte Christian Backes aus unserer Arbeitsgruppe zeigen, dass die Balance von Nekrose- zu Apoptoseinduktion einen starken Einfluss auf das globale Killingpotential von NK-Zellen ausübt. Mit Hilfe der hier gewonnenen Erkenntnis, dass diese Balance vom extrazellulären Kalziumangebot abhängt, kann die Beeinflussung der Effizienz natürlicher Killerzellen durch die Verfügbarkeit von Kalziumionen nun in Teilen erklärt werden.
Verschiedenartige Muster von Kalziumströmen in aktiven NK-Zellen wurden in der Vergangenheit bereits von anderen Arbeitsgruppen postuliert, jedoch nicht exakt quantifiziert. Neben einer solchen Quantifizierung kann die vorliegende Arbeit erstmals beweisen, dass diese Signalmuster deutlich mit den verschiedenen Killingarten assoziiert sind, zu denen NK-Zellen fähig sind.

Natürliche Killerzellen zählen zu den wichtigsten Effektoren der Tumorüberwachung. Auch im Falle von bereits entstandenen Tumoren tragen sie essenziell dazu bei, den Tumor in Schach zu halten. Unmittelbar führen Apoptoseinduktion und Lyse zwar zum gleichen Ergebnis - dem Tod der Tumorzelle -, beide Prozesse beeinflussen jedoch die gegen den Tumor gerichtete folgende Immunantwort auf stark unterschiedliche Weise. Es ist anzunehmen, dass die Frage, wie NK-Zellen Tumorzellen eliminieren und welche Kalziumsignale sie dabei präsentieren, auch einen Einfluss auf die Wirksamkeit von Chemotherapien, immunmodulierenden Therapien und adoptivem Zelltransfer haben könnte. Viele aktuelle Studien legen nahe, dass Tumorzellen von einem bestimmten immunologischen Mikromilieu profitieren. Ein solches Milieu scheint insbesondere durch nekrotische Zellen begünstigt zu werden. Ein tiefer gehendes Verständnis davon, wie verschiedene Kalziumsignale in NK-Zellen zustande kommen, könnte es erlauben, sie pharmakologisch zu beeinflussen, um das Tötungsverhalten von NK-Zellen zu modifizieren. Auf diese Weise könnte ein immunologisches Mikromilieu im Tumorgewebe erreicht werden, das bösartige Zellen schädigt, ohne gleichzeitig die Vermehrung benachbarter Tumorzellen zu stimulieren.

1 Introduction

1.1 The role of NK cells in innate and adaptive immunity

It is widely accepted that malignant cell transformation occurs randomly but frequently during cell division. Luckily, our immune system has extensive capabilities to identify and extinguish these tumors in the making [1]. If surveillance mechanisms fail, cells can gain replicative immortality [2]. They grow and form cancerous tissues which can eventually cause life-threatening diseases.

Sooner or later, virtually all cancers manage to develop mechanisms of immune evasion [3], [4]. How they escape our immune system varies among different tumor entities and has long attracted the attention of many immunologists. One evasive strategy occurring regularly in cancer cells is the downregulation or mutation of major histocompatibility complex class I (MHC I) [5], a constellation often referred to as 'missing self'. MHC I proteins are normally expressed on the surface of every nucleated cell in the body where they present intracellularly processed peptides to passing immune cells [6]. The latter investigate the molecular identity of these peptide fragments to check for structures of infectious or tumorous origin. If cells are infected by viruses or have transformed into a malignant clone, they are likely to present foreign peptides which would immediately draw the attention of B-cells, CTLs and phagocytes. Therefore, those tumor cells downregulating MHC I expression would stay incognito and gain an advantage of growth. NK cells can complement immune surveillance by recognizing cells with modified or missing MHC I peptides.

The significance of tumor control carried out by natural killer cells has been highlighted repeatedly during the past decades. Mice lacking NK cell function suffered from an increased susceptibility to implanted tumor cells [7] and healthy humans were shown to have an increased risk of developing cancer in case of lower than average in-vitro NK cell activity [8]. This heightened susceptibility to cancer is not only the result of NK cells not being able to kill malignant cells but also due to their inability to promote immune responses. Upon stimulation, certain subtypes of NK cells produce interferon gamma (IFN-γ), tumor necrosis factor (TNF) and other cytokines, which recruit other immune cells to the site of attack. This immunoregulatory function is mainly exerted by an NK cell subpopulation expressing high levels of the surface protein CD56, earning it the name 'CD56^{bright}' [9], [10]. These CD56^{bright} NK cells usually lack CD16 and are thus incapable of executing antibody-dependent cellular cytotoxicity (ADCC), [11]. While only 10% of circulating NK cells belong to this type, they highly outnumber the CD56^{dim} type in the body since they are the predominant NK cell type in lymphoid and other organs [12].

Compared to their CD56^{bright} siblings, CD56^{dim} type NK cells are considered the main

cytotoxic form of NK cells. They express different homing receptors allowing them to infiltrate tissues and release high loads of cytotoxic proteins, which are stored in lytic granules, onto target cells [13], [14]. Potential target cells or pathogens can be recognized by the ligation of natural cytotoxicity receptors (NCRs) or triggering of Fcγ-receptor/CD16-complex in an antibody-dependent manner [15].

Unlike B- or T-lymphocytes, NK cells themselves do not possess antigen-specific receptors. Therefore, they are generally considered a part of innate immunity. Recent findings suggest that NK cells do not simply kill or spare target cells obeying an all-or-none law but show very nuanced immune responses. They were found to enter an anergic state in case of chronic receptor stimulation, undergo self-selecting mechanisms to ensure self-tolerance, and certain subsets of NK cells even transform into memory cells, [16]. Since these are abilities typically limited to B- and T-cells, these findings have raised the question whether NK cells could mark an intersection of innate and adaptive immunity.

1.2   Development of NK cells and subsets

Like every other blood cell, NK cells stem from pluripotent hematopoietic stem cells residing in the bone marrow. These stem cells differentiate into two classes of progenitor cells, dividing hematopoiesis into a lymphoid and a myeloic lineage. The latter finally gives rise to erythrocytes, platelets, monocytes and granulocytes. Lymphoid progenitor cells in turn evolve into three classes of cells: B-lymphocytes, T-lymphocytes and NK cells. Every descendant of a hematopoietic lineage has their own molecular ID: a set of membrane-bound proteins called 'cluster of differentiation' or 'CD'. By identifying the composition of CD proteins on its surface, a cell can be allocated to a defined lineage as well as stage of development. As previously mentioned, early NK cells typically express CD56 but lack CD3 which is present on all T-cells [17]. Mature NK-cells can be subdivided with regard to their expression level of CD56 and CD16. Recent findings suggest that there might be a third major subset of NK cells. Predominantly residing in mucosal lymphoid tissues, this subtyp expresses the two NCRs NKp46 and NKp44. It produces high amounts of Interleukin-22 and, unlike any other NK cell, does not depend on IL-15 for survival [18].

After developing in the bone marrow, early NK cells migrate to lymph nodes, spleen and other secondary lymphoid organs to mature. A small population of mature cells then enters circulation and scans the blood stream for pathogens. In case of infection, sterile inflammation or malignant cell transformation, these cells adhere to the vessel wall and migrate into the damaged tissue to exhibit cytotoxic or immunoregulatory functions [19].

NK cell maturation and survival depends on provision with a variety of cytokines, the most important being Interleukin-15 [20]. Mice lacking IL-15 or its receptor showed

abscence of circulating NK cells [21]. A similar condition is present in patients suffering
from SCID-X1, caused by a hereditary defect in the common peptide chain γc of several
IL-receptors. Interleukin-2 [22] and Interleukin-12 [23] are other potent promotors of NK
cell proliferation as well as cytotoxicity. IL-2 was also used during the culture of primary
NK cells used in this thesis in order to expand their life span and enhance cytotoxic po-
tential.

The majority of NK cell receptors promote activation by a cytosolic signaling domain
called 'intracytoplasmatic immunoreceptor tyrosine-based activation motif' or ITAM (s.
section 1.3.1). This linkage appears to be a common feature of all lymphocytes since
B- and T-cell receptors also induce downstream signaling using ITAMs. Interestingly,
while dysfunction of ITAM-mediated signaling leads to developmental arrest in B- and T-
lymphocytes [24], NK cell evolution seems not to depend similarly on ITAM functionality.
Total NK cell counts were unimpaired in mice deficient for ITAM-bearing molecules [25].
This finding might help explain why, compared to that of other lymphcoytes, NK cell
function tends to be only mildly affected by most congenital immune deficiencies.

In contrast to B- and T-lymphocytes, malignant transformation of NK cells is rare. Most
cases of aggressive NK-cell leukemia are diagnosed in Asia. The disease affects mostly
adolescents and young adults with a slight preponderance of males [26]. The frequent pres-
ence of Epstein-Barr virus-related genome in the tumor cells point towards an involvement
of EBV infection in the carcinogenesis [27]. Prognosis of NK-cell leukemia is usually poor.

1.3 NK cell activation: From IS formation to target cell lysis

1.3.1 Activating and inhibitory NK cell receptors

NK cells possess a variety of either stimulating or inhibitory natural cytotoxicity recep-
tors (NCRs) on their cell surface. Activation is not the result of one ligand binding to
its receptor but an interplay of these receptors finally turning the balance towards stim-
ulation. Activation is promoted by several cell surface receptors, e.g, NKp46, NKp44,
NKp30, NKG2D, CD2, 2B4 and DNAM-I. Numerous ligands for these receptors have
been identified and include viral antigens such as haemagglutinines of influenza virus,
neuraminidases of parainfluenza virus [28] and proteins structurally related to MHC class
I (MHC class I-related molecules or MICs), including the so-called UL-16 binding proteins
(ULBPs) [29], [30]. NKG2D is known to detect 'stress peptides', self molecules only ex-
pressed by cells undergoing distress and certain tumor cells [31]. Another very important
activating receptor is CD16, which detects the constant part of human IgG molecules. It
enables NK cells to induce antibody-dependent cellular cytotixicity (ADCC). In unstim-
ulated NK cells, CD16 is the only receptor capable of activating the cell on its own, while

all other receptors mentioned above first need to synergize [32].

Figure 1 provides a quick overview of the most prominent NCRs as well as their adaptor molecules. The current state of investigation suggests that more or less every activating NK cell receptor uses the same polypeptide structure with a high proportion of tyrosine, called 'immunoreceptor tyrosine-based activation motif' (ITAM) for downstream signaling. These ITAMs are not part of the NCRs per se but of linker molecules non-covalently associated with them. Different NCRs can thus be classified by which of these molecules they are linked to. The three most important ITAM-containing adaptors in humans are CD3ζ, FcRγ and DAP12. While NKG2C and NKp44 are associated with DAP12, NKp30 as well as CD16 correspond with both CD3ζ and FcRγ [33], [34]. NKG2D appears to stand out since it comes in two splice variants. The long variant NKG2DL signals using DAP12, the short variant NKG2DS uses DAP10 [35].

The common pathway of NCR activation by ligand binding is the phosphorylation of ITAMs' tyrosine residues by members of the src protein tyrosine kinase (PTK) family. In turn, this phosphorylation recruits two protein kinases, Syk and Zap-70. Both PTKs were shown to exhibit redundant functions in human NK cells since either one seems to be dispensable for NK cell cytotoxicity [36]. Syk and Zap-70 phosphorylate and activate a variety of downstream signaling molecules. The final common step in NK cell activation is the production of IP$_3$ and DAG by phospholipase Cγ (PLCγ). How ITAM-based recruitment of PTKs results in activating PLC is currently unknown. There is, however, evidence that stimulation by different NCRs can result in distinctively triggering different isoforms of PLC, PLC 1 and 2 [37]. A possible connection between patterns of NCR activation and different outcomes of NK cell action are discussed in detail in **section 4.4**.

Recognizing human MHC class I molecules on target cells dampens NK cell activity. The receptors responsible for detecting MHC include those belonging to the killer cell immunoglobulin-like receptor family (KIR) and CD94/NKG2A. In analogy to ITAMs, the tyrosine-based motifs conveying inhibitory signals in NK cells are referred to as 'ITIMs'.

1.3.2 Second messengers of activation and the ER

A common feature of most, if not all, activating NCRs, is the resulting phosphorylation of PLCγ. In its phosphorylated state, PLCγ cleaves phosphatidylinositol 4,5-bisphosphate (PIP$_2$) into diacyl glycerol (DAG) and IP$_3$. IP$_3$ in turn travels to the endoplasmic reticulum where it binds to its receptor, a Ca^{2+}-specific ion channel located in the ER membrane.

In unstimulated cells, free [Ca^{2+}]$_{int}$ is usually kept at values of 100 nM or lower. Increases in cytosolic Ca^{2+} levels are quickly intercepted by the activity of plasma membrane-located calcium pumps (PMCAs) or the sarcoplasmic/endoplasmic reticulum Ca^{2+}-ATPase
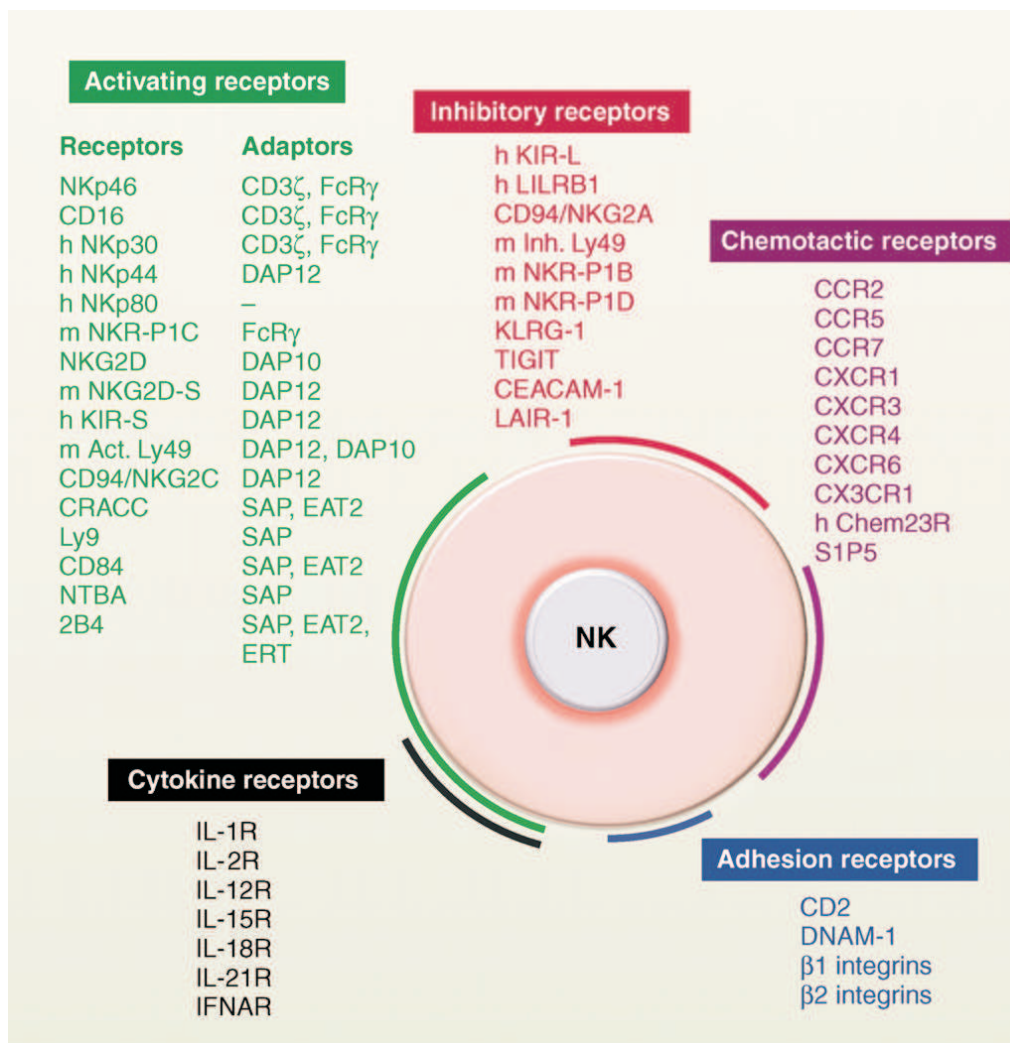
Figure 1: Activating and inhibitory NK cell receptors and their adaptor proteins

From: Vivier et al: 'Innate or Adaptive Immunity - The Example of Natural Killer Cells', Science (331), 2011

(SERCA). Ca^{2+} concentration is several orders of magnitude higher in the ER compared to the cytosol [38]. Being the most important intracellular Ca^{2+} store in humans, the ER plays a critical role in cellular Ca^{2+} homoeostasis. Recently, the translocon complex Sec61, located in the ER membrane, was found to provide an opportunity for Ca^{2+} to leak out into the cytosol [39], [40], thus functionally linking ER Ca^{2+} storage to peptide transport.

Binding of IP_3 to its receptor in the ER membrane leads to Ca^{2+} rapidly flowing from the ER into the cytosol, following an electrochemical gradient. Ca^{2+} store depletion can also be triggered pharmacologically by applying thapsigargin, a known specific inhibitor of SERCA [41], [42]. The resulting reduction in Ca^{2+} export into the ER lumen produces a gradual leakage of Ca^{2+} from the ER. This principle can be put to use in order to create

an artificial trigger for STIM and ORAI activation.

As long as no Ca^{2+} influx from outside the cell is provided, elevations in $[Ca^{2+}]_{int}$ usually stay transient because pumps shift excess Ca^{2+} back into stores or extrude it from the cytosol. Store depletion can, however, cause an even greater Ca^{2+} influx through the plasma membrane. The latter is actually responsible for definitive immune cell triggering [43].

1.3.3   STIM, ORAI and CRAC

The depletion of ER Ca^{2+} stores is sensed by a cluster of proteins called STIM [44]. They are located in the ER membrane, exposing Ca^{2+}-specific binding domains, so called 'EF-hands', to the lumen. In its resting state, STIM is saturated with Ca^{2+} ions and thus remains inactive. Once the ER Ca^{2+} storage is depleted, Ca^{2+} desaturation causes STIM molecules to autoaggregate. These aggregates in turn activate Ca^{2+}-specific ion channels located in the plasma membrane. Prior to the activation of STIM, these channels are evenly distributed across the cell surface. STIM autoaggregation recruits and gathers these channels in areas of the membrane closely neighbouring the ER membrane. In 2006, the identity of the channel-forming protein was revealed as ORAI [45], [46]. Since ORAI conductance depends on Ca^{2+} ions being previously released from stores, the resulting Ca^{2+} current across the plasma membrane was named 'calcium release-activated calcium current' or 'CRAC' [47].

Humans express two different STIMs [48] and 3 different ORAI channels [46], [49]. Out of all possible combinations of the two types of proteins, the pairing STIM1/ORAI1 appears to be by far the most important in most immune cells including NK cells [50].

The effects of Ca^{2+} entry through CRAC channels are diverse and include migration, proliferation, differential gene expression as well as the release of cytotoxic vesicles by CTLs. **Section 1.3.5** provides a detailed description of the molecular mechanisms and the Ca^{2+} dependence of vesicle release. Known transcription factors sensitive to intracellular calcium signaling by CRAC activity include the nuclear factor of activated T-cells (NFAT) and $NF\kappa B$ [51], [52]. **Figure 2** displays the players involved in the molecular activation cascade of lymphocytes.

1.3.4   The role of mitochondria at the IS

In order for cytotoxic lymphocytes to interact with their individual target cells their membranes need to come into close contact. In analogy to neurons forming synapses to ensure efficient signal transduction, these immune cell contact sites were given the name
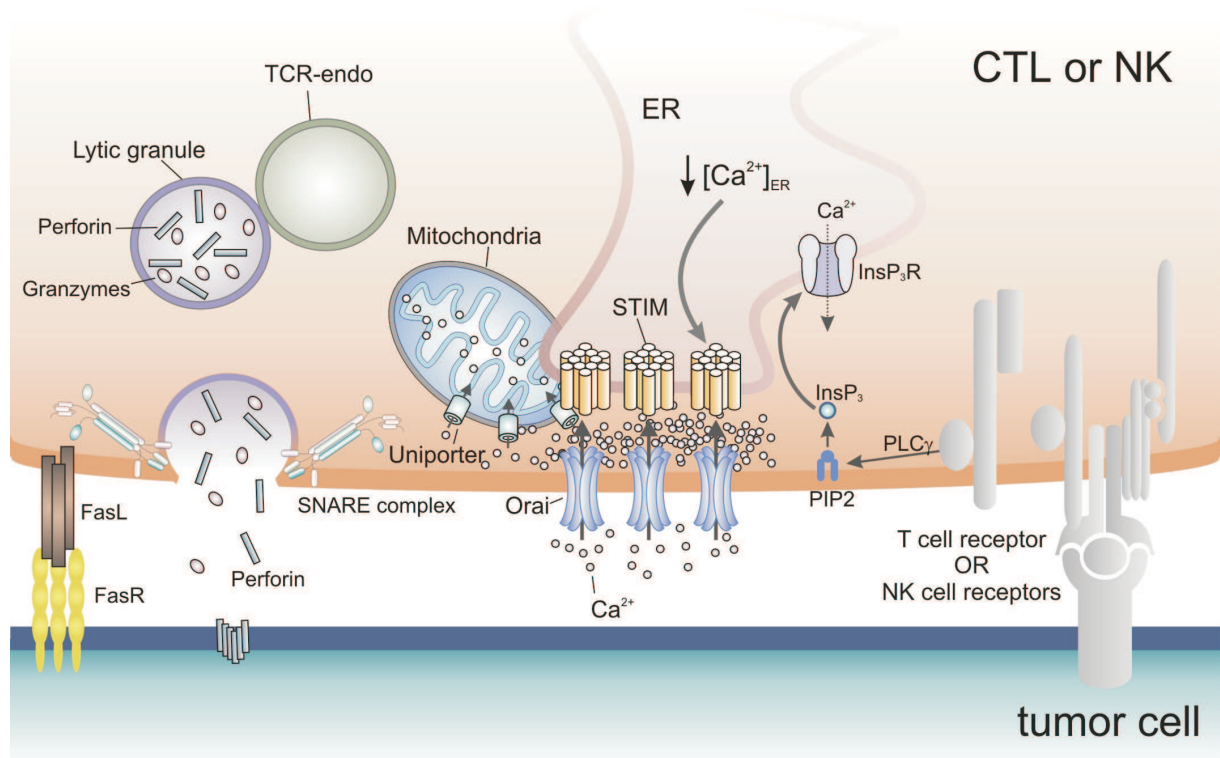
Figure 2: Molecular activation cascade in cytotoxic T-lymphocytes and NK cells
Activation of CLs occurs when their immune receptors - the T-cell receptor (TCR) or stimulatory NK cell receptors - recognize suitable ligands. PLC is activated by an out-to-in signaling cascade leading to DAG and IP$_3$ production. IP$_3$ binds to its receptor located in the ER membrane triggering a depletion of ER luminal Ca^{2+} stores. This depletion is detected by STIM molecules and followed by an autoaggregation. STIM aggregates recruit ORAI channels to the nearby parts of the cell's plasma membrane and activate them. The result is an inward current of Ca^{2+} ions. Rising intracellular Ca^{2+} concentrations mark the crucial trigger for exocytosis of cytotoxic vesicles and the modification of gene expression. Mitochondria are transferred to the IS. They take up part of the intruding Ca^{2+} ions and prevent inactivation of ORAI channels. Lytic granules (LGs) are hooked to microtubules and transported towards the IS membrane. Fusion is achieved by the action of SNARE complexes. Perforin molecules released from LGs form pores in the target cell membrane and allow granzymes to enter the cytosol.
Modified after: 'Calcium, cancer and killing: The role of calcium in killing cancer cells by cytotoxic T-lymphocytes and natural killer cells"' by Schwarz E.C. et al, Biochimica et Biophysica Acta (1833) 2013;1603-1611

'immunological synapse' (IS) [53], [54]. ISs work like a seal, allowing directed release of cytotoxic proteins onto the target cell whilst sparing innocent bystander cells. In contrast to neurological synapses, the release site of granules is not predetermined by tissue architecture but depends on where immune receptors and ligands appear in the highest density on the killer and target cells' surfaces. Upon IS formation, lytic granules are transported towards the IS. Interestingly, IS establishment comes along with a complex rearrangement of the killer cell's cytoskeleton and mitochondria. Mitochondrial translocation preceeding

NK cell cytotoxicy was first observed by Quintana et al in 2007 [55] and also seen in T-cells. In 2010, researches from our group could show that in T-lymphocytes shift of mitochondria towards the IS is necessary for sustained CRAC activity and thus effective T-cell activation [56]. When relocated into close proximity of the IS, mitochondria can take up parts of the inflowing Ca^{2+} ions. This buffering needs to occur to prevent a Ca^{2+}-dependent inactivation of ORAI channels and permits Ca^{2+} influx over a prolonged period of time [57].

Intracellular transport of organelles like mitochondria or lytic granules depends on microtubules serving as a guiding structure. Once an IS is formed, the microtubule organizing center (MTOC) is relocated towards the site of contact and the actin cytoskeleton of the cell is rearranged [58]. Next, mitochondria and lytic granules are hooked to microtubules and transported towards the MTOC in a Ca^{2+}-dependent manner. The motor proteins responsible for this movement have been identified as kinesin for anterograde transport and dynein mediating retrograde movement. In 2009 Wang and Schwarz could reveal the exact mechanism for this Ca^{2+}-dependence of mitochondrial transport in neurons [59]. Subject to a Ca^{2+}-free extracellular environment, CTLs still form immunological synapses. These synapses are, however, dysfunctional for many reasons, one being that mitochondria can no longer be relocated towards the IS [56].

1.3.5 Cytotoxicity by release of lytic granules

T-cells and NK cells have several harmful proteins at their disposal to force infected or malignantly transformed cells into cell death. These proteins are either soluble molecules released into the narrow cleft of the immunological synapse from lytic granules or membrane-bound death ligands binding their counterpart receptors on a target cell's surface. This section explains the molecular details of lytic granule formation, exocytosis and the properties of two main families of human cytotoxic proteins: perforin and granzymes.

Lytic granules are lysosome-related low-pH vesicles which store perforin and granzymes. Lysosome-associated membrane protein 1 (LAMP-1) or CD107a is strongly expressed on the surface of lytic granules [60]. In 2012, Krzewski et al could show that knockdown of LAMP-1 decreased the killing ability of NK cells by interfering with vesicle transport as well as perforin sorting into the vesicles, while target cell recognition and amounts of stored granzymes were unchanged [61]. This finding points towards a LAMP-1 dependent recruitment of motor proteins to lytic granules. Furthermore perforin and granzymes are integrated into secretory lysosomes via different transportation mechanisms, allowing for an individual dysfunction of either one.

The process of lytic granule fusion with the plasma membrane depends on a multi-

tude of priming, tethering and sensoring proteins and is far from being understood. It is sure, however, that there are parallels to vesicle fusion in neurons. Important players in lymphocyte vesicle transport or fusion include Munc 13-4 [62], Syntaxin-11 [63], [64] and Munc 18-2 [65]. Rettig and colleagues could show that both syntaxin-7 [66] and syntaxin-11 [67] are required as T-snares in cytotoxic lymphocytes. Furthermore, in T-cells VAMP8 facilitates vesicle fusion by docking early endosomes to the IS which deliver Syntaxin-11 [68]. The calcium sensor protein inducing vesicle fusion in CLs is still to be determined, but there is evidence for synaptotagmin-7 [69]. For a detailed review of molecular players in vesicle trafficking, comparing neurons and CLs, see [70].

Perforin is a 67 kDa multimeric protein stored in lytic granules. Subject to low pH, it comes as a monomer, safely contained inside the vesicle. Following release into the rim of the IS, it oligomerizes in the presence of Ca^{2+} ions and forms a pore in the target cell's plasma membrane. Perforin-1 is the major form expressed in human CTLs and NK cells and hereditary defects in perforin function account for a severe condition named hemophagocytic lymphohystiocytosis type 2 [71], [72]. The importance of perforin functionality has been further highlighted by many in and ex vivo analyses reporting impaired cytotoxicity by NK cells and CTLs in vitro as well as drastically increased vulnerability to cancerogenesis and metastasis in knockout mice [73].

Perforin consists of three functionally divided domains. Its N-terminal end forms a membrane attack complex similar to that of the complement protein C9. The middle domain has molecular resemblance to the human epidermal growth factor (EGF). Finally, the C-terminal part, more precisely its C2-domain, is responsible for Ca^{2+}-dependent target membrane binding [74].

Once released, neutral pH and available Ca^{2+} ions cause perforin molecules to form oligomers consisting of 19 to 24 proteins. These pores were estimated to have a luminal diameter of 130-200 Angström [74]. The cytolytic function of perforin is two-fold. It was shown to serve as an entrance mechanism for granzymes [75] but is also regarded to have intrinsic lytic potential [76]. Perforin having cytotoxic effects on its own is in line with results presented in this thesis which show that, depending on extracellular Ca^{2+} supply, even the majority of target cells can be killed in an apoptosis-independent fashion. Target cells were shown to be capable of repairing a certain proportion of perforin pores by using endosomes and lysosomes as donators of membrane portions [77]. The actual mechanism with which granzymes enter target cells still needs to be clarified. Some authors postulate a delivery mode which depends on clathrin-dependent endocytosis of perforin and granzymes by the target cell [78].
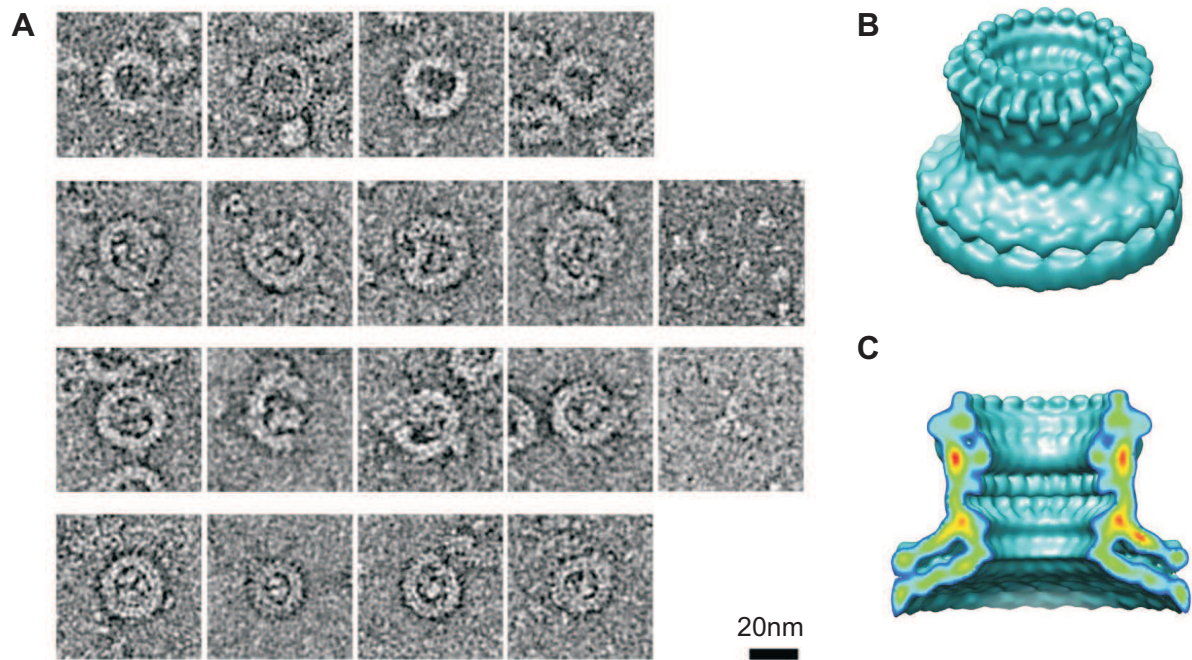
Figure 3: Electron microscopy and 3D reconstruction of perforin pores
(A) Negative stain electron microscopy of perforin pores formed on lipid monolayers, **(B)** Surface and **(C)** cutaway views of a cryo-electron microscopy reconstruction of a perforin pore with 20-fold symmetry. From: 'The structural basis for membrane binding and pore formation by lymphocyte perforin', Law R.H.P, Lukoyanova N. et al, Nature 2010, 468;447-451'

1.3.6 Cytotoxicity via death ligands and receptors

Another way of NK cells to inflict death is a family of transmembrane proteins called 'death receptors' and 'death ligands' respectively. Human NK cells express at least two types of death ligands - Fas ligand (FasL) [79], [80] and TRAIL [81], the latter being an acronym for 'Tumor necrosis factor related apoptosis inducing ligand'. Once these death ligands bind their specific receptor counterparts on a target cell's surface, they are able to induce an intracellular signaling cascade forcing the target cell into apoptosis. In contrast to the granzyme-B-dependent fashion starting directly from inside the target cell, FasL and TRAIL cause apoptosis by an out-to-in signaling pathway involving caspase 8. As recently as 2016, Zhu, Huang and Shi could show that, although noticeably expressed by both primary human NK cells as well as NK-cell lines, such as NK-92 MI, blockade of the TRAIL pathway using neutralizing antibodies did not affect granule-independent cytotoxicity, indicating that Fas-FasL-interaction is the predominant type of receptor-based cytotoxic signaling in humans [82].

While the molecular mechanisms of these death pathways are well-established, little is known about their contribution to the overall killing power of NK cells compared to perforin and granzymes. It seems likely that both modes of apoptosis induction - granzymes and death ligands - contribute to global NK cell cytotoxicity depending on an NK cell's maturation state. In the above-mentioned publication, Zhu et al also demonstrated that freshly-isolated primary NK cells killed a majority of adherent tumor cells in a vesicle-independent fashion while the proportion of lytic granule use increased with further incubation or stimulation with IL-2. It is possible that death-receptor mediated killing by NK cells may have its greatest value during early phases of NK cell maturation when the cytotoxic vesicle pool has not yet grown up to its full capacity.

1.4   NK cells in immunotherapy and adoptive cell transfer

Two of the famous cancer hallmarks postulated by Hannahan and Weinberg are the achievement of replicative immortality and the deregulation of tumor cells from cell cycle control. Tumor cells divide infinitely and more rapidly than most healthy cells. This simple fact constitutes the efficacy of chemotherapy: When administering potent inhibitors of cell division, the more rapidly a cell is proliferating, the more severely it will be affected. Chemotherapy along with surgery and radiation have been the foundation of cancer treatment for decades and still mark the most common therapeutic approaches for basically all cancer entities today.

Oncologic medicine, however, is in flux. Modern biotechnology has made monoclonal antibodies, recombinant growth factors and the group of so-called 'small molecules' broadly available. In addition, next-generation sequencing turned the complete analysis of cancerous genome into a feasible, time-economic task. These developments have found their way into cancer treatment and are currently changing the face of tumor therapy.

Immunotherapy describes the principle of modulating our body's immune response against cancer cells. Possible approaches include applying recombinant growth factors, chemokines or immunomodulating agents, such as thalidomid, to instigate already present immune cells or help hematopoiesis recover between chemotherapy cycles. Another promising approach is the administration of whole immune cells to a cancer-bearing host in the hope of boosting cellular immunity. This approach is called 'adoptive cell transfer' (ACT) and has already shown promising results in the treatment of many cancerous diseases. Cells suitable for ACT include CD8^{+} T-cells, NK cells and dendritic cells. The cells are isolated from the cancer-bearing host, purified by centrifugation and then expanded in-vitro using either recombinant growth factors or radiated tumor cell lines as stimulators. An

interesting twist to this method is the creation of T-cells expressing a cloned TCR which recognizes tumor-specific antigens in addition to their own antigenic specificity. These receptors are called 'chimeric antigen receptors' or CARs and have been used effectively against lymphoma and leukemia.

NK cells are an attractive goal for adoptive cell transfer since they do not depend on specific receptors to recognize and kill targets. Both autologous and allogeneic transfers of NK cells have been conducted in clinical trials [83], [84]. Major challenges remain guaranteeing sufficient survival of infused cells, preventing the emergence of tumor tolerance and bypassing the danger of cytokine storms or overshooting graft-versus-host diseases. In addition to primary NK cells, NK cell tumor lines have also proven suitable candidates for ACT. Recently, the FDA approved the NK-cell line NK-92 MI for the treatment of renal cell carcinoma and advanced malignant melanoma [85], [86]. By creating or exploiting an already existent specificity against tumor antigens, cell-based therapy may also contribute to avoiding the severe side-effects of conventional chemotherapy which often limit the admissible amount of chemotherapeutic drugs. Furthermore, ACT is an important representative of the emerging concept of 'personalized medicine', which aims to tailor medical treatment to every individual patient, based on cancer genome analyses, investigating the expression of tumor antigens or checking for individual anomalies in drug metabolism.

If we think of the many upcoming challenges in immune therapy development, enlightening the molecular details of cytotoxicity in CTLs might not only provide insight into our immune system but could also help to take one more step towards an effective treatment for cancer.

2 Materials and methods

2.1 Cells

2.1.1 Cell lines

2.1.1.1 Jurkat E6.1 The suspension cell line *Jurkat E6.1* was used as target cells against NK or NK-92 cells and purchased from ATCC. The official title of the cell clone used in this thesis is *Jurkat, Clone E6.1, ®ATCC, TIB-152^{TM}*. The line is cultured in RPMI-1640 medium containing 10% fetal calf serum (FCS) and P/S.

The Jurkat cell line was first established in the late 1970s from the blood of a 14-year-old boy suffering from acute T-cell leukemia. It is pseudodiploid, the modal chromosome set is 46,XY occurring in 74% with a polyploidy rate of 5.3%. The karyotype is 46,XY,-2,-18,del(2)(p21p23),del(18)(p11.2).

2.1.1.2 K-562 K-562 is a suspension cell line widely used as target cells in assays measuring natural killer cell cytotoxicity. The official title of the cell clone is *K-562, ®ATCC, CCL-243^{TM}*. The line is cultured in MDM medium containing FCS at 10% and P/S.

The K-562 cell line derives from the pleural effusion of a 53-year-old female suffering from chronic myeloic leukemia (CML). The cells were obtained during acute blast crisis and are of erythroleukemic origin [87]. The stemline chromosome number is triploid with the 2S component occurring at 4.2%.

2.1.1.3 NK-92 The cell line NK-92 is a lymphoblast cell line originating from a 50-year-old Caucasian patient suffering from malignant non-hodgkin's lymphoma. The cells are cultured in DMEM medium containing 10% FCS and 1% Penicillin/Streptomycin. Cell growth requires the addition of recombinant Interleukin-2 to the medium at levels of 100-200 U/ml. Since this cell line is highly sensitive to overgrowth, the culture density was kept below 1.6×10^6/ml at all times. NK-92 express a variety of surface antigens including CD45, CD54 and CD56 but are CD16-negative and therefore incapable of antibody-dependent cytotoxicity (FACS data from our lab technician Cora Hoxha, not published). The cell line was purchased from ATCC. The exact product name is NK-92 ATCC® CRL-2407^{TM}.

2.1.2 Primary cells

2.1.2.1 Negative isolation of primary human NK cells Primary human NK cells were isolated from peripheral blood mononuclear cells (PBMCs) retained from thrombocyte donations given at our local blood bank which is run by the Department of Hemostaseology. To isolate NK cells from these samples, they are first incubated with a mixture of mouse IgG antibodies against CD3, CD14, CD36, CDw123, HLA class II DR/DP and

CD235a to eliminate all non-NK cells in the suspension. NK cells were then negatively isolated using a Dynabead solution from LifeTechnologies. The resulting primary NK cell population was cultivated in AIMV medium + FCS at 37°C and 5% CO_2. The cells were stimulated by addition of 100 U/ml Il-2 to expand their life span. Viability was checked before every experimental procedure and isolated cells were not used for a period longer than seven days after isolation.

2.1.2.2 Expansion of primary human NK cells A basic protocol for NK cell expansion was introduced by Fujisaki and colleagues in 2009 [88]. Based on this method, our group developed a similar approach to generate large numbers of highly cytotoxic NK cells from initially low counts of PBMCs.

10×10^6 PBMCs were isolated from blood donations given by donors at the department of Hemostasiology. Cells from the leukemia cell line K-562 were irradiated with 120 Gray and the PBMCs were co-cultivated with the irradiated cells in RPMI medium containing Interleukin-2 at 50 I.U. Half of the culture medium was replaced every two days and irradiated K-562 cells were added to the culture every week. By being selectively stimulated to grow, NK cell populations increased 100-fold after one week and again by a factor of 7 after the next. Cytotoxic potential of expanded NK cells was verified using the time-resolved killing assay [89]. The cells showed high killing rates, the killing kinetics did not differ significantly between different states of expansion. NK cell expansion, culture as well as the mentioned killing assays were performed by Cora Hoxha, lab technician at the Department of Biophysics at Saarland University.

2.2 Fluorescence microscopy

2.2.1 Fluorescent dyes

2.2.1.1 Fura-2
Fura-2 is a synthetic fluorescent dye with a molecular structure similar to the Ca^{2+} chelator EGTA. It was first introduced by Grynkiewicz and colleagues in 1985 [90] and has since become a globally-used Ca^{2+} indicator. In its acetoxymethyl-estered form (Fura-2 AM), the dye is able to cross the plasma membrane of cells. Cleavage of its ester group by unspecific esterases then prevents the dye from rediffusion, trapping it in the cytosol.

Its K_D for Ca^{2+} binding varies from 135 nM to 224 nM, depending on temperature, pH and the ionic composition of the medium [90]. Free Fura-2 anions show an absorption maximum for UV light of roughly 380 nm. Upon binding of Ca^{2+} cations, this maximum shifts towards lower wavelengths, while the emission maxima of both free and bound Fura-2 remain at ± 510 nm. In all experiments conducted in this thesis, the excitation wavelengths were chosen as 340 nm for Ca^{2+}-bound and 380 nm for free Fura-2. The

excitation spectra of the free and the bound dye molecules intersect at 360 nm which allows the quantification of total dye concentration at this wavelength.

Fura-2 is a ratiometric dye, meaning that the actual concentration of free Ca^{2+}-ions can be calculated from the ratio of the emission intensities when exciting with both 340 nm and 380 nm UV light. This calculation first requires a calibration in which the minimum and maximum ratios (R_{min} and R_{max}) of the two channels are measured in both a Ca^{2+}-free and a Ca^{2+}-saturated condition respectively. For a given ratio R, the corresponding concentration of free Ca^{2+} ions can then be calculated as [90]

$$[Ca^{2+}] = \frac{R - R_{min}}{R_{max} - R} \cdot \beta,$$

β being the quotient of the proportionality factors S_f2 and S_b2 between fluorescence intensity and the free Ca^{2+} concentration in both these conditions. As long as the dye is sufficiently dilute, these factors can be replaced by the corresponding intensites measured when exciting at 380 nm, yielding

$$\beta = \frac{I_{f2}}{I_{b2}}$$

Calibration can be performed in cells loaded with Fura-2 AM or in a cell-free solution using the potassium salt of Fura-2.

2.2.1.2 NP-EGTA and 'caged calcium'

Ortho-Nitrophenyl-EGTA (NP-EGTA) is a photolabile Ca^{2+} chelator first introduced by Graham R. C. and colleagues in 1994 [91]. In its resting state it shows a high affinity to Ca^{2+} ions with a K_D of about 80 nM. Exposure to UV light (approximately 350 nm of wavelength) cleaves NP-EGTA, producing iminodiacetic acid with has a much lower affinity for Ca^{2+} ($K_D \sim 1$ mM). This photolysis leads to the release of considerable amounts of Ca^{2+} for a short period of time. In this thesis, NP-EGTA was used to investigate if necrotic killing by NK cells could be provoked by mimicking its intracellular Ca^{2+} release characteristics.

2.2.1.3 MitoTracker

Mitotrackers are fluorescent dyes which accumulate in mitochondria dependent on membrane potential. A commonly used dye is 'MitoTracker Deep Red FM' with an absorption maximum at 581 nm and an emission maximum of 644 nm of wavelength.

2.2.1.4 GFP-RFP-FRET pCasper construct

Förster resonance energy transfer or FRET is the direct radiation-free transfer of energy from one chromophore (also called donor) to another being in close proximity (acceptor, up to 10 nm). When the donor molecule is excited, it passes a transient state of increased

energy. Upon returning to its original energetic state, the energy is partly transferred onto the acceptor molecule via dipole-dipole coupling. This coupling prompts the acceptor to emit light itself. The FRET efficiency, i.e. the proportion of excitation energy which is passed via FRET, depends inversely upon the sixth power of the fluorophores' distance. This principle is put to use in genetically-engineered reporter proteins such as pCasper3, which was introduced by Shcherbo and colleagues in 2009 [92]. The donor protein GFP is connected to the acceptor protein RFP by a short peptide bridge. This bridge is specifically designed as a potential cleavage site of caspase-3. As long as this caspase stays inactive, the bridge remains intact, allowing FRET between GFP and RFP. Following apoptosis induction, caspase-3 cleaves the bridge thus separating the two fluorophores and diminishing FRET. The abrogation of FRET can be detected by an increase in GFP emission and a simultaneous decrease in FRET intensity. The following table gives an overview of the fluorescent properties of the pCasper3 fluorophores:

	excitation maximum (nm)	emission maximum (nm)
tagGFP	482	505
tagRFP	555	584
FRET	482	584

The apoptosis sensor pCasper3 was bought as a plasmid from the company Evrogen. Christian Backes stably transfected two cell lines with the construct, K-562 and Jurkat E6.1. The creation of these cell lines is described in this doctoral thesis [93].

2.2.2 Microscopes

2.2.2.1 Zeiss Cell Observer A wide-field fluorescence microscope from Zeiss, the Cell Observer allows fluorescence microscopy and bright field illumination of single samples or in a well-plate using predefined positions and a laser-based auto-focus. The sample chamber can be incubated to 37°C and inflated with CO_2 to sustain cell viability, growth and migration. For FRET measurements, the RFP excitation filter was extracted from the filter cube so that short wavelength light for GFP excitation could pass.

2.2.2.2 BD Pathway 855 BioImager The BioImager is a high-throughput automated fluorescence microscope providing environmental control and a pipetting robot. In contrast to most other high-performance fluorescence microscopes, it has a stationary sample table and an objective which is freely movable in the x-,y- and z-dimensions. The BioImager is owned by the group of Prof. Dr. Frank Zufall from the Department of Physiology at Saarland University.

2.3 Digital analysis of imaging data

2.3.1 ImageJ

ImageJ is an open-source Java-based software widely used for image editing and analysis. It was originally developed by Wayne Rasband at the National Institute of Health in Bethesda, Maryland and published in 1997. The software provides expansibility by allowing its users to implement self-written macros and plug-ins which are also traded openly via exchange platforms. After image acquisition, the single images were imported into ImageJ and concatenated. The background between cells was subtracted using a 'rolling-ball' algorithm. The following plug-ins were used for further editing or analysis:

- **Time Series Analyzer** - a plug-in developed by J. Balaji from the Department of Neurobiology at UCLA which allows for time-lapse analysis of 2D data. Its ROI manager provides a tool to define certain fixed areas of interest in a single image or an image sequence. The intensity values in every single frame are then taken from the particular ROI and saved in a table. The software version used in this thesis was 2.0, the latest version is 3.0 and was released in 2014.
- **RatioPlus / RatioPlusNaN** - The basic plug-in divides the intensity values for every pair of corresponding pixels in two given images of the same size. It was further modified by Carsten Kummerow so that all pixels for which the ratio calculation yielded a value below a user-defined threshhold were assigned the value 'not a number' and displayed in black.

- **StackReg and TurboReg** - These two plug-ins work together and allow alignment of a series of slices using an iterative algorithm, meaning that a current image is used as an anchor to calculate the shift of the following. This plug-in was necessary due to gradual drift of the well-plate throughout the course of most measurements. This drift made it impossible to work with only one ROI for every cell since the cell would gradually move out of the area of interest. To simplify ROI-tracking of cells, a new plug-in was created with the help of Carsten Kummerow. The plug-in first calculates the overall amount of drift in any user-defined channel. Secondly, the images in that channel are aligned so that a stable frame of observation can be obtained. Afterwards, this exact alignment procedure is performed with every other desired channel so that the individual channels can be merged into a false-color overlay. Finally, those areas of the image which are lost due to drifting are cropped similarly in every video. The exact code of the modified alignment plugin is printed below. Note that the names of the stacks ('blue2green', 'blue2red' and so on) in the code were chosen based on the individual fluorescent channels used specifically in pCasper measurements. They are merely place holders and can be substituted by any name to the user's liking. Comments are marked with '//' and were added to explain the functions of individual sections in the code.

```
// Define input data (GFP, FRET, ...)
stack1 = "blue2green.tif";
stack2 = "blue2red.tif";
stack3 = "Trans.tif";
stack4 = "green2red.tif";

source = "source";
target = "target";
sourceX = 0;
sourceY = 0;
targetX = 0;
targetY = 0;

// Read image dimensions
selectWindow(stack1);
width = getWidth();
height = getHeight();

// Create arrays to store shift in x and y
deltaX=newArray(nSlices);
deltaX[0]=0;
deltaY=newArray(nSlices);
deltaY[0]=0;

// Create a loop with 'nSlices' runs
```

```
for (i=1; i<nSlices; i++)

        // Create two substacks 'target' and 'source' from the stack
        {
        selectWindow(stack1);
        run("Make Substack...", "  slices="+i);
        rename("target");

        j=i+1;
        selectWindow(stack1);
        run("Make Substack...", "  slices="+j);
        rename("source");

        // Perform 'TurboReg' on 'source' and 'target'
        run("TurboReg ", "-align " + "-window " + source + " "
        + "0 0 " + (width - 1) + " " + (height - 1) + " "
        + "-window " + target + " "
        + "0 0 " + (width - 1) + " " + (height - 1) + " "
        + "-translation "
        + (width / 2) + " " + (height / 2) + " "
        + (width / 2) + " " + (height / 2) + " "
        + "-showOutput");

        // Determine old and new X and Y
        sourceX = getResult("sourceX", 0); // First line of the table.
        sourceY = getResult("sourceY", 0);
        targetX = getResult("targetX", 0);
        targetY = getResult("targetY", 0);

        // Calculate shift between source and target using old and new X and Y
        deltaX[i] = deltaX[i-1] - (sourceX - targetX);
        deltaY[i] = deltaY[i-1] - (sourceY - targetY);
        print(deltaX[i]);
        print(deltaY[i]);

        selectWindow("source");
        close();
        selectWindow("target");
        close();
        selectWindow("Output");
        close();

}
// Save values in new table and sort them
        print ("\\Clear");
        SortedValuesX = Array.copy(deltaX)
        Array.sort(SortedValuesX);

        for (jj = 0; jj < deltaX.length; jj++) {
```

```
        print (SortedValuesX [ j j ]) ;}


maxX = 0;
minX = 0;
// Determine maximal shifts in X and Y
    for (a = 0; a < SortedValuesX.length; a++) {
        maxX = maxOf(SortedValuesX [a], maxX);
    }


    for (a = 0; a < SortedValuesX.length; a++) {
        minX = minOf(SortedValuesX [a], minX);
    }



        print (minX);



        SortedValuesY = Array.copy(deltaY)
        Array.sort(SortedValuesY);


        for (jj = 0; jj < deltaY.length; jj++) {
        print (SortedValuesY [ j j ]) ;}


minY = 0;
maxY = 0;


        for (a = 0; a < SortedValuesY.length; a++) {
        minY = minOf(SortedValuesY [a], minY);
    }
    //maxY = minx;
    for (a = 0; a < SortedValuesY.length; a++) {
        maxY = maxOf(SortedValuesY [a], maxY);
        }
        print (maxY);
// Calculate parameters for the cropping rectangle
OriginX = maxX;
OriginY = maxY;
LengthX = width − abs(minX–maxX);
LengthY = height − abs(maxY–minY);

// Align and crop first channel
selectWindow(stack1);
run("Set Scale...", "distance=0 known=0 pixel=1 unit=pixel");
for (i=1; i<=nSlices; i++) {
        setSlice(i);
        run("Translate...", "x="+deltaX[i−1]+" y="+deltaY[i−1]+"
        interpolation=Bicubic slice");
}
makeRectangle(OriginX, OriginY, LengthX, LengthY);
```

```
run("Crop");

// Align and crop second channel
selectWindow(stack2);
run("Set Scale...", "distance=0 known=0 pixel=1 unit=pixel");
for (i=1; i<=nSlices; i++) {
        setSlice(i);
        run("Translate...", "x="+deltaX[i-1]+" y="+deltaY[i-1]+"
        interpolation=Bicubic slice");
}
makeRectangle(OriginX, OriginY, LengthX, LengthY);
run("Crop");

// Align and crop third channel
selectWindow(stack3);
run("Set Scale...", "distance=0 known=0 pixel=1 unit=pixel");
for (i=1; i<=nSlices; i++) {
        setSlice(i);
        run("Translate...", "x="+deltaX[i-1]+" y="+deltaY[i-1]+"
        interpolation=Bicubic slice");
}
makeRectangle(OriginX, OriginY, LengthX, LengthY);
run("Crop");

// Align and crop fourth channel
selectWindow(stack4);
run("Set Scale...", "distance=0 known=0 pixel=1 unit=pixel");
for (i=1; i<=nSlices; i++) {
        setSlice(i);
        run("Translate...", "x="+deltaX[i-1]+" y="+deltaY[i-1]+"
        interpolation=Bicubic slice");
}
makeRectangle(OriginX, OriginY, LengthX, LengthY);
run("Crop");
```

2.3.2   IGOR Pro

Igor Pro is a data analysis software developed and distributed by WaveMetrics. It provides a complete programming language and runs on Windows and Mac operating systems. Its major applications are time series analyses, curve fitting and image processing. The version used in this thesis is 6.2.2.2.

2.4   Experimental procedures

As long as not stated otherwise, chemicals, solutions and standard laboratory procedures were used or conducted as follows (for product information see **section 2.5**):

- Cells were cultured in AIMV/MDM/RPMI-medium containing FCS at 10% and Penicillin/Streptomycin at 1%.

- Killer and target cells were suspended in AIMV medium without any FCS or P/S during experiment preparation and measurements. HEPES was used to buffer the media with a concentration of 10 mM.

- Centrifugation of NK-, NK-92-, K-562- and Jurkat-cells was performed at 200 g for 5 minutes.

Improved Fura-2 staining protocol in NK-92 cells using probenecid and Pluronic F-127 (section **3.1**)

500,000 NK-92 cells were washed twice in DPBS and then resuspended in the staining solutions. These solutions contained Fura-2 AM dye at 1 μM, probenecid at 1mM or 2.5 mM and/or Pluronic F-127 at 0.1%. Cells were loaded for 30 minutes at room temperature. After completion of the loading procedure, cells were washed again in DPBS and transferred to a glass cover-slip which was previously coated with poly-L-ornithine. After adhesion to the cover slip, the medium was washed away and substituted with Ringer solution containing 1 mM $CaCl_2$. The exact composition of this solution can be taken from **section 2.5**.

Probenecid has low solubility at physiological pH. A stock solution can be created by diluting a small portion in 1 M NaOH which can then be slowly titrated using HCl. Note that this solution will have a high osmolarity compared to physiological levels.

A more efficient way to create a stock solution is to dilute a suitable amount of powder in 1 M NaOH to create a 1 M alkaline solution. The latter can then be diluted 1:1 with an equal volume of DPBS. The stock should then be thoroughly mixed and slightly heated until the powder has completely dissolved. The resulting probenecid stock contains the substance at 500 mM. In 500 ml of a Fura-2 staining solution, the addition of 2.5 μl of probenecid stock gives a final pH of 7.44.

Pluronic F-127 stock solution contained the substance at 20% solved in DMSO.

Measuring apoptosis and necrosis using the pCasper3 construct (sections **3.2 + 3.3**).

300000 Jurkat E6.1pCasper cells were washed in DPBS, suspended in serum-free AIMV medium and pipetted into wells of a black 96-well-plate by Falcon. The final target cell density was 600/μl. 875000 negatively isolated primary NK-cells were washed twice in DPBS, thoroughly re-suspended in DPBS and finally suspended in 100μl of AIMV medium. 40 μl of NK cell suspension were pipetted in each well on top of the target cells. The final volume in each well was 240μl, the killer-to-target ratio was $\sim$ 3:1. Imaging

was performed using the Cell Observer Setup, including incubation with 37°C and 5% CO_2. A 20x objective was used. 400 images (3 fluorescent channels, 1 brightfield) were taken over 2 hours. Videos and the presented image sequences derived from them were prepared in ImageJ. FRET-ratio and RFP intensities were extrapolated using the Time-Series-Analyzer Plugin and then plotted in IgorPro.

How extracellular Calcium ion concentration affects the distribution of apoptosis and necrosis by NK-cells (section **3.3.1**)

EGTA or $CaCl_2$ solutions were added to HEPES-buffered AIMV medium to yield twice the concentration that was desired for the final measurement. This step was taken to avoid the necessity of exposing killer or target cells to the altered Ca^{2+} concentrations before the actual measurement. The buffered media were preincubated at 37°C and 5% CO_2 for 24 hours. On the day of the measurement, 1,600,000 target Jurkat E6.1 cells were washed in DPBS and diluted in a total volume of 800 μl. 100 μl of this cell suspension were pipetted into 7 wells of a black 96-well-plate and incubated at 37°C and 5% CO_2 for one hour. The final target cell concentration was 200,000 cells per well. Expanded primary NK cells were washed thoroughly in DPBS, resuspended in 320 μl of HEPES-buffered AIMV medium and 40 μl of this suspension was pipetted into 7 wells of the 96-well-plate containing the preincubated EGTA- and $CaCl_2$-buffered media in adjacent wells. To start the measurement, 100 μl of these media were pipetted parallelly to all target cells, yielding the desired calcium dilutions. The Cell Observer was programmed and the pCasper measurement was initiated. After several cycles, 50 μl of the buffered media were added to the killer cell suspensions, the cells were thoroughly re-suspended and then 50 μl of the diluted suspensions were added to the measuring wells to yield a final killer-to-target ratio of 0.9 to 1. Live-cell imaging was performed over 2 hours at 37°C and 5% CO_2 with a 10x objective. The cycle time was 32 seconds. Images were later analysed with ImageJ.

How osmolarity affects the distribution of apoptosis and necrosis by NK-cells (section **3.3.3**)

Osmolality of AIMV medium without FCS buffered with 10 mM HEPES was measured several times using the osmometer listed in **section 2.5**. The average osmolality was 314 mosmol/l. To first test cell viability at different osmolalities, a dilution series was generated using distilled water or mannitol. The following concentrations were tested: 281 mosmol/l, 292 mosmol/l, 303 mosmol/l, 314 mosmol/l, 325 mosmol/l, 336 mosmol/l and 347 mosmol/l. After the cells proved unimpaired after 3 hours in these media, the lowest and highest osmolalities were chosen for the killing experiments. 420,000 Jurkat

E6.1 pCasper cells were centrifuged, washed in DPBS and pipetted into 6 wells of a black 96-well-plate at a concentration of 500 /μl, giving 50,000 target cells per well. 600,000 primary human NK cells isolated from PBMCs were washed in DPBS and suspended in buffered AIMV medium. 10 minutes before the start of the measurement, the media containing the target cells were diluted with H_2O or concentrated with mannitol so that adding the killer cells would yield the previously tested osmolalities. Killer cells were added to the target cells at a killer-to-target ratio of 1 to 1 and the measurement was initiated. The BioImager setup was used with a 10x objective for better overview and larger cell counts. The cycle time was 52 seconds. Images were analysed using ImageJ.

Correlation of intra- and extracellular calcium concentration during killing by NK cells (section **3.4.1**)

EGTA or $CaCl_2$ solutions were added to HEPES-buffered AIMV medium to yield twice the final concentration to allow for a 1:1-dilution shortly before the start of the measurement as previously explained. The solutions were preincubated at 37°C and 5% CO_2 over night. On the day of the measurement, 750,000 NK-92 cells were washed in DPBS and re-suspended in serum-free AIMV medium. The cells were loaded with Fura-2 AM dye at a concentration of 1 mM at room temperature for 30 minutes. The loading solution contained probenecid at 2 mM and Pluronic F-127 at 0.1 %. After 30 minutes, the killer cells were washed twice in DPBS and suspended in 1000 μl of serum-free AIMV medium and then 100 μl each were transferred into 8 wells of a black 96-Well-Plate. The plate was kept at room temperature to slow down dye extrusion and retained from light exposure. The media portions buffered with EGTA and $CaCl_2$ were transferred to a transparent 96-well-plate. 480,000 K-562 cells were washed in DPBS and suspended in AIMV medium at 2,000 cells/μl. 8 portions of 60 mul of this cell suspension were pipetted to 8 wells of the transparent well plate also containing the buffered AIMV media. Before the start of the measurement, 100 μl of these media were pipetted to the killer cells to give the final desired Calcium concentrations. The microscope was programmed and test images were acquired. After a few test cycles, 30 μl of the media were pipetted to the target cell suspensions. The target cells were thoroughly re-suspended and 50 μl of these suspensions were each pipetted to the corresponding killer cell wells. Measurement was performed at the BioImager setup with a 20x objective. Transmitted light images were recorded as well as Fura-2 images at 340 and 380 nm excitation wavelength. The cycle time was 59 s. After 110 to 120 minutes, the measurement was stopped. Images were analysed with ImageJ, Fura-2 ratio values were extrapolated using the Time-series-analyzer plugin and the values were transferred to IgorPro for further analysis.

Detailed analysis of intracellular calcium signals in active NK cells (section **3.4.2**)

The experimental approach was similar to that described previously for NK-92 cells. Human NK cells were positively isolated from PMBCs, cultivated in DMEM medium and stimulated over 3 days with Interleukin-2 at 1:1,000,000. On the day of the experiment, 700,000 NK cells were washed in DPBS and loaded with Fura-2 -AM at a concentration of 1 mM at room temperature for 30 minutes. The loading solution contained probenecid at 2.5 mM and Pluronic F-127 at 0.1%. The experiment was conducted in HEPES-buffered AIMV medium without addition of EGTA or $CaCl_2$. After staining, the killer cells were allowed to sit down on the bottom of a black 96-well-plate at a density of 75,000 cells per well. Jurkat E6.1 pCasper cells were used as target cells, centrifuged, washed in DPBS and re-suspended in serum-free AIMV medium. After programming the microscope and measuring one complete cycle, the target cells were added on top with a killer-to-target Ratio of 1 to 1. The BioImager Setup was used with a 20x objective. Three wells were measured in parallel, the cycle time was 32 seconds. Data was transferred to ImageJ, time series analysis was performed using ImageJ and IgorPro as previously described.

Uncaging calcium ions during killing (section **3.6.2**)

1,032,000 expanded primary NK cells were centrifuged, washed twice in DPBS and suspended in 737 μl containing 687 μl of AIMV without FCS and 50 μl of DPBS for initial suspension. Afterwards, 100 μl of this killer cell suspension were pipetted to 7 wells of a black 96-well-plate and incubated over two hours at 37°C and 5% CO_2 to allow for the cells to adhere to the bottom of the plate. Staining of killer cells was done using two separate loading solutions. Both contained the loading-facilitating agents at the previously noted concentrations. One half of the killer cells were loaded with NP-EGTA additionally to Fura-2 (concentrations of dyes in the loading solutions were 4 μM and 2 μM respectively), the other half only with Fura-2 as a control. Loading was performed for 30 minutes at room temperature. Afterwards, killer cells were carefully washed twice in DPBS in the well-plate and sit to rest in AIMV medium.

Target cell preparation was performed by first centrifuging 2,560,000 Jurkat E6.1 pCasper cells, then washing them once in DPBS containing BSA and then suspended in a total volume of 320 μl of AIMV medium. Target cells were pipetted to killer cells immediately before the start of the measurement. Effector-to-target ratio was 0.7 to 1.

Measurement and uncaging were performed at the BioImager setup. Lamp A for Fura-2 and NP-EGTA excitation was run at 100%, lamp B at 20% maximal power for pCasper measurement. Uncaging was performed according to a self-programmed protocol which started by once taking Fura-2 baseline values, but continued only with pCasper excitation for 20 minutes to avoid any previous Ca^{2+} release from the chelator. After 30 minutes,

cells in both conditions were flashed with UV light. Fura-2 was measured twice immediately before and after the flash to verify Ca^{2+} ion increase in the NP-EGTA group. A second flash was given ten minutes later. The protocol finished with pCasper measurements over another 80 minutes. Total observation time was 120 minutes. Time resolution was 18 s between flashes and 32 s separating flashing, Fura-2 excitation and the following pCasper measurement. Digital analysis ensued in a similar manner as for the experiments of **section 3.5** using the aforementioned software.

2.5 Product information

Laboratory consumables and glassware

Product	Company	Catalogue number
96-well-plate (black)	Corning / Falcon	3340
96-well-plate (transparent)	BD Becton Dickinson / Falcon	353296
Disposable pipettes	BD Biosciences	357525
Culture flasks	BD Biosciences	353108

Technical devices

Gadget	company	model
Cell counter	Beckman Coulter	Beckman Coulter Z2
Cell culture hood	Erlab	Captair flow
Centrifuge	Eppendorf	Centrifuge 5418/5418R
Incubator	Thermo Fisher Scientific	Heracell
Osmometer	Wescor	AC-061
Pipet aid	Integra	PipetBoy Acu 2
Shaker	Heidolph Instruments GmbH & Co KG	Heidolph Duomax 1030
Weighing scale	Kern & Sohn GmbH	ALT 160-4 NM
Vortex mixer	Scientific industries Inc.	Vortex Genie 2

Chemicals and solutions

Product	Company	Catalogue number / specification
AIMV medium	Thermo Fisher Scientific / gibco	12055083
BAPTA-AM	Thermo Fisher Scientific / invitrogen	B6769
BSA	Thermo Fisher Scientific / invitrogen	15561020
$CaCl_2$	Merck Millipore	102382
DMSO	Sigma-Aldrich / Merck Millipore	D8418
Dynabeads$^{®}$ Untouched^{TM} Human NK Cells Kit	Thermo Fisher Scientific	11349D
DPBS	Thermo Fisher Scientific / gibco	14190
FCS	Thermo Fisher Scientific / gibco	10270-106
Fura-2 AM	Thermo Fisher Scientific / invitrogen	F1221
Mannitol	Sigma-Aldrich / Merck Millipore	M9546
HEPES	Sigma-Aldrich / Merck Millipore	H7523
MitoTracker Deep Red	Thermo Fisher Scientific / invitrogen	M22426
NP-EGTA AM	Thermo Fisher Scientific / invitrogen	N6803
Penicillin / Streptomycin	Sigma-Aldrich / Merck Millipore	P4333
Pluronic F-127	Sigma-Aldrich / Merck Millipore	P2443
Poly-L-ornithine	Sigma-Aldrich / Merck Millipore	P3655
Probenecid	Sigma-Aldrich / Merck Millipore	P8761
Ringer solution + 1 mM $CaCl_2$	self made	155 mM NaCl 4.5 mM KCl 10 mM glucose 5 mM HEPES 2 mM $MgCl_2$ 1 mM $CaCl_2$ pH 7.4
RPMI-1640 medium	Thermo Fisher Scientific / gibco	21875

3 Results

3.1 An improved staining protocol for Fura-2-based calcium imaging in NK-92 cells and primary NK cells

Fura-2 and Fura Red are among the most frequently used dyes suitable for calcium imaging. **Section 2.2** provides an overview of the fluorescent properties of Fura-2 as well as an introduction into the mathematical principle of ratiometric calcium measurement as suggested by Grynkiewicz and colleagues [90].

For the purpose of measuring Ca^{2+} concentrations in NK cells during the attack on target cells expressing the pCasper construct, Fura-2 was chosen over Fura Red to avoid any cross-talk with the GFP/RFP fluorescence of the sensor protein.

Preliminary Fura-2 staining experiments quickly led to the observation that, while primary human NK cells showed sufficient uptake of Fura-2 following standard loading protocols for the dye, the cell line NK-92 could not accumulate sufficient amounts of dye for accurate Ca^{2+} measurements. Neither increasing the concentration of the AM-dye in the loading solution nor varying staining time had beneficial effects on imaging quality.

Many cell types, including immune cells, express organic anion transporters responsible for active export of multivalent anions [94]. These transporters are an important clearance mechanism for urate in kidney epithelial cells [95]. Being rather unspecific, they also accept Fura-2 anions as their substrates, leading to a gradual extrusion of the dye from the cytosol. The substance *probenecid* is known to be an effective inhibitor of organic anion transport [96] and has been used in treating patients with gout to block urate resorption [97]. Di Virgilio and others showed that it can also reduce both export and sequestration of anionic dyes like Fura-2 in macrophages [98].

In an attempt to slow down export of the already cleaved AM-dye, NK-92 cells were loaded according to the same protocol as before, but in a solution which contained probenecid at 2.5 mM. Interestingly, the drug greatly improved imaging quality, suggesting high activity of organic anion transport in these cells. Probenecid also increased dye uptake and brightness in primary NK cells (not shown) but the effect was not as strong compared to the cell line.

Further increase in brightness could be achieved using the substance Pluronic F-127. It is an organic copolymer consisting of a polyoxypropylene chain substituted with hydrophilic chains of polyoxyethylene. Pluronic is commonly used as a dispersing agent in chemical industry and has experimental applications in pharmaceutics. Its tendency to form micelles is useful when diluting acetoxymethyl-based dyes such as Fura-2 AM in hydrophilic fluids. Although the AM-dye was already thoroughly distributed using a vor-

tex mixer, adding Pluronic F-127 at 0.1% to the staining solution significantly improved loading quality. The effect of 0.1% disperging agent in the solution was comparable to that of the addition of 2.5 mM probenecid. Combining both substances in the staining solution synergistically enhanced Fura-2 accumulation in the cytosol of NK-92 cells, giving an even brighter fluorescence signal. The separate and combined effects of probenecid and Pluronic F-127 on Fura-2 staining are shown in **figure 4**.
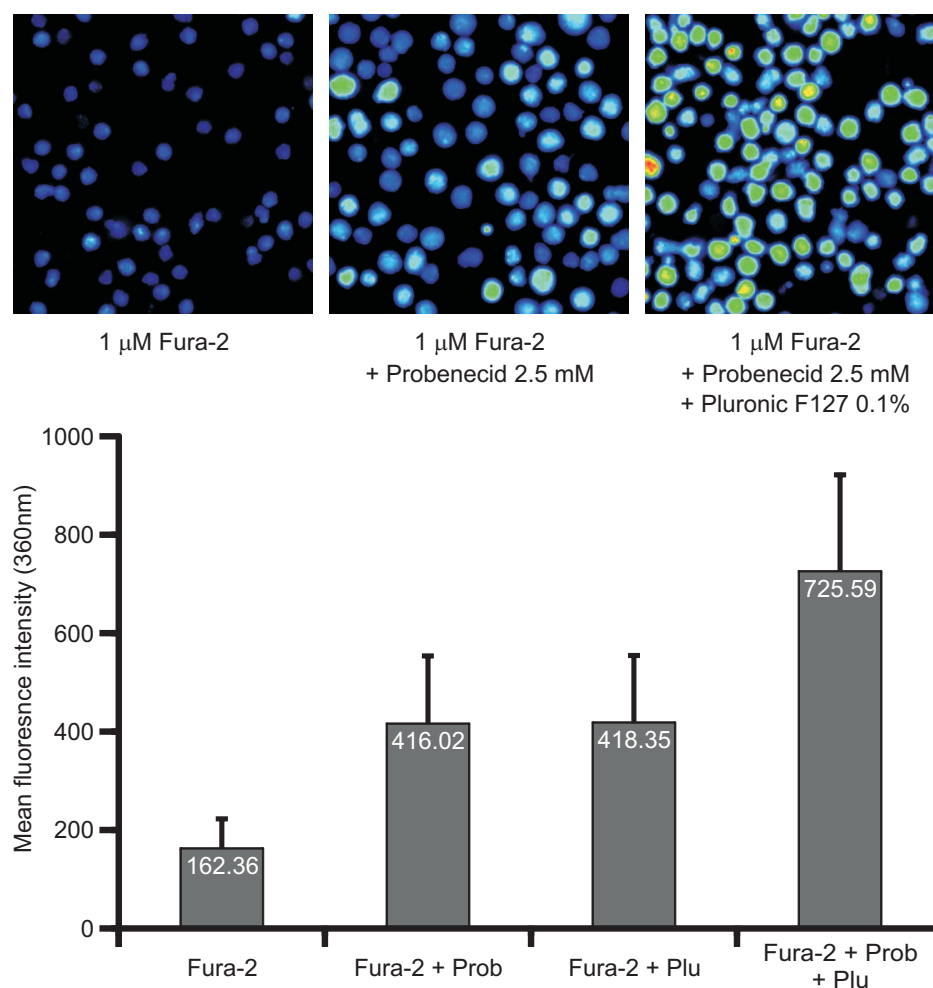
Figure 4: Probenecid and Pluronic F-127 synergistically increase staining efficiency of Fura-2 in NK-92 cells
Cells were loaded at room temperature for 30 minutes. The composition of the individual staining solutions can be taken from the captions below the three corresponding false-color images. Blue indicates low, green average, red high intensity. After loading, the cells were fixed to a coverslip coated with a layer of poly-L-ornithine and washed in Ringer solution containing 1 mM $CaCl_2$. Fura-2 was excited at 360 nm using a monochromator. Exposure time was 100 ms. An average fluorescence intensity of the cells in every condition as well as standard deviation is depicted by bars below.

To exclude any direct toxic effects of both probenecid and Pluronic F-127, NK cells were suspended in AIMV medium for two hours containing both substances at the concentra-

tions used in the loading solution. Both agents did not affect NK cell viability during the whole observation time. Drawing from several independent experiments performed with both primary NKs and NK-92 cells stained with and without the addition of both substances, it appears safe to say that their addition does not have any detectable effect on NK cell migration or killing efficiency. Therefore, the two agents were used in all subsequent Ca^{2+}-imaging experiments.

3.2 How to detect ongoing apoptosis and necrosis in target cells

Apoptosis and necrosis are associated with typical changes in cell morphology. Activating caspases is the crucial step in apoptosis induction. It is followed by chromatin condensation, DNA fragmentation and a constriction of the cell membrane [99]. These processes are microscopically detectable by an observable shrinkage and involution of the cell. The latter is achieved by a decoupling of the cytoskeleton from its membrane, forcing it to fold itself into bulges [100]. The resulting apoptotic bulges are often referred to as 'blebs'.

Necrosis, on the other hand, leads to a visible swelling of the target cell, culminating in the membrane rupturing. Although this rupture can sometimes be seen using conventional brightfield or infrared illumination, a more certain indicator is the loss of cytosolic fluorescent dyes into the supernatant.

Several ways to identify a target cell's dying type have been developed [101], [102], [103]. Assessing only the above-mentioned features visible during brightfield illumination of cells can be reliable in some cases, but it is likely to miss milder forms of ongoing apoptosis or necrosis associated with low caspase activity or very discrete membrane damage.

Combining morphological aspects of cell death types with fluorescent indicators greatly improves sensitivity and specificity in death type detection. A suitable sensor for apoptosis induction in target cells is the GFP-RFP-FRET-construct 'Casper3-GR', whose properties are explained in **section 2.2** [92]. During his doctoral thesis, Christian Backes transfected two stable cell lines with this construct, allowing for repetitive and reliable apoptosis measurement in single-cell experiments. The principle of Casper-based apoptosis indication is explained in more detail in his thesis [93]. Its basics, however, are once more outlined in this section since the sensor was regularly used in this doctoral thesis and the following approach to quantify apoptosis and necrosis was based on its mode of function.

In viable cells, the peptide sequence DEVD, combining the two fluorescent proteins GFP and RFP of the pCasper construct, remains intact, allowing the GFP-RFP-FRET. Once apoptosis is triggered, active caspase 3 will cleave this peptide bridge, thus diminishing the energy resonance transfer. The subsequent extinction of FRET causes an antiparallel increase in green fluorescence emission by GFP as well as a decrease of FRET emission. Division of FRET intensity by GFP intensity yields the so-called 'Donor Ratio' or 'FRET Ratio'. This ratio can be taken to calculate an 'Apoptotic Ratio' (AR), which corresponds to the extent of ongoing apoptosis.

Since lysis of target cells does not lead to caspase activation, the Casper-3 construct is specific for apoptosis. It can, however, also be used as an indirect necrosis indicator.

Apoptosis causes blebbing but does not impair cell membrane integrity per se. The overall amount of cytosolic fluorescent protein, corresponding to the red emission of RFP, thus remains constant over time. When a cell is lysed, there is no increase in green fluorescence or the AR, but pCasper as well as other cytosolic contents rapidly diffuse out into the supernatant. Due to the loss of indicator protein, red fluoresence intensity declines after lysis. Thus, measuring GFP, FRET and RFP will allow detecting both types of target cell death in parallel. Exemplary functions of AR and RFP intensities over time from both apoptotic and lytic target cells are shown in **figure 5**.

Obviously, apoptosis and necrosis show different both morphological and fluorescent
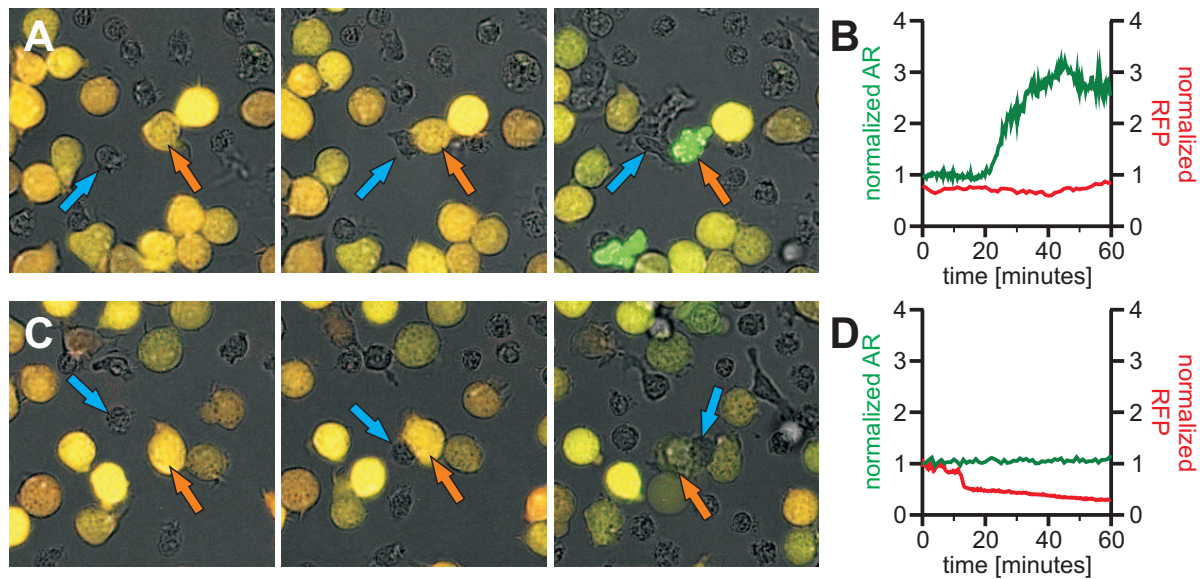
Figure 5: Killer-cell-induced apoptosis and necrosis in target cells measured with the Casper-3 sensor

Two different Jurkat E6.1 cells expressing pCasper are killed by primary NK cells through induction of apoptosis **(A)** and necrosis **(C)**. Targets cells are marked by orange arrows, primary NK cells by blue arrows. Apoptosis induction leads to an increase in GFP emission, indicated by a switch from yellow to green in the false-color image. The apoptotic target cell also shows clear signs of shrinkage and blebbing. In the lower image sequence, the target cell swells, its membrane bursts open and indicator fluorescence emission is quickly diminished.

The corresponding rRFP and AR values from the respective target cells are plotted as a function of time in **(B)** and **(D)**. Target cells which do not have any contact to an NK cell still show gradual increase in FRET as well as decrease in RFP intensity due to bleaching. Therefore, these cells were used to calculate standard AR- and RFP-curves to correct for this bleaching using a slowly exponentially growing and an exponentially declining function. Afterwards, the intensities taken from the cells being killed were normalized against these standard curves which is also the reason why both normalized AR (left y-axis) and normalized RFP (right y-axis) curves start at values of $\pm$ 1.

characteristics. It should yet be noted that they are not functionally independent of one another. If apoptosis is induced by granzymes, perforin pores are required first to grant access into the cytosol. A detailed discussion of this interdependence of both killing types as well as the limitations in their detection with pCasper is provided by **sections 4.1.1**

and **4.1.2**.

## 3.3 How to mathematically quantify apoptosis and necrosis in target cells

A frequent observation during the presented series of experiments was that pCasper reported apoptosis in target cells which showed little to no morphological changes typically associated with apoptosis. These cells would often take longer to undergo apoptosis-related changes in cell morphology and showed a rather slow turnover of pCasper in comparison to others. Obviously, programmed cell death induced by killer cells is a process which can take place with different velocities or degrees, depending on how high caspase activity accumulates inside the cytosol. The same is true for necrosis: It appears intuitive that the more perforin is released, the more pores will be formed, thus membrane lysis should occur more rapidly in these cells. In fact, using pCasper in live-cell imaging, some necrotic target cells lose the sensor protein very quickly, while others show more of a gradual leakage, often taking minutes or even hours to pale completely. Given this observation, the question was whether pCasper could not only serve as a qualitative indicator for death types but also as a means to physically quantify the degree of both necrosis and apoptosis in every target cell. Putting it simply: 'How much necrosis is going on, how much apoptosis is going on and how rapid are they?' Such a quantification could prove useful since it is likely to be linkable to the extent of granule exocytosis by NK cells or the individual strength of death receptor signaling.

The following two subsections display a new approach to mathematically quantify necrosis and apoptosis in target cells using only the fluorescence measurements of pCasper. This method can be performed for every target cell expressing the sensor protein and the results can later be correlated with parameters taken from calcium measurements in the respective killer cell.

3.3.1 Quantifying necrosis - the necrotic index

During the course of observation, every Jurkat E6.1 pCasper cell shows a slow exponential decrease in RFP fluorescence over time due to photobleaching. In order to yield an unadulterated RFP signal, a normalization can be performed using Jurkat cells not being killed nor attacked by any NK cell. **Figure 6** shows the average RFP signal in these cells over 100 minutes of observation. This signal can be approximated by a slowly-declining exponential function. The result is a standard RFP signal against which the actual target cells can be normalized by dividing their individual RFP signal. Cells not being attacked during the course of the experiment would then have a constant relative RFP signal (from this point on referred to as 'rRFP') rather than an exponentially declining absolute RFP function.
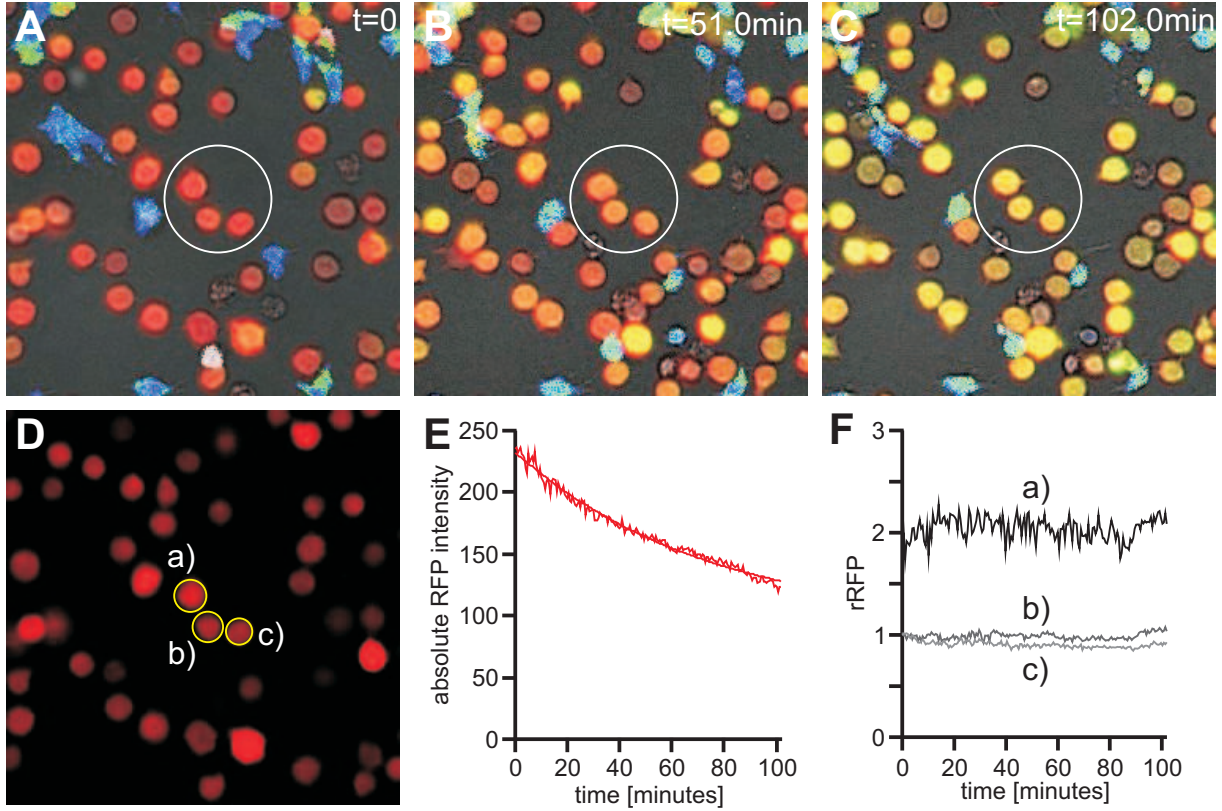
Figure 6: Correction for photobleaching - normalizing RFP intensity
The top row shows an area from the same experiment presented before. Three Jurkat cells are marked in the center. These cells do not contact any killer cells during the whole observation time (**A - C**). Picture **D** shows the same cells, but this time only the RFP channel. The background was subtracted and an image was created in which all intensity values below a certain threshhold were given the value 'not a number', which is represented by the black area in the background. All spared Jurkat cells were used to calculate a standard RFP intensity function (**E**). Afterwards, the three cells marked in **D** were divided by this RFP standard, yielding a relative RFP intensity (rRFP) for all three cells a) to c) (**F**).

If a target cell is exposed to perforin, its membrane will be disrupted leading to a loss of indicator protein into the supernatant. The speed of loss in red fluorescence - i.e. the speed of pCasper effusion - will depend on the extent of membrane damage and the concentration gradient of pCasper between the intra- and extracellular space. Presuming that the number of perforin pores stays constant over time, the diffusion rate will decline depending on the amount of protein that is left inside the cytosol. Theoretically, the relative RFP signal should therefore present an exponential decrease. **Figure 7** shows that rRFP decrement can in fact be approximated quite well using a simple exponential function. The speed of necrotic cell lysis occuring in a particular cell can then be described as the time constant of this exponential decrease. If I_{rRFP} equals relative RFP intensity, then its decline can be described as

$$I_{rRFP} = I_0 \cdot e^{-\lambda \cdot t}$$

with lambda being the necrotic index:

$$k_n = \lambda(rRFP)$$

This parameter is suitable for two reasons: First, it represents the amount of released perforin, since more perforin will very likely lead to more pores which facilitates protein diffusion. Therefore, cells undergoing a rapid lysis will have a shorter half life or a higher λ than others. Secondly, the decay constant is independent of the overall amount of protein. This comes in handy, regarding the large differences of pCasper expression levels comparing different target cells. In **figure 7**, rRFP functions from two necrotic target cells are compared against a healthy control cell. Lysis occurred more rapidly in the red cell than in the blue one (on the left), resulting in a higher necrotic index of 0.2 compared to 0.07 after exponential fit (on the right). The necrotic index k_n will be above zero for every target cell undergoing detectable degrees of lysis. In all cases of rRFP being constant over time, cells will by definition have a k_n of zero.
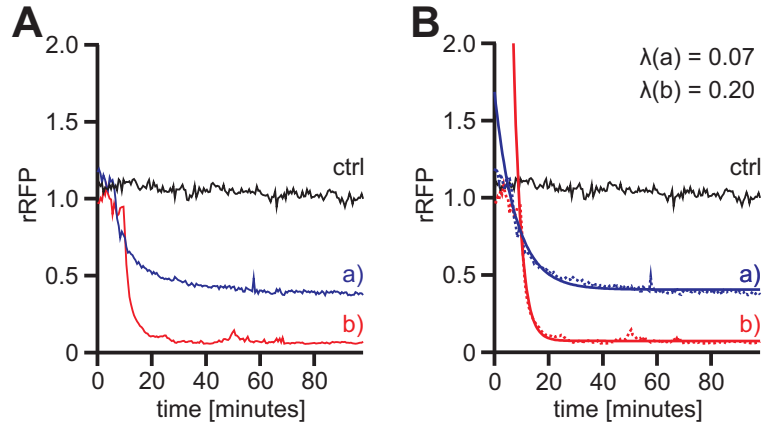
Figure 7: Comparison of different necrotic indices
A plots the rRFP values for two representative Jurkat cells being killed by necrotic lysis (red and blue) and one Jurkat cell which is not being attacked serving as a control (ctrl, black). The time span before contact formation was cut out. Following perforin release and pore formation, the indicator protein leaves the cytosol. The corresponding loss of red fluorescence is fitted with an exponential function. The two fits can be seen in **B**. Applying the definition of the necrotic index given above, the control cell would have a k_n of 0, the blue one of 0.07 and the red one a k_n of 0.20.

3.3.2 Quantifying apoptosis - the apoptotic index

Apoptosis induced by NK cells is characterized by activation of caspases through granzymes (s. **section 1.4**) or cross-linking death ligands. Caspases cleave the peptide bridge between GFP and RFP thereby extinguishing FRET. Once apoptosis has started, the intensity of GFP emission will increase since there is no more energy transfer to RFP. In parallel, FRET intensity will decline. The efficiency of resonance energy transfer can be approximated by the quotient of measured FRET intensity and donor intensity,

$$n(FRET) = \frac{I(FRET)}{I(donor)} = \frac{I(FRET)}{I(GFP)},$$

yielding the so called 'FRET-Ratio'. We can define the difference between 1 and the FRET-Ratio as the 'Apoptotic Ratio' or 'AR' because it correlates to the amount of apoptotic activity inside the cell:

$$AR = 1 - \frac{I(FRET)}{I(GFP)}$$

The target set of the AR function will depend on the individual exposure times of GFP and FRET excitation. With those exposure times chosen uniformly for all experiments, values ranged between roughly 0.15 (non-apoptotic cells) to 0.9 (apoptotic cells).

The AR can be described by a logistic function. This type of function is often used in biochemistry to describe the kinetics of cooperative ligand binding to enzymes. If AR_{min} is the lower and AR_{max} the higher limit, then the equation can be written as

$$AR = AR_{min} \cdot (1 + \frac{AR_{max} - 1}{1 + (\frac{x_h}{x})^n})$$

or

$$AR = AR_{min} + \frac{AR_{max} - AR_{min}}{1 + e^{-n \cdot (x - x_0)}}.$$

n is often referred to as the 'Hill coefficient'. It is a measure of cooperativity in ligand binding. For all $n > 1$, a cooperative effect is visible, while $n = 1$ equals no cooperative effect. The value of n is visualized by the steepness of the sigmoid curve.

If we attempt to quantify the extent of apoptosis, we need to quantify intracellular caspase activity. Caspases are enzymes turning over their substrates, one of which is - among a vast majority of other proteins - pCasper. Hence, if a high number of caspases is being activated, the AR curve will have a steep increase, and a lower steepness if the overall caspase activity inside the cell is low. The value n or its common logarithm can therefore serve as an estimator for apoptosis activity. The apoptotic index k_a would then be defined as

$$k_a = lg(n_a)$$

Defining k_a by the common logarithm of n and not by n itself is not a necessity. It is handy though, since $lg(n)$ will yield values which are of the same size as those for k_n. k_a will be positive for all cells showing measurable extent of apoptosis. All cells which showed no visible extent of sigmoidal AR increase were regarded as 'non-apoptotic' and allocated the value zero.

With these simple mathematical tools at hand, we can assign both a necrotic index k_n and an apoptotic index k_a to every target cell observed during a killing experiment. Hence, we yield a pair of values (k_n,k_a) for a specific cell which will always suit one and only one of the following constellations:

$$k_n = 0 \wedge k_a = 0$$

$\rightarrow$ no necrosis, no apoptosis,

$$k_n > 0 \wedge k_a = 0$$

$\rightarrow$ necrosis, but no apoptosis,

$$k_n = 0 \wedge k_a > 0$$

$\rightarrow$ no necrosis, but apoptosis and

$$k_n > 0 \wedge k_a > 0$$

$\rightarrow$, both necrosis and apoptosis, mixed type.

Figure 8 shows how a video directly representing the AR can be generated from the GFP and FRET measurements. **Figure 9** demonstrates that, as predicted, AR does in fact increase over time according to a sigmoid function, and that differences in apoptotic speed translate to differences in k_a.

Drawing from several experiments performed, the forth group, i.e. the mixed death type, is the rarest but also the most complex. While it is reasonable to assume that both k_n and k_a are sensitive enough to detect that both types of target cell death are enrolling in the same cell, the question remains whether their respective extent can be reliably expressed using the method described in this section. For a detailed discussion of this problem see **section 4.1.2**.
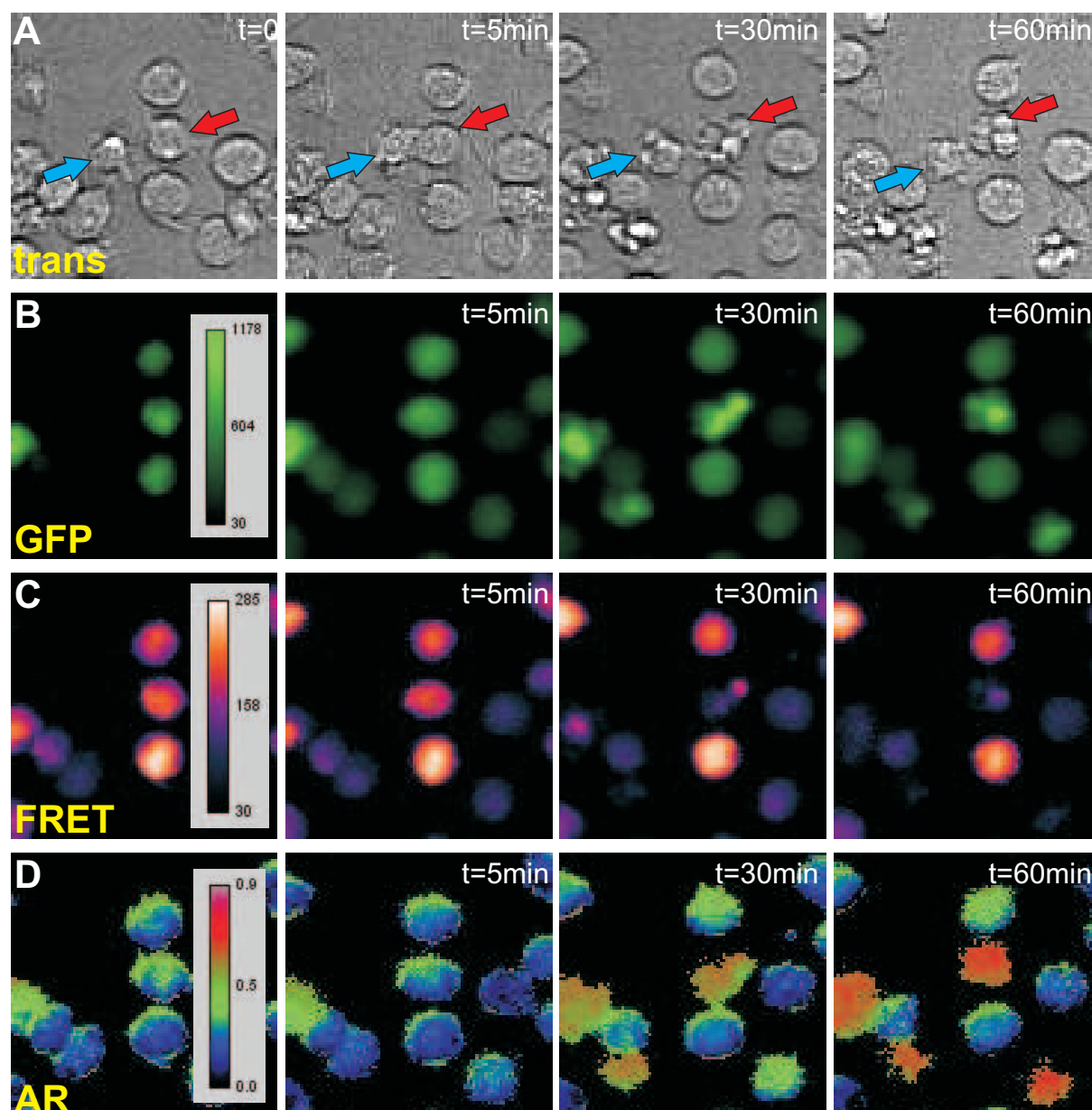
Figure 8: Calculating the apoptotic ratio (AR) for target cells using GFP and FRET measurements

Row **A** shows brightfield images of a target Jurkat cell (red arrow) entering apoptosis after being contacted by an NK cell (blue arrow). Rows **B** and **C** show colored images taken from the GFP and the FRET measurement for the given time points. Both are divided and the result is subtracted from 1 to yield the Apoptotic Ratio or AR **(D)**. The pseudocolor scale shows that those cells not undergoing apoptosis have a stable AR. After apoptosis initiation, the target cell's AR increases quickly and converges maximal values. AR values can be extrapolated from the video and plotted in IGOR to calculate the apoptotic index. For further details see **Figure 9**.
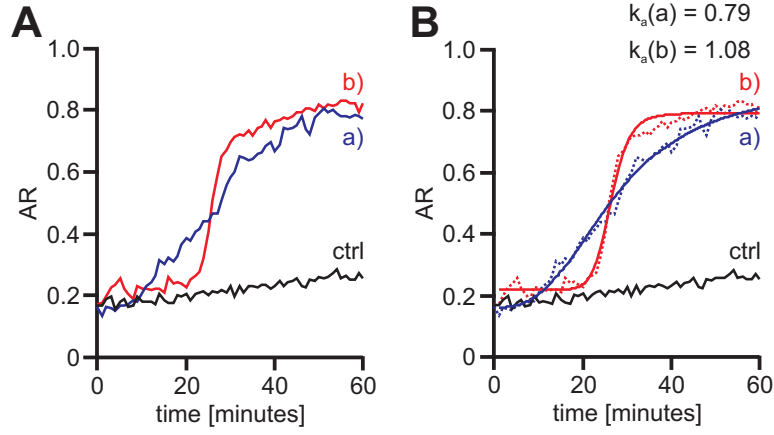
Figure 9: Comparison of different apoptotic indices
A plots the AR values for two representative Jurkat cells being killed by apoptosis (red and blue) and, as a control, one Jurkat cell which is not being attacked at all (black, ctrl). The time span before contact formation was cut out. After cleavage of the peptide bridge, FRET is diminished and the apoptotic Ratio increases, but with different velocities in cells a) and b). The two Hill fits can be seen in **B**. Applying the definition of the apoptotic index given above, the control cell would have a k_a of 0, the blue one of 0.79 and the red one a k_n of 1.08.

3.4 Statistical distribution of apoptosis and necrosis by NK cells

Under physiological conditions, NK cells can induce apoptosis as well as necrosis in Jurkat E6.1 pCasper cells. Interestingly, the distribution of both killing types is not random but *necrosis* appears to be the dominant type. Experiments in this subsection show how the frequency distribution of apoptosis and necrosis induction by NK cells depends on extracellular Ca^{2+} supply.

3.4.1 Extracellular free calcium concentration

NK cells and Jurkat E6.1 cells expressing Casper3 were brought together to make contacts exposed to varying extracellular concentrations of free calcium ions. The concentration gradient was produced by either buffering standard AIMV medium with different amounts of the Ca^{2+} chelator EGTA or adding increasing amounts of $CaCl_2$.

EGTA/CaCl$_2$ added [mM]	measured $[Ca^{2+}]_{ext}$ [mM]	standard deviation [mM]	calculated $[Ca^{2+}]_{ext}$ [mM]
1.00 E	0.004	0.005	0.0029
0.95 E	0.008	0.006	0.0107
0.94 E	0.011	0.007	0.0128
0.93 E	0.014	0.009	0.0150
0.92 E	0.019	0.011	0.0175
0.91 E	0.020	0.011	0.0201
0.90 E	0.025	0.008	0.0231
0.80 E	0.074	0.006	0.0724
0.70 E	0.193	0.013	0.1930
0.60 E	0.268	0.025	0.2652
0.50 E	0.364	0.021	0.3549
0.40 E	0.451	0.033	0.4447
0.30 E	0.508	0.034	0.5344
0.20 E	0.599	0.034	0.6241
0.10 E	0.684	0.033	0.7138
0 (AIMV)	**0.783**	**0.019**	**0.8036**
1.0 Ca	1.730	0.03	1.7009
2.0 Ca	2.600	0.13	2.5733
3.0 Ca	3.930	0.045	3.9833
4.0 Ca	5.420	0.26	5.3933

Calculating the concentrations of free Ca^{2+} ions in media is not trivial due to varying degrees of protein Ca^{2+} ion binding. Based on calcium electrode measurements performed

by many colleagues, in particular Eva Schwarz and Kim Friedmann, a calibration curve for $[Ca^{2+}]_{ext}$ as a function of the amount of EGTA or CaCl$_2$ added to AIMV medium was calculated. This approximation was done using linear regression for concentrations higher than 200 μM ($R^2 = 0.999$) and an offset exponential function for lower concentrations. Measured and calculated concentrations are given in the table above. After 2 hours of observation, all detectable target cell killings were counted and allocated to either apoptosis or necrosis according to the associated changes in pCasper target cell fluorescence. Target cells were counted as apoptotic if they showed an increase in GFP in combination with a steady rRFP signal and as necrotic in all cases of rRFP loss. This means, that, regarding the analysis of this particular experimental setting, mixed-type killings were counted as necrotic killings. The entity of mixed-type target cell killing is discussed later
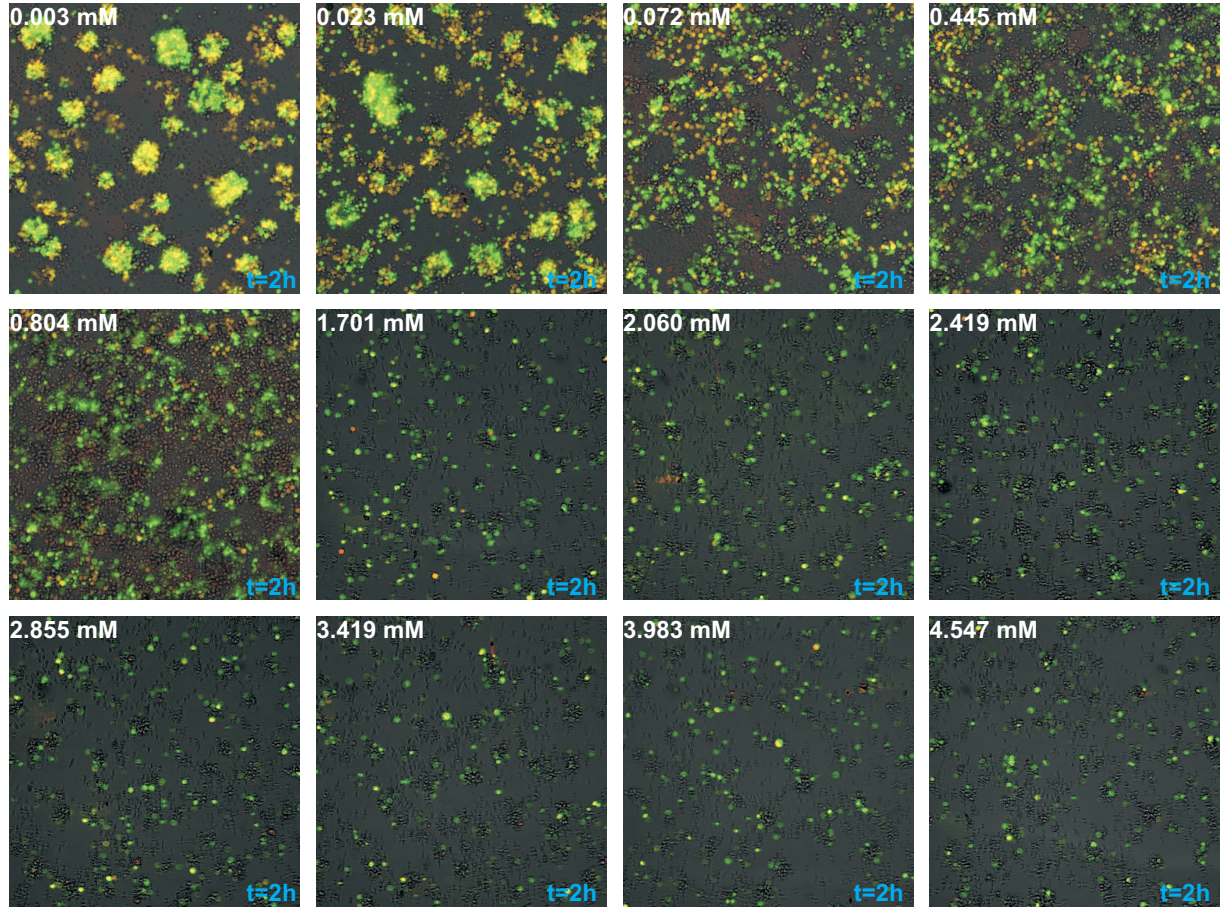
Figure 10: Calcium shifts the balance of apoptotic and necrotic killing by NK cells - live cell imaging
The amount of free Ca^{2+} ions was reduced by addition of EGTA or raised by addition of CaCl$_2$ to create a wide range dilution series. Pictures show killing of Jurkat E6.1 pCasper cells by NK cells two hours into the measurement at different Ca^{2+} concentrations. In case of Ca^{2+} levels lower than +0.9 mM EGTA or 0.072 μM (top row), no lysis of Jurkat cells occurred. Instead, apoptotic target cells formed aggregates with migrating NK cells. The rate of necrotic cell lysis increased steadily with the amount of Ca^{2+} available in the medium (middle and bottom row) and reached a plateau.

in this section.

Figure 10 shows the influence of $[Ca^{2+}]_{ext}$ on NK cell killing behavior: When buffering $[Ca^{2+}]_{ext}$ to low micromolar levels, necrotic killing completely stopped occurring. This phenomenon was already described by Christian Backes [93] and was consistently reproduced in these experiments. However, apoptotic killing appeared to be unimpaired. Since the target cells were not lysed, they stuck to the killer cell after apoptosis induction and formed dense cell aggregates appearing as green bulks. Starting from 72 μM (top row, third image), these cell aggregates could no longer be observed. Instead, first signs of necrotic lysis appeared in parallel to apoptotic killings. The proportion of lysed targets increased continuously as the amount of free Ca^{2+} ions outside was raised and culminated at roughly 85% (top and middle row). Further addition of $CaCl_2$ did not have any additional effect on the distribution of the two killing types (bottom row). The exact distribution of apoptosis and necrosis for the whole range of Ca^{2+} concentrations tested can be seen as a bar chart in **figure 11**.

The experiment was repeated twice. Primary NK cells from two different donors were
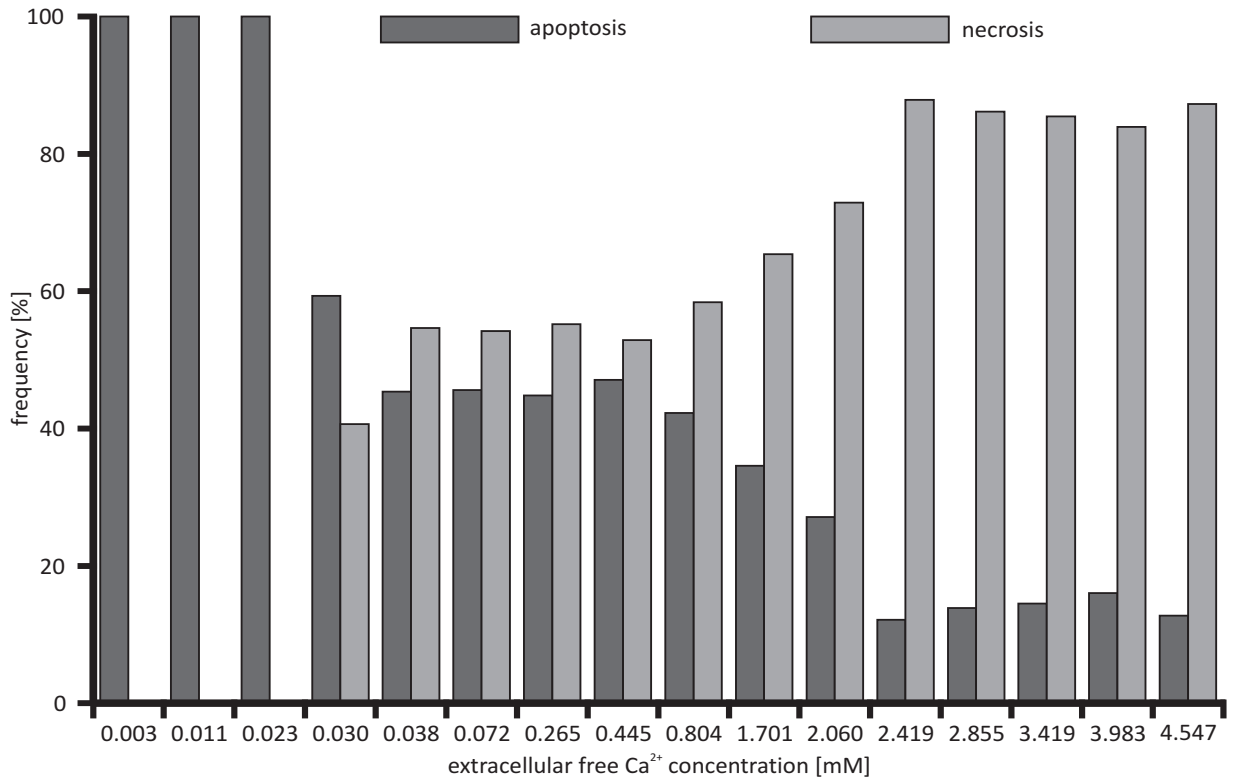
Figure 11: Calcium shifts the balance of apoptosis and necrosis induction by NK cells - statistical analysis
Frequency of apoptosis and necrosis of target cells, expressed in %, is plotted against free $[Ca^{2+}]_{ext}$. For necrosis to occur, the concentration needed to be above 20 - 30 μM. The interval [30 μM ; 2,400 μM] marked the dynamic range in which changes in $[Ca^{2+}]_{ext}$ had a large effect on the distribution. Further addition of Ca^{2+} favored necrosis over apoptosis. Beyond 2,400 μM, the distribution remained steady with necrosis being the dominant type ($\sim$ 85%).

tested, each population had been previously stimulated with IL-2 for two days. Counting every Ca^{2+} condition, 3,418 target cell killings were counted altogether. Looking closely at those target cells being lysed, it was noticeable that a considerable proportion of this group also showed weak signs of apoptosis. The full extinction of FRET intensity was, however, not reached in these cases, probably because the cells died from necrosis before granzymes could reach their maximal activity. Most of these cells presented with an immediate but apparently not fatal swelling of the cell membrane succeeded by a gradual increase in green fluorescence. This death type might hence be counted as 'secondary apoptosis'. Expanding observation time to several hours will lead to more and more target cells showing both death types in reversed order (not shown): Upon IS formation with an NK cell, some targets reacted by blebbing and an increase in GFP emission, indicating ongoing apoptosis, but succumbed to secondary membrane lysis afterwards. This event can analogously be counted as 'secondary necrosis'. An unmistakable allocation which type came first is not possible relying only on qualitative changes in pCasper fluorescence because in most cases both processes were initiated in close sequence. Such an allocation can, however, be attempted by calculating k_n and k_a for the same cell and determining half-life constants for both rRFP decrease and AR increase. Since this method depends on visually fitting both functions as well as determining the time span between the point of IS formation and the individual half-life, it may be applicable to single cells but would first need automatization in order to analyze a greater number of cells.

For the time being, both sequences can be categorized as a mixed killing type. In a
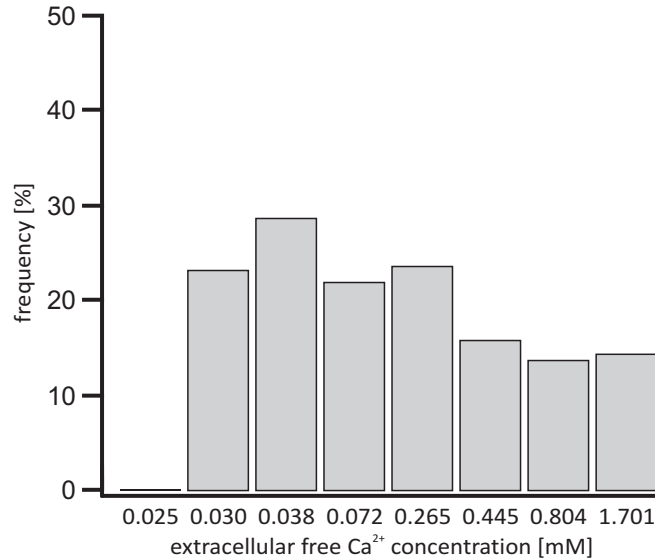
Figure 12: Frequency of mixed-type killing is inversely correlated to extracellular calcium supply

Frequency of E6.1 pCasper cells showing features of both apoptosis and necrosis when killed by primary NK cells. First events were observed at $[Ca^{2+}]_{ext}$ of 0.030 mM or higher. Mixed-type killing was most common at 0.038 mM Ca^{2+}. Afterwards, frequency dropped as $[Ca^{2+}]_{ext}$ increased.

subsequent experiment, the likelihood of mixed-type killings by NK cells killing Jurkat E6.1 pCasper cells was investigated using a slightly smaller Ca^{2+} concentration range than before. The results are presented in **figure 12**. This time, the population of lytic target cells was split into two subgroups, the first containing all purely necrotic target cells and the second one incorporating all targets featuring both necrosis and apoptosis. Statistical analysis showed that mixed-type killing occurred most often at a $[Ca^{2+}]_{ext}$ of 380 μM. Further increase in $[Ca^{2+}]_{ext}$ reduced the frequency, indicating that secondary apoptosis could be turned into primary necrosis if sufficient amounts of Ca^{2+} were to be supplied to the killer cells.

The absolute number of target cells killed differed considerably among the different Ca^{2+} conditions (not shown). Lowest overall killing was registered at 0.003 mM $[Ca^{2+}]_{ext}$, which was also the lowest Ca^{2+} condition tested. Both the frequency of necrosis induction and the total number of target cells killed increased steadily from 0.003 mM to 0.265 mM. Interestingly, further increase in $[Ca^{2+}]_{ext}$ did provoke more necrosis but reduced the total number of successfully killed target cells. As **figure 12** demonstrates, this increase in lytic killing rate was mainly at the cost of mixed-type killing.

3.4.2 Increasing osmotic stress boosts NK-cell-inflicted target cell lysis

The previous section demonstrated that primary NK cells can modify their killing behavior depending on the amount of free Ca^{2+} at their disposal. Direct membrane lysis depends on the formation of perforin pores. These pores put an osmotic strain on the target cell. The mechanism probably responsible for target cell lysis is a consecutive influx of fluid, which first leads to the cell swelling and - if it fails to withstand the resulting osmotic pressure - secondly to its membrane rupturing. Judging from the results presented in **section 3.4.1**, higher Ca^{2+} levels seem to favor this process, possibly by prompting the killer cell to release more perforin-containing vesicles. The following experiments were designed to study whether an increase in osmotic strain on target cells could also facilitate direct cell lysis by NK cells.

For this purpose, killer and target cells were exposed to artificially high, normal and low osmolalities and the occurrence of target cell necrosis, apoptosis and mixed death types was assessed by single-cell microscopy. The working hypothesis was that target cells should be lysed more violently when subjected to lower than normal osmolalities. Standard HEPES-buffered AIMV medium served as a control condition. The osmolality of this medium was measured with 314 mosmol/l. To create conditions with increasing osmotic stress, the medium was diluted with distilled water, lowering osmolality by steps of 11 mosmol/l. The lowest osmolality tested was 281 mosmol/l. On the opposite site of the spectrum, step-wise increase by 11 mosmol/l using mannitol produced media with unphysiologically high osmolality. The highest one tested was 347 mosmol/l. The calculated resulting osmolalities were experimentally confirmed with an osmometer prior to recreation in the final killing experiments.

Since the added solutions did not contain $CaCl_2$, they would inevitably dilute $[Ca^{2+}]_{ext}$. In both the lowest and highest condition, the residual $[Ca^{2+}]_{ext}$ was calculated to be 720 mM compared to 800 mM in the undiluted medium. The impact of this dilution on the distribution of apoptotic and necrotic events can be estimated based on the results presented in **figure 11**. At this point of the concentration spectrum, differences in Ca^{2+} levels as low as 80 μM were thus deemed unlikely to confound the outcome of the experiment.

To exclude any directly toxic effects of these unphysiological osmolalities on the killer or target cells, Jurkat E6.1 cells and NK cells were separately exposed to the respective media and rate of spontaneous cell death (apoptosis or lysis) was determined for a period of two hours with AIMV medium serving as a control. After 2 hours of exposure, the rate of spontaneous apoptosis or necrosis of Jurkat cells was 4% at 281 mosmol/l, 4% in the control condition and 5% in hyperosmolalic medium. NK cell viability, assessed visually

by the absence of necrosis- and apoptosis-related changes in cell morphology, was higher in all conditions compared to target cells (99.5% in low osmolality, 99% in control and 99% in high osmolality). There were no significant differences between the three conditions for both killer and target cells.

The viability of both NK cells and Jurkat E6.1 pCasper cells verified, experimentation proceeded to analyzing the statistical distribution of killing events using the same osmolalities. Killing events were registered over 2 hours of observation and allocated to the three previously outlined groups. The experiment was performed three times, using NK cells from two different donors. The cells had been stimulated with IL-2 for 2 and 3 days respectively. The results can be taken from **figure 13**.

Frequency of apoptosis induction differed slightly between the three conditions with
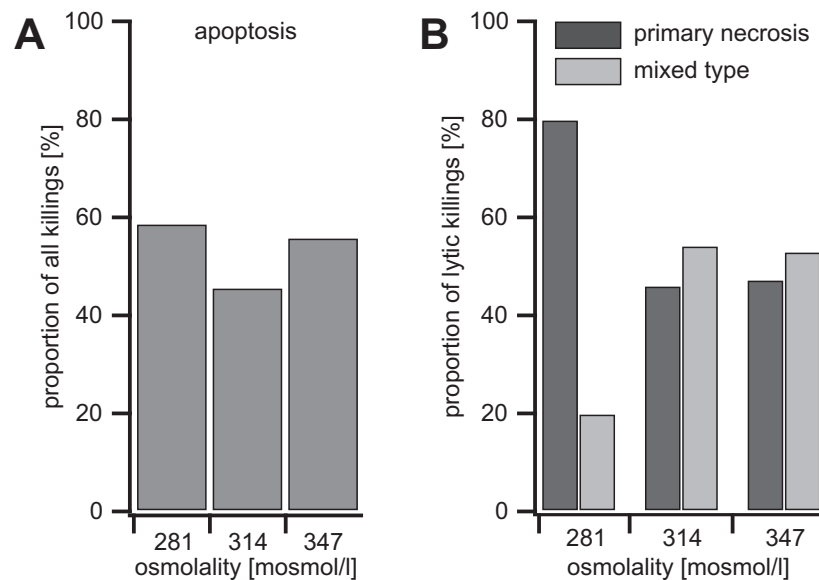
Figure 13: Low osmolality facilitates immediate target cell lysis by NK cells and reduces the occurence of mixed-type killings
(**A**) The likelihood of apoptosis induction by NK cells was slightly lower in the control condition (314 mosmol/l), while apoptosis rates were similar comparing low (281 mosmol/l) with high (347 mosmol/l) osmolalities. The percentage of primary necrotic killings of all lytic killing events was roughly below 50% in control and high osmolality but increased drastically when the cells were subjected to the low osmolality (**B**).

58.9% in low, 45.5% in normal and 55.7% in high osmolality. A more prominent effect could be observed regarding the occurrence of lytic events. While the proportion of lysis was not increased by the reduction in osmolality, the ratio of mixed types to primary necrosis differed significantly among the three groups. While this ratio was roughly 1:1 at 347 and 314 mosmol/l, primary necrosis occurred four times more often than the mixed type when osmolality was lowered to 281 mosmol/l. This finding indicates that lysis can not only be prompted on the side of the killer cell by increasing the availability of Ca^{2+}

ions but also on the side of the target cell by an increase in osmotic pressure.

3.5 Analysing intracellular calcium signals in active NK cells

3.5.1 Correlation of intra- and extracellular calcium concentration during killing

After IS formation, depletion of intracellular calcium stores and consecutive CRAC activity are crucial steps for immunocompetent cells towards eliminating their targets. The previous section showed how the amount of extracellular free Ca^{2+} ions can have an effect on total killing competence as well as on the likelihood of apoptotic and necrotic killing. The following experiments were aimed to address the mechanism of this dependence. If NK cell killing behaviour is shaped by outside Ca^{2+}, it is plausible to assume that changes in $[Ca^{2+}]_{ext}$ will be reflected in height or duration of intracellular Ca^{2+} signals. The second purpose of this series of experiments is linked to the Ca^{2+} dependence of global killing efficiency which applied to both CD8$^+$ lymphocytes and NK cells. As mentioned in the abstract, our research group made the discovery that this dependence is bell-shaped, meaning that both NK cells and CD8$^+$ lymphocytes kill more target cells at moderate extracellular Ca^{2+} concentrations and less when subject to either lower or higher $[Ca^{2+}]_{ext}$ (manuscript in preparation). This observation raised the question whether $[Ca^{2+}]_{int}$ of killing NK cells was also bell-shaped. This chapter presents Fura-2-based measurements and analyses of Ca^{2+} signals in NK-92 cells killing target cells while both were being exposed to a variety of different Ca^{2+} concentrations.

To study intracellular Ca^{2+} signals in NK cells, cells must be observed using high magnification (20x objectives or higher). This increase in resolution comes at the cost of total numbers of observable cell-cell contacts. In addition, every time a target cell was being contacted by more than one killer cell, the killer cells involved were not included into the analysis since there may be an indeterminate mutual influence on their Ca^{2+} signals. The third restriction was that only those NK-92 cells were considered which successfully killed their target cell. This restriction was not applied when buffering $[Ca^{2+}]_{ext}$ to the low micromolar range since these conditions prohibit killing of K-562 cells by NK cells in the first place.

To eliminate any effect of the killing type itself - i.e. apoptosis or necrosis - on the killer cell's Ca^{2+} signal, the cell line K-562 was used as target cells. They lack Fas ligand and are therefore not susceptible to apoptosis induction by the death receptor pathway. Employing our group's killing assay with this pairing of cells, interference with vesicle acidification by incubation of killer cells with concanamycin A nearly extinguished any killing of K-562, while Jurkat E6.1 cells were still killed to a lower extent (manuscript in preparation). This finding confirms that K-562 are mainly killed by NK cells via vesicle release. Instead of primary NK cells, the highly killing-competent cell line NK-92 was used in these experiments. They are easy to cultivate and show lively migration and killing after stimulation with Interleukin-2.

Figure 14 shows an exemplary contact between an NK-92 cell and a K-562 target cell. Shortly after the killer cell makes contact, its intracellular calcium levels begin to rise (color: blue equals low, red equals high). The amount of Ca^{2+} inside the killer cell reaches a local maximum, usually within 1 to 2 minutes after IS formation, and then drops to a plateau. The target cell is lysed shortly after $[Ca^{2+}]_{int}$ has peaked. After extrapolating the resulting function of $[Ca^{2+}]_{int}$ over time, Ca^{2+} kinetics can be analyzed in detail and compared among all killer cells.

Cell preparation, especially centrifugation and adhesion to the bottom of the well plate, can cause pre-excitation of killer cells. To exclude any adulteration of the Ca^{2+} signal measured, a baseline of at least 10 minutes was taken before target cells were added to the media. Different Ca^{2+} conditions were again generated by adding EGTA or $CaCl_2$ as
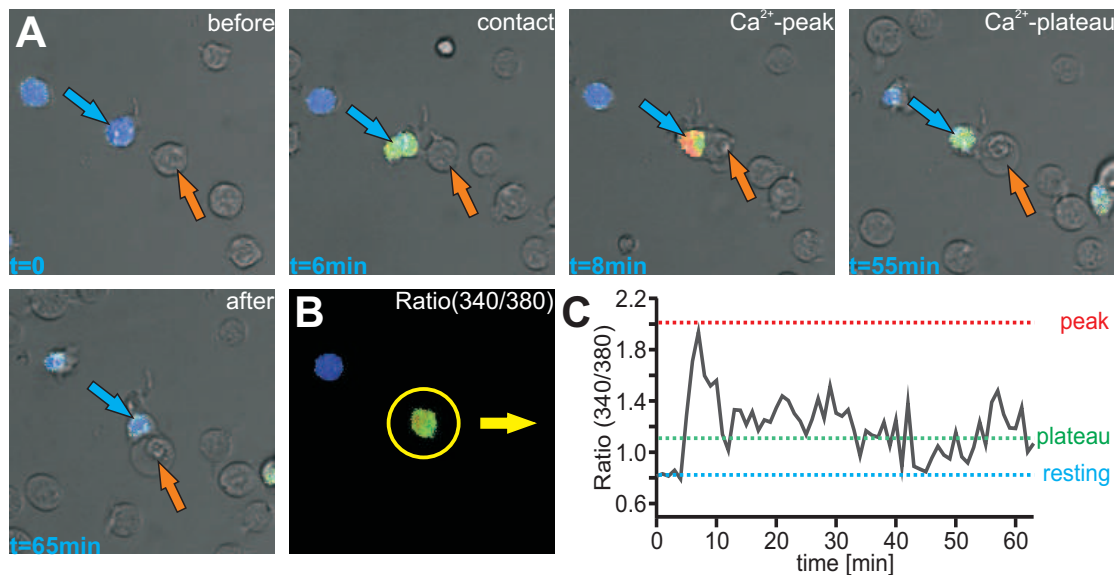
Figure 14: Measuring intracellular Ca^{2+} signals in NK-92 cells during killing
(A) This sequence of images shows an NK-92 cell stained with Fura-2 (blue arrow) contacting and killing a target K-562 cell (orange arrow). Immediately after contact formation, intracellular Ca^{2+} levels begin to rise (indicated by false color: blue equals low, red equals high). Two minutes later, $[Ca^{2+}]_{int}$ reaches a maximum, the target cell is already visibly damaged but not yet completely lysed. After reaching its peak, $[Ca^{2+}]_{int}$ does not drop back to resting levels but remains elevated for a significant amount of time, even after the target cell is completely lysed. After about 60 minutes, intracellular Ca^{2+} levels return to normal values. This cell could now go on to contact and kill another cell. **B** shows how intracellular Ca^{2+} signals can be extrapolated and then analyzed using ImageJ and IgorPro. By division of the two Fura-2 fluorescence channels (340 nm and 380 nm), a new video is achieved in which the background between cells is eliminated. The ratio values are extrapolated using the "'Time Series Analyzer"' plugin for ImageJ and then transferred to IgorPro. **C** shows the function for Fura-2 ratio plotted against time for the cell shown in B.

already described in **section 3.4**. After taking all signals from the killer cells of a single Ca^{2+} condition, they were temporally aligned so that the time span before contact for-

mation was exactly 5 minutes for every cell. The signals were then averaged for all killer cells and compared with regard to the height of their plateau Ca^{2+} levels. The latters were calculated as the mean of all ratio values over one hour after the initial peak. For control purposes, a condition was created by adding both EGTA and $CaCl_2$ at 1mM to check for any direct effects of EGTA addition on the Ca^{2+} signals .
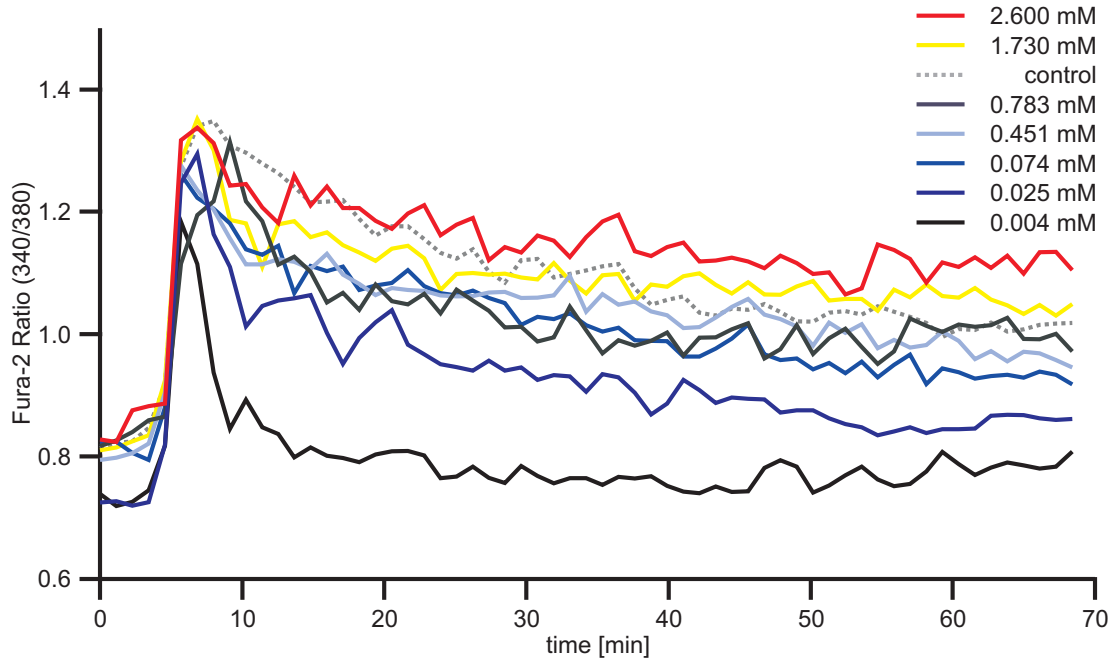
Figure 15: Kinetics of $[Ca^{2+}]_{int}$ over time for different extracellular Ca^{2+} concentrations Average Fura-2 ratios representing $[Ca^{2+}]_{int}$ over time for NK-92 cells killing under different extracellular Ca^{2+} conditions ranging from 0.004 mM (black) over moderate concentrations to high levels of $[Ca^{2+}]_{ext}$ up to 2.6mM (red). After successful target cell elimination, the killer cells' cytosolic Ca^{2+} concentrations decreased and finally remained steady for a significant period of time. The height of these plateaus seemed to correspond monotonically with the amount of free Ca^{2+} ions outside the cell.

Figure 15 shows the average kinetics of $[Ca^{2+}]_{int}$ from all killer cells. During the first five minutes of the experiment, killer cells rested on the bottom of the well plate and showed stable $[Ca^{2+}]_{int}$. The measured ratio values were ~ 0.72 on average for the two lowest conditions and slightly higher (~ 0.8) for the rest.

Contact formation occurred after 5 minutes. Intracellular Ca^{2+} levels reached a peak upon cell-cell interaction and then dropped towards a plateau. The height of these peaks was not analyzed in this experiment since time resolution of one value per minute was deemed insufficient. In contrast, the plateau levels appeared to be quite steady. Final decline of $[Ca^{2+}]_{int}$ towards original values can be expected after detachment from the target cell. This drop in intracellular Ca^{2+} levels was, however, not recorded in all cases since observation time was limited to 90 minutes and some cell-cell contacts occurred later than others. When comparing the plateau height of the averaged signals, it was obvious that

$[Ca^{2+}]_{int}$ rose monotonically with $[Ca^{2+}]_{ext}$. This rise is visualized by a semi-logarithmic plot in **figure 16**. The exact values of $[Ca^{2+}]_{ext}$ used can be taken from **figure 15**.
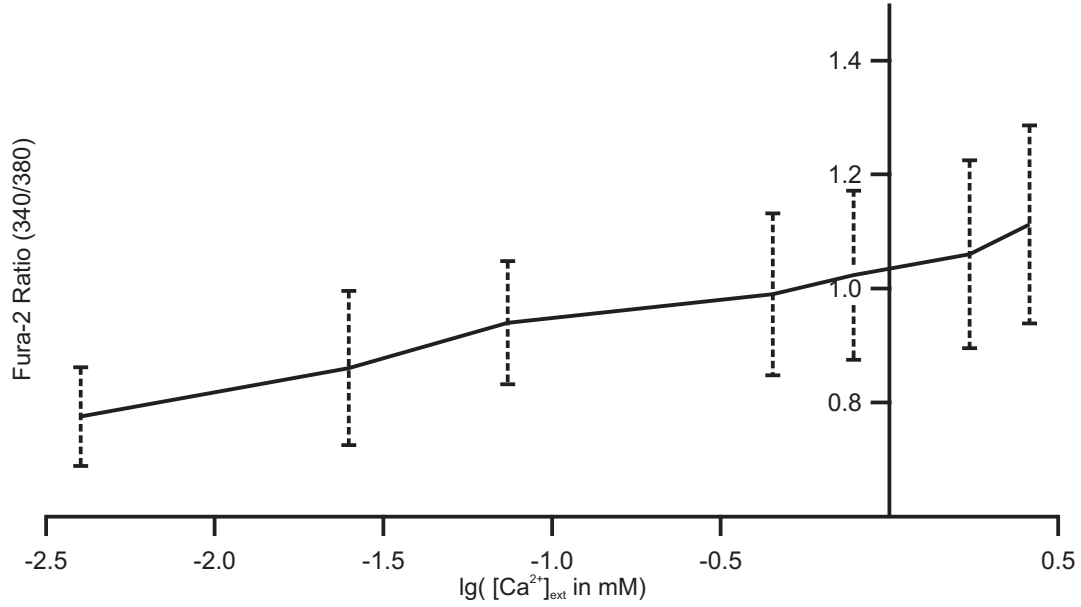
Figure 16: Height of intracellular plateau Ca^{2+} levels after killing as a function of $[Ca^{2+}]_{ext}$
This semi-logarithmic plot shows a monotonic increase in plateau height when extracellular Ca^{2+} supply is raised.

The experiment was conducted four times. Since NK-92 cells are a cell line, the employed killer cells in these 4 experiments can be expected to have identical properties in contrast to primary NK cells whose function will always be donor-dependent.

Regarding the two main questions mentioned in the introductory part of this section, a first conclusion is that $[Ca^{2+}]_{ext}$ is in fact mirrored by $[Ca^{2+}]_{int}$ during killing. While this is not too much of a surprise given that a greater driving force for Ca^{2+} ions can be expected to produce higher intracellular Ca^{2+} levels, the monotonous rise of plateau $[Ca^{2+}]_{int}$ appears to be in conflict with the bell-shaped dependence for global killing. This finding confirms that the Gaussian shape of this dependence is not created by the killer cell clamping its intracellular Ca^{2+} levels to an optimum range which cannot be maintained when $[Ca^{2+}]_{ext}$ becomes too low or too high. Especially the descending part of the bell-shaped function requires a more complex mechanism since $[Ca^{2+}]_{int}$ is sufficient for exhaustive vesicle release. Our group has found evidence that the two-sidedness of the Ca^{2+} dependence is reducible to the fact that vesicle release itself has a bell-shaped Ca^{2+} dependence in both NK cells and CD8^{+} lymphocytes (manuscript in preparation).

3.5.2 Detailed analysis of intracellular calcium signals in active NK cells

Section 3.3 demonstrated that the frequency distribution of apoptosis and necrosis induction is highly dependent on extracellular Ca^{2+} supply. This finding points towards Ca^{2+} being one of the key players in determining which type is to be pursued. After establishing a fluorescence-based method to distinguish both types of ongoing target cell death (**sections 3.1** and **3.2**), the next step was to study intracellular Ca^{2+} signals in active NK cells to check for any correlations with the ensuing killing type. Jurkat E6.1 pCasper cells were used as target cells since they are prone to both necrosis and apoptosis induction by NK cells.

Primary NK cells were stained with Fura-2 and live-cell-imaging of contacts to Jurkat E6.1 pCasper cells was performed for two hours. Afterwards, the Fura-2 measurements of those NK cells which were able to kill at least one target cell were transferred into Igor-Pro and analyzed quantitatively. Again, only those cells were selected for analysis which presented single-cell contacts to exclude any cooperative effect which could potentially adulterate the calcium response of every individual cell. pCasper measurements in target cells were performed in parallel so that Ca^{2+} signals could later be correlated with the specific type of target cell death they provoked. A total of 40 cells was measured, 36 of which could be included into subsequent analysis. Two of the missing four cells moved too quickly and showed transient overlapping with other NK cells so that tracking could not be performed. One killer cell managed to kill its target but entered apoptosis immediately afterwards. The last one showed considerable pre-excitation before contacting its target cell and was therefore not incorporated. Three wells were measured per run, yielding a time resolution of 0.53 minutes between two images. Observation time was 2 hours and limited by bleaching and extrusion of Fura-2. Spontaneous Ca^{2+} signals of killer cells with no contact to target cells were also observable but not included in this analysis.

First, pCasper signals from the 36 E6.1 Jurkat cells which were successfully eliminated were analyzed and necrotic and apoptotic indices were calculated as explained in **section 3.3**. Out of the total amount of 36 target cells, 11 were killed by necrosis without any signs of apoptotic activity. Their necrotic indices ranged from 0.57 to 1.72. 15 cells showed apoptosis with no indication of cell membrane damage. Out of this group, the lowest apoptotic index registered was 0.90 and the highest 2.12. The remaining 10 cells showed mixed forms of cell death with varying degrees of both types (**figure 17**).

Except for one target cell out of this group, which had both rather high k_n and k_a $(1.27, 1.32)$, cells of the mixed-type group had below-average apoptotic indices, meaning that if both necrosis and apoptosis were happening in parallel, apoptosis was rather slow. Surprisingly, in these cases, necrosis was not significantly slower compared to pure
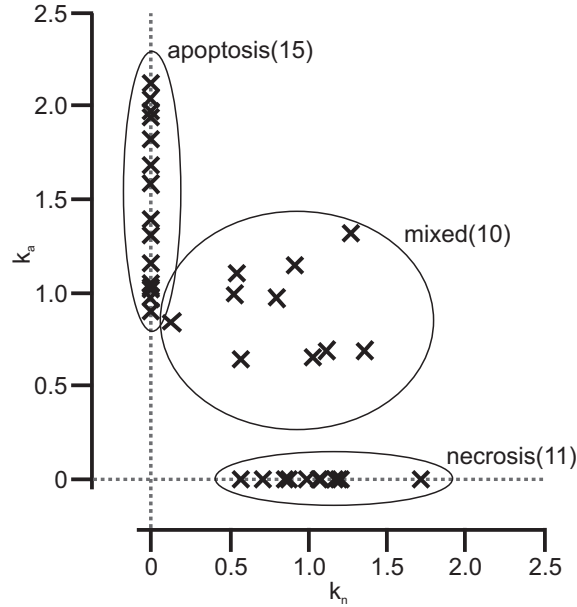
Figure 17: Target cell populations grouped by necrotic and apoptotic indices
Grouping every successfully killed target cell by its value pairs for k_n, k_a gives three populations which
are marked by circles. All cells on the dotted horizontal line have a k_a of zero and therefore classify
as pure necroses. Fifteen cells on the vertical line entered apoptosis and showed no sign of membrane
damage. These events were hence regarded as purely apoptotic. A total of 10 cells showed characteristics
of both killing types.

necroses. Obviously, lytic activity seemed to limit the speed of apoptosis in the same
target cell but not vice versa. A possible explanation for this observation is discussed in
section 4.1.2.

Apart from quantifying lysis and apoptosis extents, defining a value pair k_n, k_a for a
target cell could also give objective information about when it could be considered dead.
Of course, both lysis and apoptosis are processes taking minutes to hours, and on first
sight it appears strange if not counter-intuitive to define a single 'time point of death'. It
is possible, however, since rRFP and AR show exponential decrease and sigmoid increase,
both having a distinct half-life constant. We can hence define a time point of death or
PD:

i) for necrosis as the half-life time point of the rRFP curve called PD_n

ii) for apoptosis as the half-maximum time point of the AR curve called PD_a

Applying this method also provides a tool to discriminate which process, i.e. necrosis or
apoptosis, came first, the two scenarios being:

i) $PD_n < PD_a \rightarrow$ Primary necrosis, secondary apoptosis

ii) $PD_n > PD_a \rightarrow$ Primary apoptosis, secondary necrosis

In the given experimental series, three out of the ten cells of the mixed population were
identified as secondary necroses, the other seven showed membrane lysis first and then
initiation of apoptosis.

The second step of evaluation was to look at the killer cells' Ca^{2+} signals in more detail. The basic shape of a Ca^{2+} response in NK cells following target cell recognition was already described in **section 3.5**.

Although similar in principle, the 36 Ca^{2+} responses measured had distinct characteris-
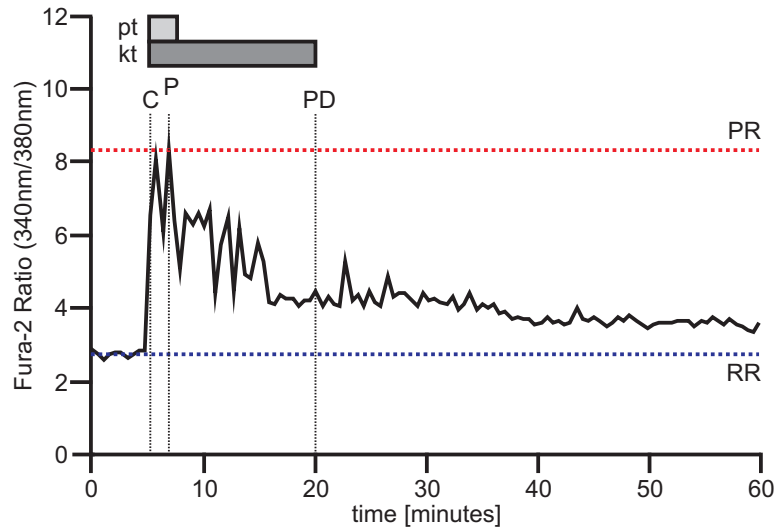
Figure 18: Key parameters of intracellular calcium signals in active NK cells
An exemplary signal measured inside a killing NK cell is shown to demonstrate which parameters were taken into analysis. Before making contact to its target cell, the killer cell was in its resting state and its Fura-2 ratio had the value RR. Shortly after contact formation (C), intracellular Ca^{2+} levels reached their peak (P). This target cell was lysed roughly 12 minutes later (PD). The time span from IS formation to the Ca^{2+} peak is referred to as pt (peaking time), that from IS formation to target cell death as kt (killing time).

tics. In order to perform a detailed analysis, it was necessary to define certain parameters which - despite all differences - were common features of all signals:

- **Resting Ratio (RR)**: the mean of the resting Fura-2 ratio values, i.e. before the killer cell had contact to any other cell, calculated over a time span of 5 minutes.
- **Peak Ratio (PR)**: the global maximum of the Fura-2 ratio function which was always reached shortly after IS formation
- **Peaking time (pt)**: the time from contact initiation until PR was reached
- **Killing time (kt)**: the time from contact initiation to the target cell's individual PD_n or PD_a. In case of simultaneous necrosis and apoptosis, the lower of the latter two was chosen to calculate the kt.

The above-listed parameters are visualized in **figure 18** using an exemplary Fura-2 ratio signal.

A comparison of all 36 signals quickly showed that there were patterns which seemed to correlate to the mode of target cell death which followed them. Every signal could be dissected into two basic elements - Ca^{2+} spikes and Ca^{2+} plateaus. *Spikes* could be defined as very short and transient elevations in intracellular Ca^{2+} levels. These elevations usually lasted one to two minutes and cytosolic calcium levels returned to their previous state afterwards. *Plateaus* were rather slow but more sustained rises in Ca^{2+} lasting up to 30 minutes or longer depending on how long cell-cell-contact was maintained. Both Ca^{2+} oscillations of similar frequency and Ca^{2+} plateaus have been described in CTLs [43].

After detailed analysis to what extent an individual Ca^{2+} response was composed of spikes and plateaus, it was obvious that all recorded Ca^{2+} signals fitted into one of the three following groups:

3.5.2.1 Type A - Oscillatory type   This type was composed only of Ca^{2+} spikes and lacked any significant plateau-like elevations. Before initiating cell-cell contact, base ratio values were stable. After IS formation, the NK cell responded with a repetition of Ca^{2+} spikes while calcium ion levels would always drop to base level in between. After killing the target cell, spikes were usually no longer detectable or showed greatly reduced amplitude.

3.5.2.2 Type B - Plateau type   As opposed to type A, this type was characterized by one large and sustained Ca^{2+} influx starting immediately after IS formation. Intracellular calcium concentration would not return to its original level until the killer cell had succeeded in killing its target. Even afterwards, Ca^{2+} levels would stay elevated in every NK cell showing this signal type throughout the entire measurement.

3.5.2.3 Type C - Mixed type   A combination of the previous two in which plateau-like elevations in intracellular Ca^{2+} levels would superpose with spikes.

Figure 19 visualizes the characteristics of these three signal types using 3 exemplary cells for each one.

25% of all killer cells had an A-type Ca^{2+} response. All of these cells later induced apoptosis while primary or secondary necrosis was never associated with this type of signal. The peaking time was the longest, averaging 6.2 minutes. Peaks of type-A signals were also the overall lowest with a mean Fura-2 ratio of 6.3, which equalled 2.2-fold the resting ratio value for these cells. NK cells which had an A-type signal took the longest to successfully kill their targets. The kt was about 37 minutes on average, thus more than twice as long compared to type C and more than four times as long as for type B. After target cell apoptosis was initiated, Ca^{2+} influx terminated and no subsequent spikes nor plateaus were detectable.
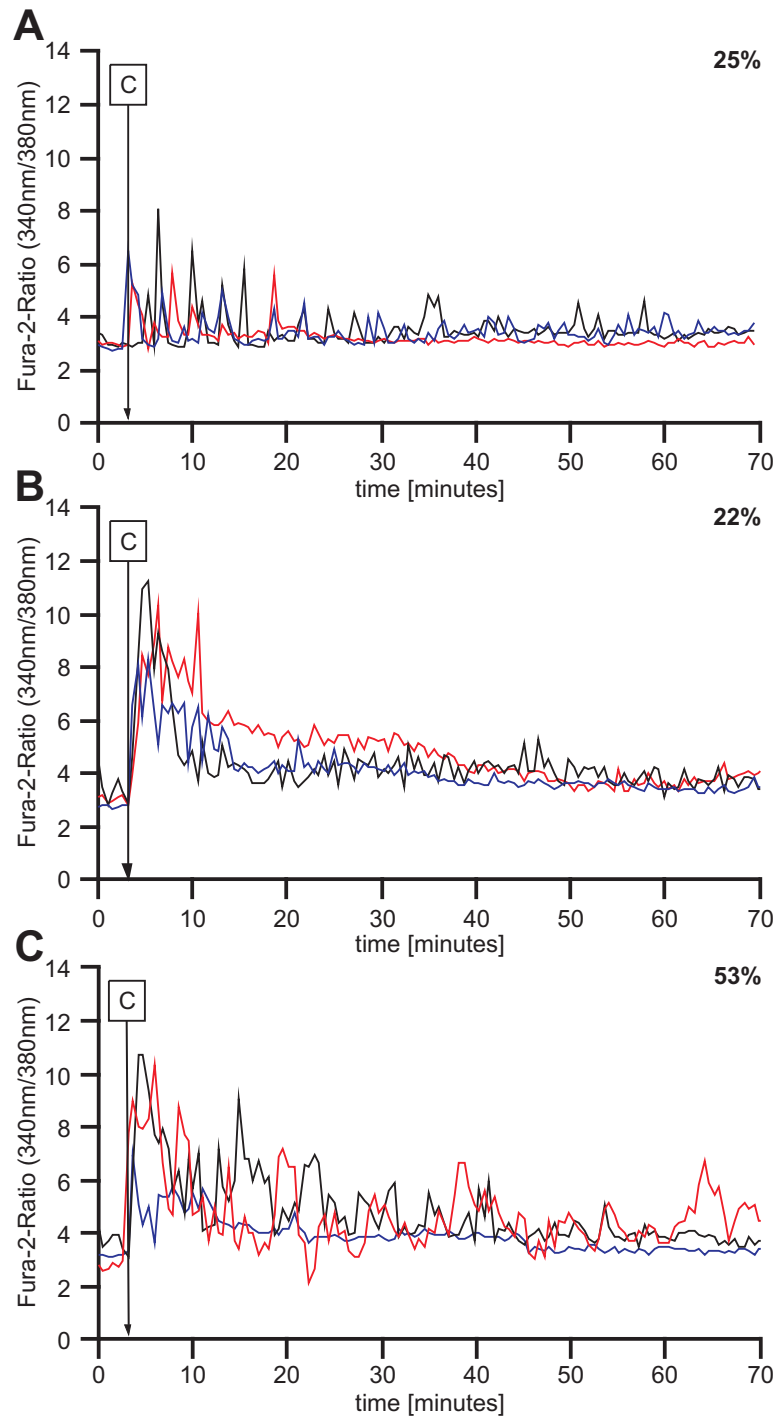
Figure 19: Three different types of calcium responses shown by active primary NK cells
The three types of recorded Ca^{2+} signals are displayed. For each signal type, three representative killer cells are shown in black, red and blue. **A** - oscillatory type, **B** - plateau type and **C** - mixed type. The time point of IS formation with the target cells (C) is marked with an arrow.

Type-B signals occurred in 22% of NK cell killings. Necrosis of the target cell was observed in every single case, while no apoptosis (primary nor secondary) would follow this

signal type. The peaking time was quite short in all cases, on average 2.5 minutes. The peaks were the highest with an average PR of 9.6 ($\sim$ 3-fold RR) . These cells achieved target cell death most quickly, needing only 7.9 minutes on average. Before Ca^{2+} influx was initiated, type-B cells showed slightly higher RR values than the other subtypes. In contrast to the previous type, Ca^{2+} levels stayed elevated in all cells even after cell-cell contact was ceased and the target cell had died. Comparing the average cytosolic Ca^{2+} levels over a period of 5 minutes before and one hour after contact formation, base levels had increased by $\sim$ 14%, indicating that these killer cells may have stayed in a more activated state compared to those showing oscillations, even after detachment from the target cell had been completed. Noticeably, these NK cells would also show spikes or new plateaus without contacting another cell in between.

Type C signals were the most common type, shown by 53% of the entire NK cell population. Interestingly, every type of target cell death could be observed in these cases, primary apoptosis occurring most often (53%), followed by secondary apoptosis (32%) and, most rarely, primary necrosis (15%). The average peaking time was 3.4 minutes, the mean peak height was measured at 8.0, both ranging between those for types A and B. Target cell killing took roughly 18 minutes, the mean RR value was 2.8 and well comparable to that of the oscillatory type. C-type signals were also accompanied with an increase in basal Ca^{2+} levels, measuring 21% on average, which was even higher than for type B. **Figure 20** summarizes these differences in Ca^{2+} signal parameters for the different signal types.

To summarize, type A signals strictly correlated with apoptosis. They were not followed by any lytic activity of the killer cell. Cells presenting this type of signal took longest to kill their targets and they tended to have rather low peak levels of intracellular free Ca^{2+}. The opposite was true for type B signals - they were succeeded by necrosis induction every single time. Nk cells showing this signal type took only a few minutes, sometimes even less than a minute, to kill their target cell by direct lysis. Intracellular Ca^{2+} levels reached very high figures compared to the other types and the target cell was eliminated 2 to 3 times faster than in cases of types A or C. RR values were similar in all three groups and showed no significant differences. This makes it unlikely that high-peaking Ca^{2+} responses as type B signals were caused by pre-excitation.

Similar differences between intracellular Ca^{2+} patterns associated with apoptosis and necrosis were already described by Honda and Miyazaki in 1996 [104]. They found differences in both height and duration of intracellular Ca^{2+} signals in NK cells in case of apoptosis and necrosis induction in target cells similar to the ones found here. They did, however, not propose the existence of distinct types of Ca^{2+} signals.
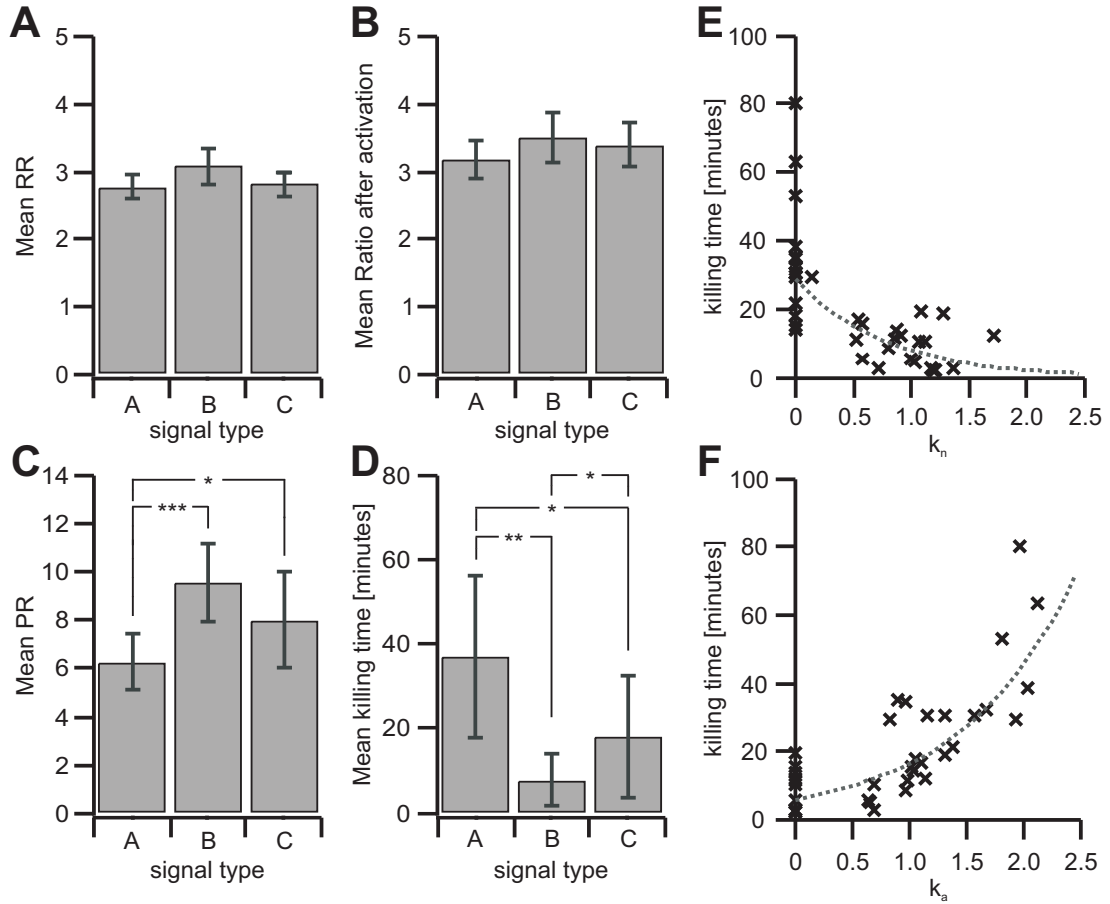
Figure 20: How the three signal types differ in individual calcium signal parameters
Every parameter displayed was first tested positive for standard distribution using a Kolmogorov-Smirnoff-test. **A**, **B** show discrete but not significant differences between Resting Ratio and the mean Ratio after activation, calculated over a time span of 5 minutes one hour after the peak, comparing the three signal types. In contrast, the average Ca^{2+} peak abbreviated with PR was measured highest for type B signals, lowest for type A and between the two for type C, as is shown in **C**. **D** demonstrates that target cells are killed most quickly after type B signals, most slowly after type A signals and after an intermediate time span following type C signals. **E** and **F** display the killing time (kt) as a function of k_n and k_a. The more rapid the lysis, the more quickly the cell is destroyed. The faster apoptosis is going on, the longer the target cell needed to enter the apoptosis cascade.

Figure 20 also shows how the kt behaved as a function of the necrotic and apoptotic index of the corresponding target cell (parts **E** and **F**). It appears intuitive that those cells with a k_n above zero took considerably less time to die than those target cells entering apoptosis. If there was any lysis at all, kt dropped as k_n increased, since more rapid necrosis is likely associated with higher perforin release which deals more damage to the plasma membrane thus shortening IS conjugation time. When looking at the dependency of kt on the apoptotic index, it comes as a surprise that it increased monotonically as k_a did. Hence, the longer it took the target cell to enter apoptosis, the more quickly the resulting apoptosis turned out to be.

While signal types A and B were quite distinct and showed the largest differences to one another, the implications of the mixed signal types are less clear. Those signals might merely be a weaker form of type B signals. Another possibility is that type C Ca^{2+} signals are the superposition of both A and B happening in parallel. The question to what extent types A and C can be regarded as Ca^{2+} signaling patterns of their own is discussed in **section 4.4.4**.

Necrosis occurence clearly depended on a strong influx of calcium ions and this influx had to last for several minutes. This is likely attributable to the fact that necrosis is linked to release of perforin from cytotoxic vesicles, a process which is known to be Ca^{2+}-dependent. Interestingly, when comparing the peak heights for type A and B signals, some of apoptosis-inducing NK cells had higher Ca^{2+} peaks than those inducing cytolysis. Apparently, successful vesicle release depends not on the total amount of free calcium ions in the cytosol but rather on how long the intracellular Ca^{2+} concentration stays elevated above a certain threshold. Spikes as short as 1 minute in duration or less did not allow for necrosis to occur, no matter how high the Ca^{2+} concentration may have peaked in these cases. Taking into consideration that higher levels of Ca^{2+} outside the cell favor necrosis, one may raise the question if sustained Ca^{2+} increase may not only be a necessary but also sufficient condition for vesicle release and subsequent target cell lysis.

3.6 Is calcium a sufficient condition for necrosis induction by NK cells?

Using a similar approach as described before, primary NK cells and Jurkat E6.1 cells were used to study the role of Ca^{2+} boosts for necrosis induction. The aim was to create a considerable sudden increase in intracellular Ca^{2+} supply completely independent of any cytotoxic signaling pathways going on in the cell. If Ca^{2+} was sufficient to induce lysis, then releasing high amounts of Ca^{2+} during target cell engagement could provoke an active NK cell to induce necrosis or could even turn an apoptotic killing into a necrotic one.

3.6.1 Releasing calcium ions into the cytosol of NK cells using the photochelator NP-EGTA

Photolysis of NP-EGTA which has previously been loaded into cells allows for an immediate and large release of Ca^{2+} ions into the cytosol. To this point, the dye had mainly been used in neurons [105], glia cells [106], epithelial cells [107] and muscle cells [108], [109], [110]. This first series of experiments serves as a 'proof of principle' and demonstrates that NP-EGTA can be used efficiently in primary NK cells. Preliminary experiments were conducted to study the release kinetics of NP-EGTA in primary NK cells using different loading regimens as well as varying degrees of UV light exposure to achieve de-chelation.

Primary NK cells were loaded with the AM form of the photochelator for 30 minutes. To verify if Ca^{2+} was released effectively, the cells were also stained with Fura-2. After incubation with both compounds, the cells were washed several times and then transferred to the bottom of a black 96-well-plate in AIMV medium containing no serum. Primary NK cells loaded only with Fura-2 served as a control. Different dye concentrations were tested, including varying concentration ratios of NP-EGTA to Fura-2. Since both substances compete for the same ligand, it proved challenging to titrate how much of each dye could be used to ensure both a high photolytic release as well as sensitive measurement of free Ca^{2+} ion concentration at the same time.

Figure 21 visualizes the course of cytosolic Ca^{2+} ion concentration in primary NK cells during a representative experiment. At the beginning of the measurement, killer cells in both groups had comparable resting ratio values. Fura-2 was measured in every condition during the following minute. At $t = 0$, the cells in both conditions were flashed with high intensity UV-light and Fura-2 was measured immediately afterwards. While ratios in the control condition stayed unchanged, intracellular Ca^{2+} levels in the chelator group reached a peak of roughly double to three times their resting value. Afterwards, Ca^{2+} levels inside the cell gradually dropped over the course of 2 minutes but stayed elevated

in those cells containing NP-EGTA compared to the control cells having only the Fura.
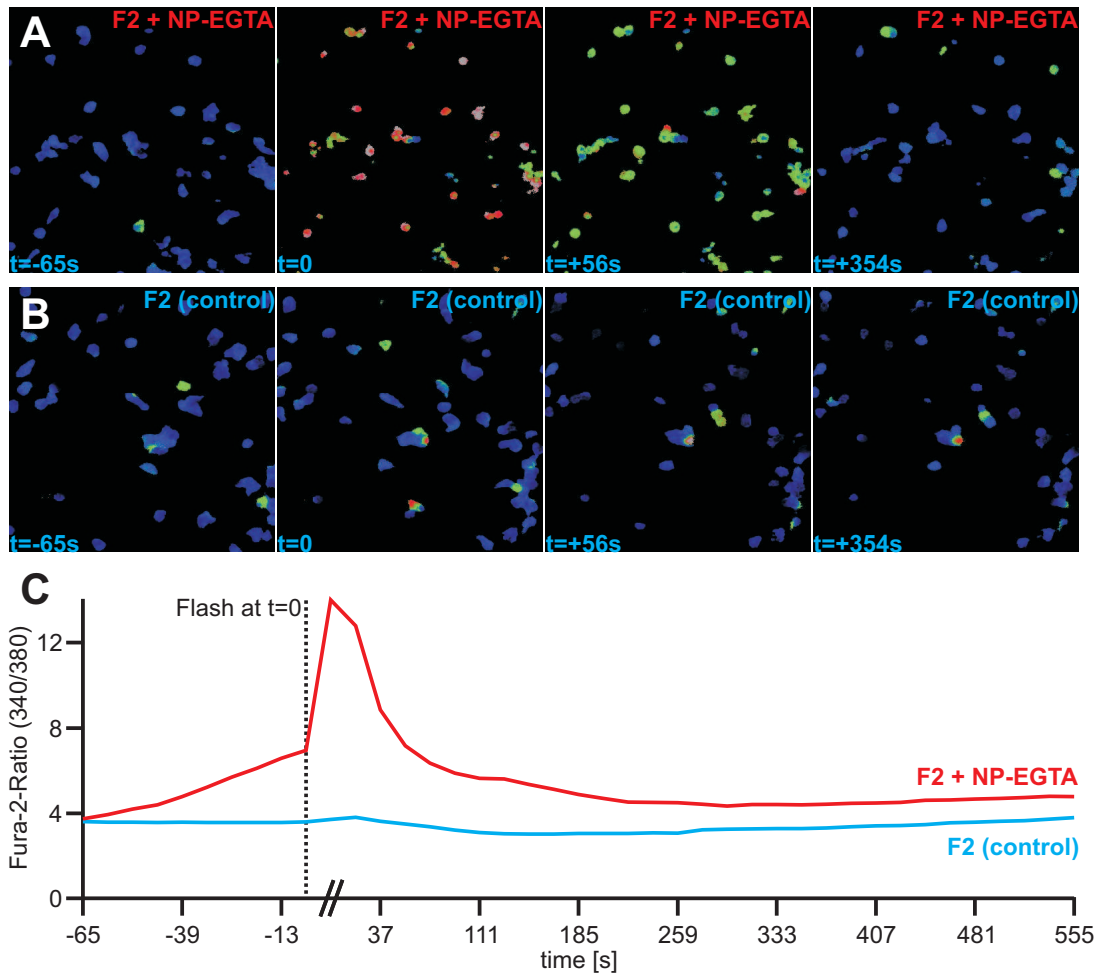
Figure 21: Releasing Ca^{2+} ions into the cytosol of NK cells by photolysis of NP-EGTA
When loaded with NP-EGTA, Ca^{2+} ions can be released in large quantities into the cytosol of NK cells. To test release potential of NP-EGTA, NK cells were split into two groups. One was loaded with both NP-EGTA and Fura-2 (**A**), the other only with Fura-2 as a control (**B**). Images display Fura-2 ratio values as a false-colored image with blue equalling low and red corresponding to high ratios. At $t = 0$, cells in both groups were exposed to a short but strong UV light flash. Ca^{2+} ion levels increased drastically in the first group and returned back to resting values during the following minutes. Fura-2 ratio values as a function of time are plotted for both groups in **C**.

This experiment demonstrates that it is well possible to uncage Ca^{2+} ions in NK cells using NP-EGTA and UV light. However, even before the UV flash was initiated, ratio values of the NP-EGTA-group steadily rose compared to control. This slow increase in the concentration of intracellular Ca^{2+} was probably due to the fact that Fura-2 measurement itself repetitively uncaged a small quantity of ions which accumulated over time. This effect was reproduced on purpose in a following series of measurements which was aimed to test whether a continuous, high-frequency Fura-2 measurement instead of one single UV light flash could supply an alternative release pattern for photolysis. Experiments shown in **section 3.4** suggested that necrosis by NK cells is induced rather after more sustained,

longer-lasting calcium ion influx than after short Ca^{2+} spikes. Therefore, a smaller but more sustained photolysis could prove more suitable to provoke necrosis. **Figure 22** shows that this method works in principle. It comes, yet, with two problems:

Firstly, in order to detect any effect on the distribution of necrosis and apoptosis, a parallel measurement of the pCasper construct in target cells is necessary. Measuring its three channels - GFP, RFP and FRET - requires at least 20 seconds for two wells (chelator and control). Having only one lamp available, this limits the possible UV excitation frequency of the cells to a maximum of 3 releases per minute. Although every Fura-2 measurement is answered by a small uncaging, the frequency is too low in order to create a cumulative effect. Using this strategy, only a very limited increase in intracellular Ca^{2+} ion concentration could be achieved, as shown in the figure below.
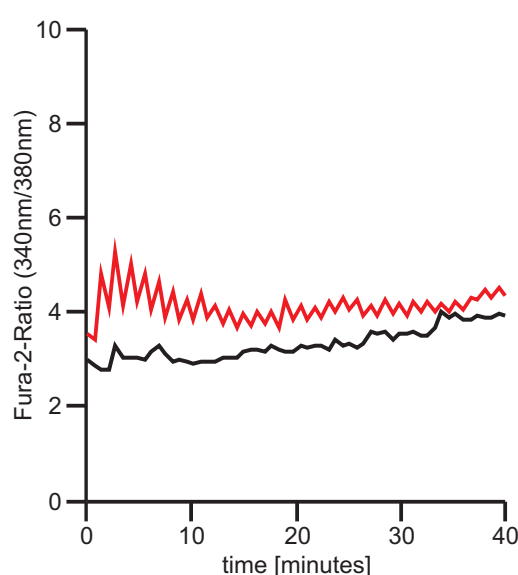
Figure 22: Repetitive UV light exposure leads to lower, more sustained uncaging
NK cells were loaded with NP-EGTA and Fura-2. Although no target cells expressing pCasper present, the pCasper channels were measured as well so that the resulting time resolution for UV light exposure would resemble that of an actual killing experiment. Here the time span between two consecutive UV light exposures in one well was 81 seconds. Short and high intensity flashes would alternate with a standard Fura-2 take every 40 seconds. A total of four wells was measured, limiting the highest possible uncaging frequency for one well to 20 seconds. The red curve represents the Fura-2 Ratio of those killer cells containing NP-EGTA. Although these cells had higher Ca^{2+} levels compared to control cells (black) throughout the whole experiment, the possible maximum inrease in Ca^{2+} ion concentration was rather low compared to that of the single flash which can be seen in **figure 21**.

Secondly, primary NK cells as well as Jurkat E6.1 cells proved much more resilient to small but intense UV flashes than to continuous, moderate intensity UV light exposure. Since lamp power needs to be sufficient to achieve uncaging from NP-EGTA, the cells take significant damage. To ensure a good cell viability during a live-cell killing experiment, Fura-2 control measurements should therefore be restricted to a necessary minimum.
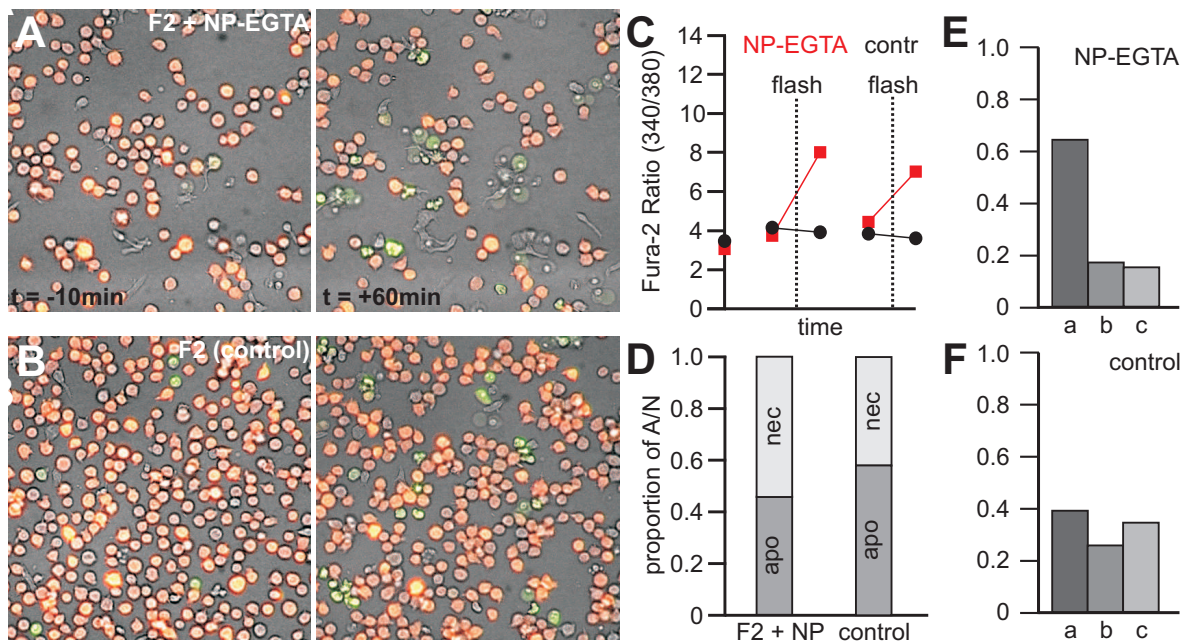
3.6.2 Uncaging calcium in NK cells during killing

Using the BioImager setup, only the single flash protocols proved suitable to create a suffi-
cient uncaging without threatening the killer cells' viability. This method was then taken
to the test in a killing experiment using a similar approach as described in **sections 3.4**
and **3.5**. Again, Jurkat E6.1 cells expressing pCasper were used as target cells. Primary
NK cells loaded with Fura-2 and NP-EGTA as well as primary NK cells loaded only with
Fura-2 as a control were brought together with the Jurkat cells. After a few minutes,
Fura-2 was measured once in every condition as a baseline ratio value. Afterwards, the
pCasper construct was excited every 30 seconds and a UV light flash was given once ev-
ery 30 minutes in every condition tested. To verify release from the chelator, Fura-2 was
measured once before and after every flash. Afterwards, chelator and control group were
checked for statistical distribution of target cell apoptosis and necrosis.

The results are presented in **figure 23**. Two wells of cells were tested in both condi-
tions. NK cells of both groups managed to kill a comparable number of E6.1 Jurkat cells
during the one hour measurement. Necrosis of target cells was detected by an exponen-
tial decrease in rRFP, apoptosis by an increase in the apoptotic ratio (AR) as described
before.

The Fura-2 control measurement is displayed in **C** and verifies that Ca^{2+} ions were
effectively released in the first condition (red), but not in the control group (black). All
target cell deaths - apoptoses and lyses - were counted and their distribution was an-
alyzed. Plot **D** shows that necrosis did in fact occur more often in the chelator group
compared to control. To check whether this predominance was in fact due to uncaging,
necrotic target cells were analyzed with regard to when they had shown the first signs
of necrosis-associated membrane damage, indicated by a clear drop of the rRFP signal.
Since the first UV light flash was timed 30 minutes into the experiment, all necroses were
allocated to three groups:

a) First group: Earliest signs of necrosis occurred within the first 30 minutes, hence before
the first uncaging.

b) Second group: Necrosis became visible between 30 and 40 minutes, so during the first
ten minutes after the first flash. These events were of highest interest since they would
likely be correlated to the Ca^{2+} release in NK cells.

c) Third and last group: Target cell lysis was induced later than 40 minutes into the ex-
periment. Given that free Ca^{2+} ions are quickly exported after uncaging, necrotic killings
belonging to this group were deemed unlikely to be impacted by the uncaging process.

Although the ratio of both killing types was shifted in favor of necrosis in the chelator
group, plots **E** and **F** show that most killings were initiated *before* the flash was actually
given. This was true for both groups. Furthermore, the proportion of group b necroses

Figure 23: Uncaging calcium ions in active NK cells during killing
Image sequences **A** and **B** show false-color overlays. Killer cells (not coloured) and Jurkat E6.1 pCasper cells (orange) were observed over 70 minutes. NK cells in A were loaded with NP-EGTA in addition to Fura-2, those in B had only Fura-2 and served as the control condition. Graph **C** shows that Ca^{2+} ions were indeed released in NK cells loaded with the chelator but not in the control group. Since no continous Fura-2 measurement was performed, ratio values are plotted as dots. NK cells from the NP-EGTA-group showed a slight excess of lytic killings compared to control (**D**). All necrotic killing events were allocated to three groups a, b and c depending whether they occurred before, immediately after or later than 10 minutes after the first flash. **E** and **F** show that most necrotic killings took place before the first Ca^{2+} ion release. Furthermore, the proportion of necrotic killings which were initiated after the first photolysis of Ca^{2+} ions was higher in the control group. Taken together, the experiment could not provide evidence that lysis of target cells by NK cells could be provoked by Ca^{2+} ion de-chelation from NP-EGTA.

was higher in the control group than in the chelator group. This observation makes it very unlikely that the slight predominance of necrosis was traceable to the Ca^{2+} uncaging since one would expect more necrosis to happen in the NP-EGTA-group.

To summarize, the uncaging experiments could not prove that Ca^{2+} ions were sufficient to provoke lysis by NK cells. Due to the difficulty of the experiment, the yield of analyzable cells per run is very low. Similar experiments using the same protocol or an improved version should be repeated for sufficient statistical backup. A detailed discussion of the results obtained from Ca^{2+} uncaging is provided by **section 4.1.4**.

4 Discussion

The experimental work of this thesis was dedicated to gaining new insight into the calcium dependency of NK cell function. While it has long been known that Ca^{2+} influx is key for proper immune cell action, little was known about how extracellular Ca^{2+} ion concentration can influence NK cell cytotoxicity. Our group discovered that Ca^{2+} ion concentration outside the killer cell can have a dramatic influence on the overall killing efficiency of a killer cell population. The conducted experiments prove that not only total killing efficiency but also the proportion of necrotic and apoptotic cytotoxicity depends strongly on extracellular Ca^{2+} ion supply. Upon activation, NK cells do not reply by an all-or-nothing influx of Ca^{2+} ions but show nuanced response patterns which are clearly associated with different outcomes of cytotoxic action. Three types of intracellular Ca^{2+} signals were identified, quantified and compared. Certain signal types could be connected to consecutive apoptosis or necrosis induction in target cells with very high significance.

If activated NK cells show distinct Ca^{2+} responses, why do some killer cells prefer to inflict necrosis and others apoptosis? What are the molecular players determining which type of killing is to take place? The final section of this thesis provides several models which could help explain these differences and proposes experiments to put them to the test. The final part of this section deals with possible biological implications of necrosis and apoptosis induction by NK cells in the context of immunogenicity and tumor surveillance.

4.1 Critical review

4.1.1 Limitations of pCasper-based detection of cell death

The physical functionality of the pCasper apoptosis sensor was explained in detail in **section 2.2.1**, its biological value for the discrimination of cell death types in **section 3.1**. There is currently no data available concerning the overall sensitivity of pCasper. It seems intuitive that there is a minimum caspase activity necessary for a detectable change in its fluorescence properties. This activity level is not necessarily identical to that of caspase-mediated proteolytic cleavage of other proteins which partake in the apoptosis cascade. Thus, it is possible that apoptosis detection by pCasper comes with a significant temporal delay. This is all the more true for necrosis detection by pCasper which is not even an inherent property of the sensor itself but is based on its diffusion through the damaged target cell membrane. Compared to small molecule cytosolic dyes such as Calcein or Fura-2, pCasper can be expected to diffuse out of the cell with much lower velocity due to its high molecular weight. Therefore, low concentrations of perforin pores might lead to lytic stress on the target cell which could be dectected by these dyes but

not with the construct.

4.1.2 Interdependence of necrotic and apoptotic index

The aim of the necrotic and apoptotic index definition was twofold. Firstly, it should allow not only a qualitative but semi-quantitative description of target cell death. Secondly, by calculating half-life points for rRFP and AR functions for each cell, one should be able to distinguish the sequence of apoptosis and necrosis when both types happen in parallel in the same target cell. The frequency distribution of apoptotic to necrotic events in a target cell population can now be determined applying two methods: The first is based only on visual assessment of target cell behaviour during microscopy. By combining visible effects such as cell swelling or blebbing with the qualitative changes in pCasper fluorescence, cells can be assigned to both types of target cell elimination with already high precision. Using the second method, the calculation of apoptotic and necrotic indices provides an objective and reproducible method of allocation. The counted numbers of apoptotic and necrotic target cell killings based on k_n, k_a-pairings fitted very well to that gained from the first method. This finding supports that apoptotic and necrotic indices are reliable tools at least when it comes to identifying the type of target cell death.

How valid this method is, regarding the quantification of both types with equally high reliability, is not as clear. If a cell is lysed quickly, more and more sensor protein will be lost for reporting apoptosis. We can therefore expect that apoptosis detection as well as the quantification of its speed expressed by the apoptotic ratio will be the more imprecise the faster a target cell is being lysed. Since only one sensor protein is used to measure both processes, necrotic and apoptotic ratio are not independent of one another. This correlation is clearly visualized by **figure 18** in **section 3.4.2**. The higher the k_n, the lower the k_a and vice versa. While this effect is, in principle, expected, since ongoing lysis or apoptosis will always limit the possible degree of the other death type, it is unclear to what degree the limitation in exact quantification is due to the underlying biology or to the weakness of the quantification method.

Another problem arises from the fact that correct calculation of both indices requires individual fitting of AR and rRFP by hand. This process is time-consuming and would need automatization if intended for high-throughput analysis of imaging data.

4.1.3 Calibration of the Fura-2 ratio function in NK cells

As outlined in **section 2.2.1**, Fura-2 is a ratiometric Ca^{2+} dye. Because Ca^{2+}-bound dye has a different absorption maximum for UV light than unbound dye, one can deduce the present Ca^{2+} concentration using the ratio of emission intensities in both channels. For the calculation of exact Ca^{2+} concentrations, a calibration of the Fura-2 dye is needed in which the two extreme values, R_{min} and R_{max}, are determined in the absence as well as

the saturating presence of Ca^{2+} ions [90].

When first attempting this calibration in NK-92 cells triggered with thapsigargin and ionomycin, the rapid extrusion of Ca^{2+} ions out of the cytosol turned out to be a recurring problem, making it impossible to measure a true R_{max}. This extrusion was not preventable using Caloxin 1b1, a potent inhibitor of membrane-located Ca^{2+} ATPases [111], nor depriving the cells of glucose which should limit ATP supply to Ca^{2+} pumps.

A similar problem occurred using primary NK cells. A Fura-2 calibration was attempted following two separate approaches. The first one was to measure R_{min} and R_{max} once again using ionomycin and thapsigargin in two wells in a 96-well-plate at the BioImager microscope. One well contained cells in a medium which had high concentrations of EGTA, the other high concentrations of calcium chloride. In the second approach, using the same EGTA and Ca^{2+} concentrations in two separate wells, the minimum and maximum ratio values were measured using Fura-2 potassium salt. Although identical lamp powers as well as exposure times were chosen for both conditions, R_{max} was significantly higher when using the Fura-2 salt. Thus it remained unclear which pair of values was in fact adequate. For this reason, a calculation of Ca^{2+} concentrations based on the Fura-2 ratio was not performed. R_{max} was slightly higher in NK cells loaded with probenecid which delays the extrusion of Fura-2 dye from the cytosol, but the corresponding values were still lower than the ones derived from the cell-free method. The observed discrepancies in the maximal ratio values derived from the two methods could also be due to the AM form of the dye being sequestered by mitochondria and other organelles [112]. To circumvent this process, NK cells could be electroporated with the potassium salt of Fura-2 and calibration results could be compared to those of the cell-free approach.

4.1.4   Photolysis of NP-EGTA in NK cells

Regarding how necrotic killings by NK cells were linked temporally to the applied UV flashes (**section 3.6.2**, **figure 23**), it appears justified to deduct that singular high-intensity photolysis did not facilitate necrosis induction by NK cells. There was, however, a higher proportion of necrotic killings in the chelator group compared to control, occurring *prior* to the first UV flash. Since Fura-2 was only measured twice within the first 30 minutes, for the first time at the very beginning, and again immediately before flashing, we can exclude an active uncaging of Ca^{2+} by UV light during this particular period of the experiment. It might yet be that Ca^{2+} ions were released gradually by a UV light-independent mechanism. Such an unnoticed 'spontaneous uncaging' could have led to Ca^{2+} being transferred to Ca^{2+} binding proteins, being refilled into Ca^{2+} stores, or being extruded from the cytosol. These processes, escaping direct detection by Fura-2

measurement, could have accounted for the slight preponderance of necrotic killings in the chelator group during the first 30 minutes of the experiment.

At the moment, it seems more likely that uncaging Ca^{2+} ions from NP-EGTA in NK cells, independent of the individual uncaging pattern, did not increase the fraction of necrotic killings. There are many conceivable reasons for this observation. As already mentioned in **section 3.6.2**, the easiest would be that the underlying hypothesis that Ca^{2+} ions are sufficient for necrosis induction is invalid. Putting it simply: The experiment worked and invalidated a faulty presumption. Another possible explanation concerns the function of Ca^{2+} microdomains. Upon loading with NP-EGTA, the substance should be evenly distributed in the cyotosol of the killer cell. Hence, photolysis can be expected to produce a homogeneous Ca^{2+} release with little to no spatial variance in ion density. Numerous research groups have provided evidence that for many cellular functions, localized Ca^{2+} signals, so-called Ca^{2+} microdomains, are of greater importance than overall Ca^{2+} concentrations inside the cell [113], [114]. Experiments in this thesis from **section 4.2** underline the importance of Ca^{2+} microdomain generation particularly for necrosis induction by NK cells. That in mind, it might also be that Ca^{2+} release from NP-EGTA was not suitable to provoke necrosis induction in killer cells, since it affected only global Ca^{2+} concentrations.

Regarding the complexity of the experimental setup, further improvement of experimental protocols is necessary for final judgement. Necrosis induction by CLs may still be solely dependent on sufficient Ca^{2+} supply but might only be achieved if photolysis is induced at the right moment. This sensitive period might be located somewhere in a cascade involving the interplay of receptors and ligands, IS formation, CRAC, vesicle trafficking and their subsequent release. Uncaging Ca^{2+} ions at the right time might thus be a matter of precise timing and higher numbers of repetitions could be necessary to prove it possible.

An interesting experimental approach would be to shift the experimental setting described in **section 3.6.2** to a low-Ca^{2+} environment. As discussed in the following section, extracellular Ca^{2+} concentrations lower than 20 to 30 μM prohibit target cell killing by NK cells but not IS formation nor the partial depletion of Ca^{2+} stores. Uncaging Ca^{2+} ions under these conditions might serve as a replacement for ORAI-mediated Ca^{2+} influx across the plasma membrane and might restore killing competence in killer cells.

4.1.5 Applicability to the in-vivo system

NK cells performed both necrotic and apoptotic killing against Jurkat E6.1 cells in in-vitro experiments. Since both processes are probably unalike regarding their immunogenicity,

it would be of great value to investigate their statistical occurrence in living organisms. Unfortunately, this enterprise is much more complex than it might appear at first sight. As long as there are no identified biological markers for both, the discrimination between apoptotic and lytic tumor cell killing still depends on single-cell microscopy. The task is hence to create an environment in which such microscopy is possible without interfering with the integrity of the examined tissue. 3D-microscopy could prove an important step towards this goal. Using our light sheet microscope, Carsten Kummerow, Rouven Schoppmeyer, Christian Backes and many other colleagues worked together to establish functioning models for 3D analysis of NK cell migration and killing rates. Killer and target cells are transferred into a collagen-based matrix which marks an important improvement in physiology compared to the flat ground of a well plate. In the long run, transgenic mice could be created expressing the pCasper apoptosis sensor and killing of tumor cells in a living mouse could be performed using two-photon microscopy.

4.2 How environmental factors influence killing mode

When observing NK cells killing target cells under a fluorescence microscope, one can determine the outcome of cell-cell contacts by changes in fluorescence if the target cells stably expresses an apoptosis sensor. This outcome - i.e. target cell lysis or target cell apoptosis or both - is the final step in a complex cascade of cytosolic processes. Therefore, the question why some killer cells induce necrosis and some apoptosis is tough to tackle. A very simple approach is to first reduce the problem to three key factors which can be expected to have an influence on NK cell killing behavior: the killer cell, the target cell and their surrounding environment.

Which type of cytotoxicity a killer cell will induce appears to depend partially on the pattern of Ca^{2+} influx upon activation. In contrast to cell lines, primary NK cells are heterogeneous. They can be expected to have varying expression levels of receptors, signaling molecules or cytotoxic proteins. Some killer cells might simply be more suitable to produce a certain type of signal than others. On the other hand, target cells might also tip the scales: Low counts of perforin pores are more easily repaired, hence target cells might avoid direct lysis in theses cases. A possible influence of NCR ligands expressed on the surface of a target cell is discussed below. In the long run, target cells might develop resilience against certain types of cytotoxicity through a change of phenotype. Mutations of apoptosis-regulating proteins might provide immunity against the proteolytic activity of granzymes or caspases activated via death receptor signaling. Enzymes present in the target cell's cytosol could deactivate granzymes, providing further resistance against apoptosis induction.

We learn something important about the influence of environmental factors from the results in **section 3.3**. The more Ca^{2+} ions there are in the supernatant, the more likely necrosis induction will be. This effect was seen both in negatively-isolated NK cells stimulated with IL-2 as well as in expanded NK cells. Adding sufficient amounts of EGTA completely eliminated necrosis occurrence. Necrosis by NK cells therefore depends on a minimum amount of free Ca^{2+} ions. Perforin is the key player in granule-dependent necrosis induction by CTLs. During the past decades, numerous research groups have presented converging evidence for its cytolytic function being absolutely dependent on the presence of Ca^{2+} [115], [116], [117], [76]. Hence, there are several possible explanations for the absence of necrotic killing in low-Ca^{2+} environments, two of which will be discussed in detail. The first one is that too low concentrations of Ca^{2+} do not allow sufficient vesicle release. The second one is that even at low Ca^{2+} concentrations, vesicles are still released but there is not enough Ca^{2+} available for perforin to autoaggregate.

To find out what is in fact the limiting factor for necrosis in low-Ca^{2+} environments, the threshold concentration was approximated using a narrower gradient than the one used for the basic experiments from **section 3.4**. Final Ca^{2+} concentrations of the sera were again calculated based on the Ca^{2+} electrode data referenced in that section. Following this approach, the threshhold could be narrowed down to a free Ca^{2+} concentration range of 20 and 30 μM. In 2005, Voskoboinik et al tested the calcium and pH dependency of perforin pore formation. They used purified human perforin to lyse sheep erythrocytes [118] and found that a minimum of 20 to 30 μM free Ca^{2+} ion concentration was necessary for auto-aggregation (s. **figure 24**). This threshold fits surprisingly well to the one found here in the cell-based system. Voskoboinik reported that full perforin activity would require free $[Ca^{2+}]_{ext}$ of 200 μM or higher. By determining at which concentration 50% of maximal erythrocyte lysis was achieved, they calculated the K_D of the perforin C2 domain to be $\pm$ 70 μM of free Ca^{2+} ions. The percentage of necrotic killing by NK cells was roughly 55% at 72 μM and changed insignificantly to 56% at 265 μM. Combining these results, it seems plausible that necrosis is limited by auto-aggregation when Ca^{2+} concentrations are lower than the K_D and becomes release-limited as $[Ca^{2+}]_{ext}$ is elevated.

The second step was to test if vesicle release ceases at exactly this Ca^{2+} concentration, a result which would point towards a release limitation of perforin function at low $[Ca^{2+}]_{ext}$. The difficulty was to reduce only the concentration of *cytosolic* Ca^{2+} without lowering the amount outside the cell. To mimic such a condition, a similar killing experiment was performed with primary NK cells and Jurkat E6.1 pCasper as target cells, but the killer cells were previously loaded with the fast-acting Ca^{2+} chelator BAPTA-AM. Being a
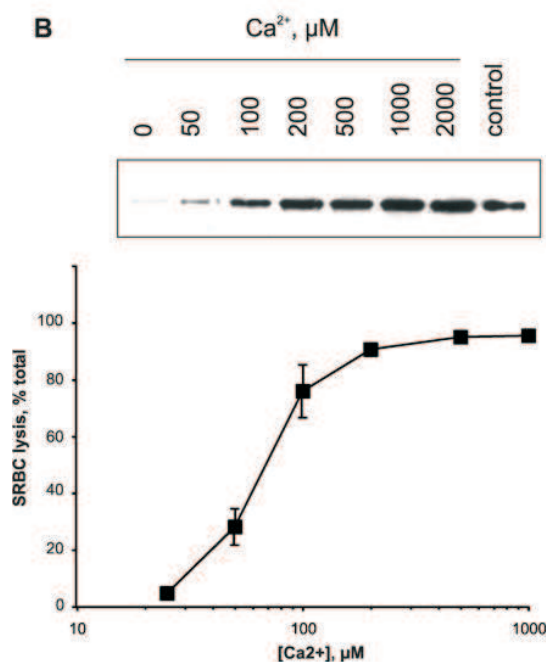
Figure 24: Calcium dependence of target cell membrane lysis by purified human perforin from 'Calcium-dependent Plasma Membrane Binding and Cell Lysis by Perforin Are Mediated through Its C2 Domain', Voskoboinik et al, The Journal of Biological Chemistry, 2005, 280, 8426-8434

rapid-acting chelator, BAPTA interferes with the generation of Ca^{2+} microdomains, which have been demonstrated to be necessary for transmitter release in neurons [119], [120] and for efficient T-cell activation [113].

Figure 25 shows how loading the NK cells with BAPTA significantly reduced the frequency of target cell necrosis. The distribution of lysis and apoptosis induction was even reversed. Furthermore, those killer cells still able to induce target cell lysis took significantly longer to kill their targets compared to those not loaded with BAPTA.

Apparently, buffering intracellular Ca^{2+} concentration with BAPTA diminishes release of perforin. Thus, necrosis frequency is reduced although the amount of free Ca^{2+} in the supernatant is unchanged. This result points towards vesicle release being the limiting factor for necrosis at lower Ca^{2+} concentrations. A definite answer, however, cannot be given at this point. A possible experimental approach to provide such an answer could be a TIRF-based analysis of vesicle release while buffering outside Ca^{2+} with EGTA below the necrotic threshold. Another approach could be staining NK cells after killing, using monoclonal antibodies against CD107a. CD107a or LAMP-1 is located in the membranes of cytotoxic vesicles [60], [70]. If the cells manage to release vesicles in a low-calcium environment, LAMP-1 should be detectable on the cell surface afterwards.
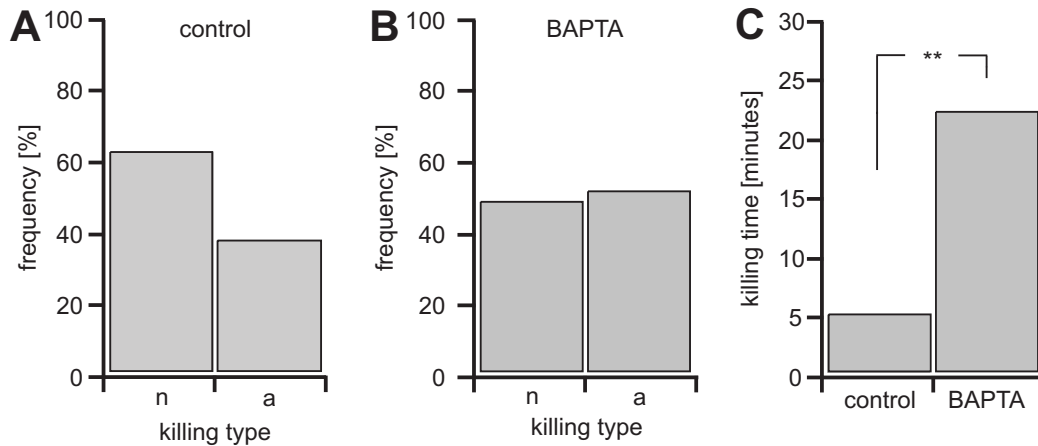
Figure 25: Interfering with calcium microdomain formation in NK cells reduces necrosis potential and delays killing
A, **B** Primary NK cells loaded with BAPTA performed necrosis 49 % of the time compared to control cells (61 %), which is about the standard necrosis frequency in AIMV medium. **C** Those cells that managed to induce target cell lysis when loaded with BAPTA needed significantly more time (22.1 minutes) to kill their targets compared to control (5.1 minutes), 'n' = necrosis, 'a' = apoptosis

Looking at the other end of the Ca^{2+} concentration spectrum, **figure 11** from **section 3.4.1** shows how the likelihood of necrotic killing rises monotonically with extracellular Ca^{2+} ion supply until it reaches a plateau. The highest frequency of necrosis was measured at about 80 to 85 % and could not be increased regardless of how much Ca^{2+} chloride was added to the medium. Apparently, there is always a certain proportion of killings which is not sensible to modifications of the surrounding Ca^{2+} concentration. This observation suggests that those remaining 15 to 20 % apoptotic killings could be performed in a Ca^{2+}-independent way. This assumption could be tested using blocking monoclonal antibodies against FAS or FAS-ligand. If this small fraction of apoptosis is induced independently of granzymes, and, given the fact that Fas is the main death receptor system employed by NK cells, the occurrence of apoptosis should be diminished.

4.3 Different tumor targets require different cytotoxic mechanisms

The measured distribution of apoptotic and necrotic killings is likely to be specific for the pairing of NK cells with the Jurkat E6.1 target cell line. Hence, the mode of target cell death will most likely depend on the molecular identity of the target cell. One very obvious example is the aforementioned difference in lytic and apoptotic killing distribution comparing Jurkat E6.1 and K-562 as targets. NK-92 cells killed K-562 mainly through direct cell lysis. Parts of this observation are certainly traceable to the fact that this target cell line lacks Fas-receptor, an important conductor of pro-apoptotic signaling. Since

we know that death ligands convey extrinsic but not intrinsic apoptosis as granzymes do, this explanation is valid but not sufficient for the one-sidedness of this distribution. It is more likely that, compared to Jurkat E6.1, K-562 also have a lower tolerance for perforin action. This tolerance can be the resultant of a cell's capability to withstand osmotic stress and to repair already formed perforin pores. That way, after perforin has been released, the cells do not live long enough for granzyme activity to become visible. These factors should be taken into account when analyzing the distribution of different killing modes shown by NK cells or CD8$^+$ lymphocytes. In 2016, Yanting and colleagues even reported that both naive and stimulated primary NK cells kill a considerable proportion of adherent target cell lines solely by death ligands [82].

The respective contributions of death ligands and perforin/granzyme seem to differ not only depending on the type of tumor target but also on whether NK cells are involved mainly in local or systemic anti-tumor responses. Drawing from experience gained through a variety of mouse models, CTLs from perforin-1 knockout mice were unable to effectively kill certain melanoma and sarcoma cell lines [121], [122] but proved just as efficient in controlling liver metastases of the same melanoma cell line dependent on IL-12 [123], [124]. A similar ambivalence of perforin function was found in the context of mAb immunotherapy. While in-vivo elimination of colon, prostate and breast carcinoma cell lines seemed not to depend on perforin-1 [125], its functionality was necessary for the control of melanoma cells when immunotherapy with BRAF inhibitors and anti-CD137-Ab was administered. There is evidence that the contribution of death ligands to total NK cell cytotoxicity is equally diverse [126].

4.4   How are different NK cell calcium responses generated?

After discovering that NK cells answer activation by different intracellular Ca^{2+} responses, the obvious question was how exactly those were generated. What or who determines what type of Ca^{2+} signal a killer cell is to induce and, consequently, what type of killing is to be performed?

An intuitive assumption would be that different cytosolic Ca^{2+} responses in killer cells could be generated by different Ca^{2+} channels. In 2011, Omilusik and colleagues have provided evidence that voltage-gated Ca^{2+} channels, especially the subtype Ca$_v$1.4, is expressed in T-cells and may contribute to controlling the maturation of naive T-cells [127]. Whether this subtype or other voltage-gated Ca^{2+}-selective channels are expressed in NK cells and whether they partake in modulating cytolytic effector functions is currently unknown. Another group of possible Ca^{2+} channels is marked by the so-called 'transient receptor potential' channel group (TRP channels). Out of the large variety of identified

TRP channels, subtypes TRPV5 and TRPV6 are regarded as Ca^{2+}-selective [128]. So far, their contribution to immune cell function is unclear, since they do not appear to be consistently expressed in immune cells [129], [130]. It thus appears likely that STIM and ORAI proteins are the major source of Ca^{2+} influx into lymphocytes [131], [132], [43], . If we assume that all three signal types A, B and C are generated by Ca^{2+} entering the cell through ORAI, then there must be additional factors controlling the shape and extent of ion inflow through these channels, thereby generating the different signaling shapes. Information could be encoded in both the degree of cytosolic Ca^{2+} elevation as well as its frequency of oscillation. This section enlightens possible mechanisms which could be responsible for the differences in intracellular Ca^{2+} signals in killer cells as well as possible linkers between Ca^{2+} signal types and ensuing modes of cytotoxic action.

A recurrent feature of A-type calcium signals was that cytosolic Ca^{2+} concentrations dropped back to resting levels in between. This characteristic was inherent to that type of response. Another feature was the low height of the Ca^{2+} concentration peaks compared to B- and C-type signals. The reduction in Ca^{2+} peak heights together with the absence of sustained Ca^{2+} elevations gave rise to the hypothesis that the A-type Ca^{2+} response could be the result of Ca^{2+} store depletion without subsequent ORAI activation. Current literature provides compelling evidence that vesicle release from NK cells is blocked in the absence of SOCE [130], [133]. If missing SOCE was in fact responsible for the oscillatory signal, it could hence explain the lack of necrotic killing associated with this signal type. In that case, the type A could be regarded as a dysfunctional B-type response. The question would then be why some killer cells do not show sustained SOCE upon target cell recognition.

In normal AIMV medium containing $\pm$ 800 μM free Ca^{2+}, 22% of cells had A-type Ca^{2+} signals. Given the major importance of SOCE for a variety of vital processes in immune cells, it appears highly unlikely that SOCE should in principle be dysfunctional in these cells. A more likely explanation is that both STIM and ORAI proteins function properly but target cell recognition led to missing or abbreviated ORAI conductance. Since sustained CRAC relies on the concerted action of STIM, ORAI, MTOC relocation, mitochondria repositioning and other processes, the list of possible interferences is long. Although unlikely, one should first test basic CRAC functionality in these cells. This could easily be done by stimulating the cells with thapsigargin in the absence of Ca^{2+} and then re-supplying it which should lead to considerable Ca^{2+} ion influx into the cells by activated ORAI channels. If SOCE is unimpaired in basically the entire killer cell population following artificial store release as one would expect, then inadequate SOCE in some killer cells would be connected to the individual target cell.

4.4.1 NCRs and their ligands

Ca^{2+} release from the ER is mainly caused by IP_3 binding to its receptor. Production of IP_3 in turn depends on the activity of PLCγ. As described in the introduction, the vast majority of activating NCRs convey intracellular signals by activating the two protein tyrosine kinases Syc and Zap-70 which activate PLCγ. This step appears to be canonical for lymphocyte activation. It is, however, unclear to what extent each individual NCR contributes to PLC activation. The triggering of some NCRs might provide only weak stimuli for PLC. The resulting low IP_3 production consequently leads to only small amounts of Ca^{2+} released from the ER, which does not invoke full SOCE capacity. If so, then different intracellular Ca^{2+} signals in NK cells might be the consequence of an individual pattern of NCRs being activated upon target cell recognition.

When investigating the contribution of activating NCRs to NK cell cytotoxicity in 2006, Bryceson et al found that distinct groups of receptors synergized with each other, while coactivation of other receptors did not boost resting NK cell activity [32]. Using a redirected antibody-dependent assay, they studied the influence of different coactivation patterns on NK cytotoxicity against tumor cells, the extent of NK cell degranulation, cytokine secretion and intracellular Ca^{2+} responses upon activation.

Interestingly, coactivation of distinct pairs of NK cell receptors did not only lead to varying degrees of cytotoxic potential, but induced different intracellular Ca^{2+} responses in NK cells similar to the ones presented here. In unstimulated NK cells, only CD16 was sufficient to induce cytotoxicity. While singular activation of receptors like NKG2D or 2B4 still led to influx, these stimuli were insufficient to provoke target cell lysis on their own. Upon activation of 2B4 and CD16, the correspondent NK cells showed a large, sustained inflow of Ca^{2+} ions, while NKG2D induced a lower and oscillatory response pattern similar to the A-type signal. If these signals were in fact the consequence of a certain pattern of receptors being cross-linked at the same time, then NKG2D could be associated with the A-type signal while 2B4 or other receptors could lead to Type B or C signals. Intriguingly, out of all aforementioned NCRs, NKG2D is the only natural cytotoxicity receptor employing DAP10 as its ITAM-bearing signaling molecule, possibly making way for a separate downstream signaling cascade.

The presented Ca^{2+} signals were measured in a cell system and were not gained from in-vitro stimulation of NK cells by receptor cross-linking. It seems unlikely that only one type of NCR would be activated at the time in a cell-based system since one would expect NCRs as well as their ligands to be evenly distributed across the plasma membrane before polarization. It might yet be the case that target cells express NCR ligands at different quantities, making the activation of a certain type of NK cell receptor or combinations

of them more likely than others. Consequently, the influx pattern and the type of target cell elimination associated with it would be determined by the molecular composition of NCRs and their ligands and not by modifications occurring downstream in the killer cell.

An obvious approach to put this hypothesis to the test would be to first try and induce type A, B and C signals by cross-linking a distinct combination of NCRs with monoclonal antibodies and an anti-IgG cross-linking mAb. Secondly, the same population of NK cells could be used in a single-cell experiment against different target cell lines to see whether the Ca^{2+} signals measured resemble those induced by antibody engagement. In a second step, certain NCRs or ligands could be blocked using monoclonal antibodies to check whether the frequency of types A, B or C changes.

When studying the role of MCU-mediated Ca^{2+} uptake, Parekh and colleagues stimulated mast cells using leukotriene C_4 (LTC4) [134]. They employed sub-maximal concentrations of the substance to recreate more physiological levels of stimulation. In contrast to high concentrations, moderate levels lf LTC4 induced cytosolic Ca^{2+} oscillations. This principle might also translate to NK cells: Low to moderate degrees of NCR activation could translate to low levels of IP_3 production. The consecutive weak release of Ca^{2+} from the ER allows the quick refilling of ER Ca^{2+} stores, thus abrogating Ca^{2+} inflow through ORAI. In contrast, high degrees of NCR stimulation would lead to high levels of IP_3, causing substantial storage emptying. In that case, Ca^{2+} refill rate would not be sufficient to stop SOCE through activated ORAI channels. The result would be a high and sustained rise in intracellular Ca^{2+} levels as seen in types B and C.

An important addition to the already acquired data would be examining how ADCC in contrast to NCR activation influences the distribution of Ca^{2+} signal types in primary NK cells. CD16 has repeatedly been shown to be a potent activator of NK cell cytotoxicity and degranulation. If ADCC in NK cells was found to trigger predominantly one type of Ca^{2+} signaling pattern, then this finding would be a supporter of the theory that the compositions of different NK cell receptors are responsible for turning the switch towards a distinct type of Ca^{2+} response.

4.4.2 Mitochondria and CRAC

Low or short-lived SOCE in some killer cells might not only be caused by incomplete storage emptying but also by interference with the resulting Ca^{2+} influx through ORAI channels that usually follows store depletion. A variety of cellular processes is known to regulate SOCE in activated B-, T- and NK cells. In addition to their significance for cellular energy metabolism and apoptosis control, mitochondria have been demonstrated to actively partake in shaping cytosolic Ca^{2+} responses in immune cells [135], [136], [137].

In 2006, Ariel Quintana, Christian Schwindling and other colleagues investigated the role of mitochondria translocation in activating immune cells. Our group found that sustained calcium influx across the plasma membrane of active T-cells through ORAI channels depends on mitochondria being moved to close proximity of the IS-forming membrane [56], [55]. After travelling to the inside of the immunological synapse, mitochondria take up parts of the inflowing Ca^{2+} ions, which prevents Ca^{2+}-dependent ORAI inactivation. It is possible that an A-type Ca^{2+} pattern is the result of this mechanism being disturbed. In those cases where mitochondria are not transported closely enough to CRAC channels or their uptake capacity is reduced, CRAC activity will be limited by intrinsic channel deactivation. This self-regulatory mechanism would quickly abrogate Ca^{2+} influx which could explain the absence of cytosolic Ca^{2+} plateaus in type A signals.

The main Ca^{2+} transporting protein in the inner mitochondrial matrix has been identified as the 'mitochondrial Ca^{2+} uniporter' or 'MCU'. According to Parekh et al, this protein acting properly is necessary for efficient Ca^{2+} uptake into mitochondria and pharmacological blockade leads to rapid decline of cytosolic calcium ion flux [134]. More importantly, functional uptake of ions into mitochondria allows the cell to refill its Ca^{2+} stores. By periodically filling and emptying intracellular stores such as mitochondria and the ER lumen, cells have been shown to generate Ca^{2+} oscillations, for example in mast cells, a type of immune cell related to lymphocytes [138]. These measured oscillations resemble the type of Ca^{2+} signal by NK cells associated with apoptotic target cell killing.

To examine the possible role of mitochondria in generating different Ca^{2+} signals in NK cells, a first approach could be to perform live-cell analysis of NK cells stained with a fluorescent mitochondria dye, for example MitoTracker red. Afterwards, the cells are brought together with Jurkat E6.1 pCasper cells. The mitochondrial localization in regard to the IS can then be compared in those killer cells which induced necrosis versus those that induced apoptosis. Another suitable experiment would be to measure intracellular Ca^{2+} levels in killer cells using Fura-2 or Fura-Red and in parallel interfere with mitochondrial Ca^{2+} uptake. This interference could be achieved pharmacologically by incubating the killer cells with Ru-360, a known high-affinity MCU blocker [139], [140], or by siRNA-based knock-down. Another approach would be to use carbonyl-cyanide p-trifluoromethoxyphenylhydrazone or FCCP, a protonophore which diminishes the electro-chemical gradient of the inner mitochondrial membrane, the main driving force for calcium uptake into mitochondria. Although in principle suitable for this purpose, it should be employed carefully since the breakdown of inner mitochondrial membrane potential will also severely affect the killer cell's energy metabolism.

No matter the reason for the oscillatory shape of the Ca^{2+} response, it clearly leads to successful NK cell killing. Oscillatory Ca^{2+} signals were shown to have intrinsic signaling quality in a variety of cell types [141], [134] and also in cancer cells [130]. From this perspective, it is also conceivable that A-type Ca^{2+} responses in killing NK cells are not simply the occasional failure to produce high Ca^{2+} elevations but that they are distinctively generated to trigger apoptosis induction.

4.4.3 Possible connectors of cytosolic Ca^{2+} oscillations and apoptosis induction

If we assume that large SOCE is necessary for the release of perforin and granzymes, then apoptosis is probably induced in a more ORAI-independent way, probably by death-receptor signaling. Although often offhandedly regarded as being Ca^{2+}-independent, the question remains how FasL accumulation is achieved at the IS-forming part of the killer cell membrane. Possible mechanisms include the vesicle-based transport of FasL to the membrane and the subsequent fusion of these vesicles as well as already present FasL molecules travelling to the IS by lateral diffusion. In 2011, Schmidt and colleagues employed TIRF microscopy to provide evidence that, in human T-lymphocytes, FasL as well as perforin/granzymes are stored and transported in separate vesicles [142]. An obvious implication would then be that both granules are also trafficked via distinct pathways. If this applies to NK cells, then A-type signals might be the driving stimulus for FasL vesicles to be transported to the IS but not those vesicles storing perforin and granzyme B. How these vesicles are then fused with the plasma membrane would still be unanswered. It is conceivable that the amount of Ca^{2+} ions necessary for the fusion of FasL-containing vesicles is lower than that of the perforin/granzyme-vesicles. Low to moderate Ca^{2+} influx across the plasma membrane or the mere redistribution of Ca^{2+} ions between stores might not be sufficient for the Ca^{2+}-dependence of perforin-vesicles but might allow the fusion of FasL-vesicles with the membrane. Another explanation would be that, if a killer cell does not manage to create sustained Ca^{2+} influx after IS formation, the contact is kept alive but the target cell cannot be killed at this point because of the cell's inability to fuse its vesicle pool with the membrane. Instead, the killer cell accumulates already-present FasL molecules at the IS by an unkown mechanism which then eliminates the target cell by apoptosis induction. This hypothesis could explain in parts why sometimes apoptosis could be induced quite rapidly while other cells took time spans from several minutes to even hours. Rapid apoptosis can be achieved through granzymes entering the cell which is only possible if granzyme-vesicle fusion is functional. If not, death ligands must first be gathered at the right location which takes significantly more time until a strong enough death signal is induced in the target cell.

4.4.4 How different are signal types B and C?

These types of Ca^{2+} signals were the only ones which allowed direct lysis of the target cell. In contrast to type A, both types were characterized by the occurrence of large, sustained elevations in cytosolic Ca^{2+} ions. Taking into account what is known about the Ca^{2+} dependence of immune cell function, it seems safe to assume that these elevations are produced by SOCE which is the necessary condition for the release of lytic granules. The question is whether type B and C signals are in fact distinct types of cytosolic Ca^{2+} signals or if C is merely a weaker form of B.

This assumption is backed up by the observation that, while B was followed exclusively by necrosis induction, C lead to all three types of target cell killings. Current scientific literature suggests that both perforin and granzymes are stored together in lytic granules [143]. Since perforin acts more rapidly than granzymes, a higher number of released vesicles will most likely lead to a quicker cell death. In some cases of very high cytosolic Ca^{2+} peaks - measurable as type-B signals - enough vesicles will be released at once so that the target cell is lysed even before granzymes could activate caspases inside the target cell's cytosol. In case of sustained but not as high-peaking Ca^{2+} influx, fewer vesicles fuse with the membrane. This will be registered during Ca^{2+} imaging as a type-C signal. The target cell is able to withstand the immediate osmotic pressure and endures until granzymes force it into apoptosis by activating cytosolic caspases.

How high Ca^{2+} levels will peak inside an individual killer cell will depend on a variety of factors. Possible candidates are the amounts of STIM and ORAI, their individual isotypical compositions, the buffering capacities of mitochondria and efflux efficiencies of Ca^{2+}-specific pumps which work together to clear the cytosol of excess Ca^{2+} ions, as well as energy metabolism. Some cells might, by chance, be able to create higher Ca^{2+} currents than others, explaining the slight differences in height and cell-cell contact time between types B and C. This model is also in line with the influence of extracellular Ca^{2+} concentrations on the distribution of killing types. As experiments from **section 3.4.1** have demonstrated, the increase in necrosis frequency at higher Ca^{2+} concentrations is partly at the cost of mixed type killing. The latter is likely to result from the cytotoxic effects of both perforin and granzymes balancing out. Perforin pores do considerable, but not always lethal damage to a cell, granzymes then induce apoptosis, so both processes take long enough for pCasper to detect them. Increasing the supply of extracellular Ca^{2+} ions also increases ion influx into the killer cell and boosts vesicle release. These conditions empower more cells to kill by direct membrane lysis which would otherwise have depended on the combination of perforin and granzyme action to kill their target cells. **Figure 26** provides a detailed summary of all the above-mentioned mechanisms which could be responsible for shaping Ca^{2+} responses in NK cells. It should be noted, however,
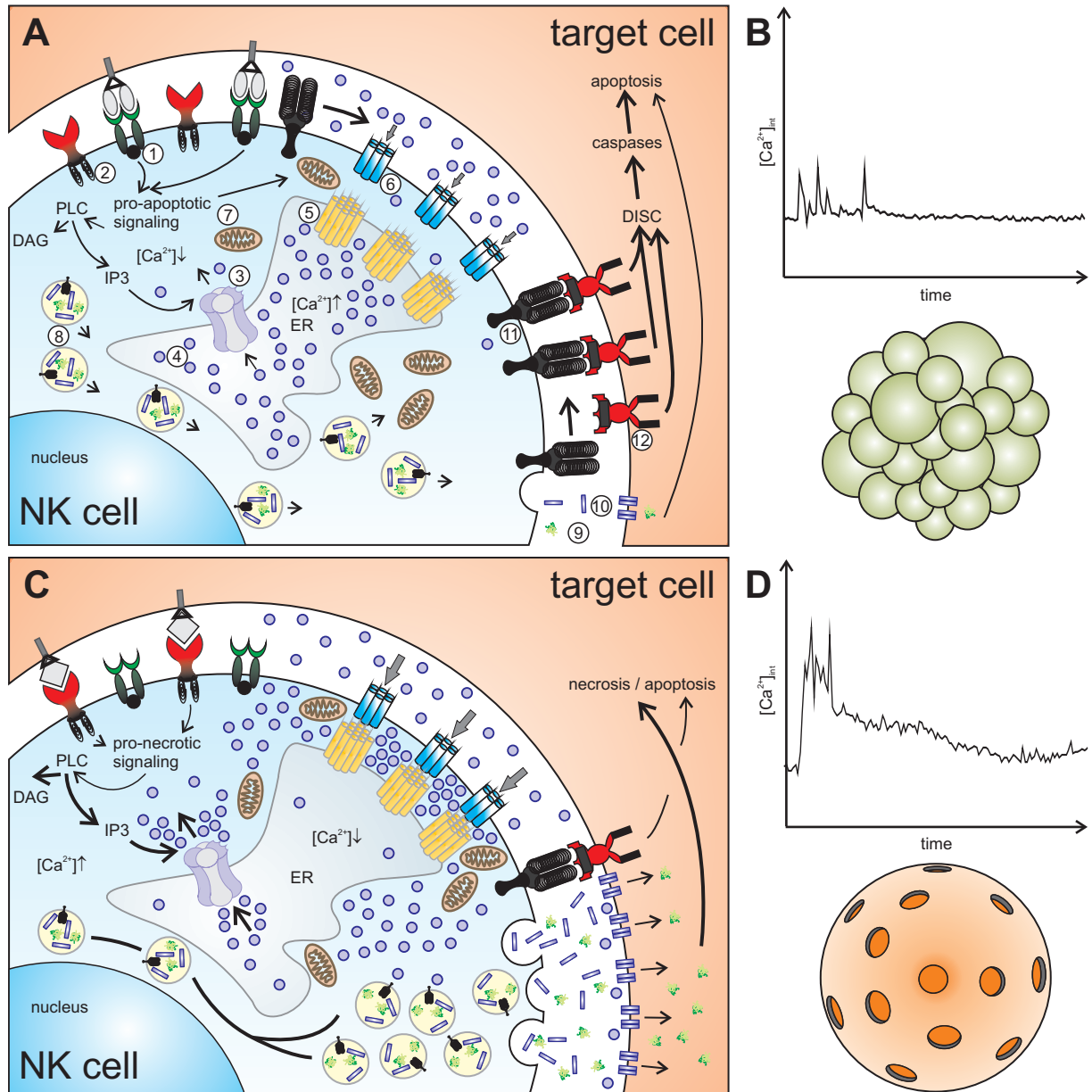
Figure 26: How NK cells could generate different calcium response patterns upon target cell recognition

(**A**) One NK cell inducing apoptosis, associated with an oscillatory Ca^{2+} response (**B**) and one inducing necrosis (**C**), showing a B-type signal (**D**). In **A**, apoptosis-promoting NCRs (1) lead to low levels of IP_3 production. After receptor activation (3), low amounts of Ca^{2+} ions (4) are released from the ER. The extent of consecutive STIM (5) and ORAI (6) activation is weak. No sustained CRAC is generated, possibly also due to mitochondria (7) not being shifted closely enough to the IS. The majority of cytotoxic vesicles (8) cannot be released. Instead, the killer cell gathers membrane-bound FasL (11) to the site of the IS, finally promoting apoptosis in the target cell by activating DISC. In contrast, NK cells showing B-type Ca^{2+} responses (**C**, **D**) generate sustained SOCE after the activation of pro-necrotic NCRs (2). Large amounts of vesicles containing granzymes (9) and perforin (10) being released cause direct lysis of the target cell or rapid apoptosis.

that not all of the depicted mechanisms would necessarily work together in the same cell.

All Ca^{2+} signals were taken from single-cell contacts, i.e. only one killer cell killing one target cell at the time. A valuable addition of data would be to analyze killing behavior in case of NK cell cooperativity. Can different NK cells boost each other's cytotoxic potential when attacking the same target cell?

Another interesting observation is that CTLs are able to kill a series of target cells in a row. This effect can be called 'serial killing'. It is present in basically all killer cells and, as Christian Backes has presented in his thesis, seems to follow a strict order of killing types: Almost all NK cells killing in sequence first induced necrosis and then switched to apoptosis afterwards. Some cells would not be able to inflict direct lysis at all. They would start with apoptosis and not at any time switch to inducing necrosis. This finding clearly suggests that NK cells, a priori, have different lytic capabilities. Those cells limited to apoptosis would probably show Ca^{2+} signals similar to types A or possibly C, while those cells being able to release high quantities of vesicles would likely start with types B and then move on to lower C-type signals. It would be interesting to see whether killer cells can also switch between types A and B/C respectively. If not, then this would be in strong support of the theory that both types have functionally distinct underlying cellular processes. This characteristic could therefore be used to group NK cells not only depending on cell surface markers but also on the cellular mechanism employed. Especially, in the case of CD56^{dim} NK cells, it would be possible to distinguish those more inclined to apoptosis from those more inclined to necrosis.

4.4.5 Outlook

A variety of experiments can be conducted to further unveil the origin of different Ca^{2+} signals in CTLs. The presented experiments provide sufficient data to assess kinetics and basic shapes of these signals. Still, time resolution of 30 seconds between data points, as was achieved here, should be increased to get a more detailed impression of the signal shapes. High-frequency Fura-2 measurement of Ca^{2+} signals may also help to verify if A-type signals resemble the typical known properties of ER store depletion.
Another valuable information that could help to clarify the origin of the difference in signals would be how the relative distribution of A-, B- and C-type Ca^{2+} responses differs when NK cells are exposed to varying extracellular Ca^{2+} concentrations. By addition of large amounts of EGTA, SOCE is likely to be prevented in all killer cells since there is simply no Ca^{2+} available to enter the cell. If ORAI-mediated Ca^{2+} influx is the key difference between type A and B signals, then every killer cell should be restricted to A-type signals. Repeating these killing experiments using increasing $[Ca^{2+}]_{ext}$ could then be used to

determine the minimum Ca^{2+} concentration necessary for B- and C-type signals to occur.

4.5 Apoptosis, necrosis and total killing efficiency

What determines the biological function of NK cells in an organism is not the distribution of killing types or Ca^{2+} signal types but their total cytotoxic potential. The task is to recognize and kill as many pathogens or tumor cells as efficiently as possible. Our newly-developed killing assay allows time-resolved analysis of killer cell action [89]. Total killing efficiency was analyzed for NK cells at different Ca^{2+} concentrations (Xhiao Zhou, Yan Zhou, manuscript in preparation). Interestingly, the function presents as bell-shaped, meaning that there is an optimum concentration for economic NK cell action. This maximum was measured at 1.7 mM free calcium ions. At first, it seems intuitive that the more necrosis an NK cell is capable of inducing, the more damage it deals to cell membranes. Furthermore, necrosis kills much faster than apoptosis, as can be seen from the drastic differences in NK cell contact time. Therefore an NK cell's overall killing capacity should increase as its necrosis potential does. Results from **section 3.4** show that at 1.7 mM $[Ca^{2+}]_{ext}$, when NK cells show the highest killing rates, necrosis is indeed the dominating type but not at the peak of its relative frequency. This means that, while necrosis by perforin is a powerful tool, further increasing necrosis potential in NK cells beyond this point does in fact impair total killing capacity. A maximum killing rate could hence be achieved by creating a fine-tuned balance between necrosis and apoptosis induction at moderate levels of $[Ca^{2+}]_{ext}$. This finding is congruent with results presented by Christian Backes in his doctoral thesis. He analyzed total killing efficiency by NK cells and came to the conclusion that NK cells tend to kill less target cells if their lytic potential is too high [93]. This observation is backed up by results presented in section 3.4.1. When analyzing the total number of killed target cells as a function of $[Ca^{2+}]_{ext}$, it turned out highest for a concentration of 0.265 mM (not shown in the plot). Compared to physiological Ca^{2+} blood levels of 1.1 to 1.4 mM, this concentration is rather low. Interestingly, this was exactly the concentration at which necrosis, apoptosis and mixed-type killing had the smallest differences in proportion (31.1% vs. 44.8% vs. 24.1%). These results suggest that while high Ca^{2+} concentrations favor the occurrence of direct target cell lysis, a fine-tuned equilibrium of all three killing types is probably more effective for NK cells in the long run. In this doctoral thesis, Christian Backes came to a similar conclusion. He identified three NK cell populations based on their preferred killing type and found that those NK cells starting with necrosis and then switching to apoptosis killed more target cells than those limited to either one [93]. A possible explanation for this phenomenon was already presented by Markus Hoth and colleagues in 2014. They suggested that, given that every killer cell has a limited storage pool of cytotoxic

vesicles, releasing too many vesicles onto one target cell would leave too few for further contacts [130].

4.6   NK cytotoxicity in the light of calcium homoeostasis

Serum Ca^{2+} levels are frequently measured in clinical practice. Roughly 50% of the total amount of Ca^{2+} ions in blood and tissues is bound by plasma proteins, leaving a free ion concentration of about 1.15 to 1.35 mmol/l. Data from **section 3.4** shows that this concentration range fits in the middle of that in which Ca^{2+} concentration has a large impact on NK cell killing type. The amount of free Ca^{2+} ions in a tissue is a complex resultant of the overall amount of Ca^{2+} in the body and the degree of ion binding by plasma proteins. Total Ca^{2+} levels in the serum depend on diet, enteral uptake, release from bone tissue and renal extrusion. These processes are in turn regulated by the interplay of several hormones, the most important being parathyroid hormone, calcitonin and vitamin D3. Free $[Ca^{2+}]_{ext}$ depends, additionally, on plasma protein levels and pH. Like that of any other electrolyte in the body, the concentration of Ca^{2+} ions is closely regulated and usually kept constant. Small variations in Ca^{2+} levels can cause arrhythmia, muscle hypotonia, spasms and central nervous system dysfunctions leading to dizziness, somnolence or seizures. If these regulatory mechanisms fail and hypo- or hypercalcemia is present in patients, these conditions might also affect killing by CLs. Too low or too high Ca^{2+} levels are frequently found in cancer patients. Roughly 30% of all tumor patients suffer from hypercalcemia [144]. The most common pathomechanisms involve autonomous production of parathyroid-hormone-related peptide (PTH-rp), Vitamin D3 or the release of Ca^{2+} from bone tissues, caused by osteolytic bone metastasis. The latter is especially common in patients with multiple myeloma in which serum calcium levels are used as a staging criterion. Cancer-related hypocalcemia is less common (10 %), but also significantly more prevalent than in healthy individuals. The mechanisms are manifold and include pseudohypocalcemia associated with hypoalbuminemia, chelation of Ca^{2+} ions by citrate after blood transfusions, increased phosphate levels due to tumor lysis syndrome, hemolysis or rhabdomyolysis and many others [145]. Given that fluctuations in free $[Ca^{2+}]_{ext}$ might greatly affect immune cell function, close attention to these conditions could not only help prevent the above-mentioned complications but influence immune cell action which is a key factor for tumor control. In 2014, Jörg Bittenbring and colleagues from the local department of internal medicine published evidence for a correlation between low vitamin D levels and impaired antibody-dependent cytotoxicity. Elderly patients who suffered from diffuse large B-cell lymphoma responded significantly better to treatment with the monoclonal antibody Rituximab when vitamin D levels below 8 ng/ml were substituted. During a three-year follow-up, this improved response correlated to increased event-free survival, progression-free survival and overall survival

rates. In patients not treated with Rituximab, vitamin D substitution did not significantly improve the outcome [146]. Antibody-dependent cytotoxicity (ADCC) is assumed to be the major effector mechanism of antibody-based tumor therapy. Since vitamin D is a strong inductor of gene expression, it is reasonable to assume that immune cells respond directly to the molecule binding to its nuclear receptor. Another possibility is that vitamin D levels influenced the patients' Ca^{2+} storages. Vitamin D deficiency could allow for hypocalcemia which could have a detrimental effect on NK cell cytoxocity. Bittenbring et al did not publish the patients' calcium levels. It would be interesting to know if low vitamin levels also translated to mild or severe hypocalcemia in those patients prior to substitution therapy.

4.7 Apoptotic and necrotic NK cell killing in the context of tumor microenvironment and the immune system

Cancerous tissues are not merely a conglomerate of malignantly transformed cells which keep on growing. They are a composition of cancer cells, stromal cells, endothelial cells, pericytes, immune cells and other cell types which together create a distinct microenvironment. This environment is currently the subject of great scientific interest. Tumor cells were shown to misuse stromal cells such as fibroblasts to produce growth-promoting cytokines [147], immune cells to supply proangiogenetic peptides to endothelial cells and to produce enzymes which digest extracellular matrix components, thereby abetting invasiveness and metastasis [2]. The biology of tumor microenvironments is vast and cannot be elucidated in detail at this point. This section focusses on a feature which seems inextricable from tumor microenvironment - the presence of immune cells. Cancer evolution and immune responses are closely linked and are known to promote each other. Cancers are recognized by immunocompetent cells as foreign and prompt an immune reaction. Inversely, chronic inflammation often serves as a breeding ground for tumors as can be seen in colorectal carcinoma following chronic inflammatory bowel disease, liver cancer following alcohol abuse and chronic hepatitis or the emergence of Burkitt's lymphoma after a smoldering infection with Epstein-Barr virus [148]. Tumors not originating from chronically inflamed tissues still benefit from immune cells which originally infiltrated the tumorous tissue to attack but failed. They reside in the tumor and produce cytokines which are intended to call other immune cells for aid but at the same time serve as growth promoters to surrounding malignant cells. NK cells as part of innate immunity are key players in tumor control. Since they have different molecular arms at their disposal to eliminate tumor cells, it should be discussed which of these arms are likely to be employed in tumor control and what implications their use could have for the tumor microenvironment as well as our whole immune system. Necrosis is generally considered an unregulated process of cell destruction. It often occurs when thermic stress, chemical noxa or radiation

damage tissues. As many other groups have suggested and as this thesis demonstrates, necrosis is also a way of CTLs to kill target cells by directly disrupting their cell membranes. This disruption leads to the uncontrolled exposure of cytoplasmic cell contents to the surrounding environment. This process can have two important consequences:

1. Bystanding immune cells can be prompted by necrotic cell debris to produce cytokines, a mechanism to recruit other cells which remove remnants and initiate healing processes. This recruitment is necessary to maintain our tissue integrity in the long run and at first glance appears favorable since it might also lead to more immunocompetent cells launching a concerted attack against the tumor. That being true, there is increasing evidence that a pro-inflammatory micromilieu could also promote tumor growth and metastasis. Interleukin-1 released from necrotic remnants is a potent inductor of the transcription factor NF-κB [149]. This factor induces the expression of anti-apoptotic and pro-mitotic regulator proteins in tumors thus promoting tumor growth [2]. Another potent pro-oncogenic transcription factor is STAT-3. The two taken together show abnormally high activity in over 50% of all cancers [150], [151], [152]. Macrophages attracted by the release of Interleukin-1 are in turn stimulated and activate NF-κB which boosts the production of cytokines such as Interleukin-1, Interleukin-6 and proteins from the tumor necrosis factor family. That way, a vicious circle may occur in which tumor necrosis activates immune cells and immune cells promote tumor growth.

2. Cells of the adaptive immune system are usually naive towards peptides and structures which are not exposed on the outside of cells or present in the extracellular space. If a cell bursts open, its cytoplasmic contents are swept into the supernatant and could stimulate B- and T-lymphocytes to act against autoantigens. Many autoimmune diseases are characterized by the production of antibodies against molecules usually kept from the eyes of adaptive immunity, for example ANCAs (anti-neutrophil cytoplasmic antibodies) in vasculitis, anti-DNA-antibodies in systemic lupus or anti-centromere-antibodies associated with the CREST syndrome, a subcategory of scleroderma. Tumor necrosis induced by CTLs on a massive scale could therefore facilitate the occurrence of autoimmune diseases.

Until now, tumor cell apoptosis appears to be favorable. Recent findings have provided insight into immunological dimensions not only of necrotic death but also of apoptotic cells. When tumor cells are targeted by certain chemotherapeutic agents such as anthracyclines or oxaliplatin, they were found to undergo apoptosis using a distinct pathway. This pathway involved the accumulation of the protein calreticulin [153]. The latter normally resides in the ER membrane and, upon apoptosis induction, was excluded from the

ER and transported to the plasma membrane in small vesicles. According to Zitvogel et al, the presence of calreticulin on the cell surface facilitated the subsequent incorporation of apoptotic remnants by dendritic cells and enhanced the presentation of tumor-derived antigens. In that case, apoptosis as well as necrosis induction in tumor cells could act as a boost for anti-tumor responses by CTLs.

Given these considerations, one might be tempted to judge that tumor cell apoptosis is beneficial and tumor necrosis is harmful. This might be true in some cases but there is certainly a catch in it.

Unlike direct lysis by osmotic stress, apoptosis will always depend on intact downstream signaling. This is true for both intrinsic apoptosis conveyed by granzymes as well as extrinsically induced apoptosis via death receptors. Tumor cells are feared for their high genetic instability, constantly putting them on the cusp of evading control by immune cells or tackling by chemotherapy. It is easily conceivable that tumor cells gain immunity against CTL attacks by expressing modified caspase targets or apoptotic enzymes. These strategies of evasion would severely disturb the physiological process of apoptotic cell involution. If CTLs could only kill by apoptosis induction, they would prove appallingly ineffective against such tumor cells, which could explain in parts why some tumors become refractory to chemo- or immune cell therapy.

Another potential disadvantage of apoptosis induction against tumor cells was recently discovered regarding the death receptor pathways. In 2015, von Karstedt and colleagues investigated the role of TRAIL signaling in tumors harboring mutations in the regulatory protein KRAS. They found that activation of TRAIL-R in these cells increased tumor progression, metastasis and shortened survival in mice [154]. Since TRAIL is also involved in NK cell-mediated cytotoxicy, engagement of TRAIL receptor might even promote tumor progression. KRAS mutations are common among a variety of tumor entities including non-small-cell lung cancer (NSCLC) and colorectal carcinoma, two of the most deadly tumor types in western civilization. A similarly detrimental effect was associated with the Fas-FasL-system. In cancer cells resistent to FAS-induced apoptosis, activation of FAS receptor on the tumor cell increased motility and invasiveness. This paradoxic effect was found to rely again on NF-κB, Caspase 8 and proteins from the ERK family inducing a variety of metastasis-promoting genes [155]. It appears that apoptosis induction by CTLs via death receptors is beneficial as long as tumor cells are still sensitive towards pro-apoptotic signaling but turns into a self-harming mechanism once tumor cells have managed to evade apoptotic downstream signaling. The same ambivalence seems to apply to granzyme-B-mediated apoptotis. On the one hand a potent inductor of apoptosis in tumor cells, it might also contribute to extracellular matrix degradation, thus facilitating invasive and metastatic growth [156], [157]. Furthermore, elevated levels of soluble granzyme B can be found frequently in patients suffering from chronic inflamma-

tory diseases [158], pointing towards a possible connection between high employement of granzymes by CTLs and the occurence of autoimmunity.

At this state, a definite answer - if there even is one - what type of target cell killing by CTLs is favorable in tumor cell killing cannot be given. Both necrosis and apoptosis seem to come with a variety of possibly beneficial as well as harmful consequences. Another factor which is currently not determined is how high or low free Ca^{2+} levels are in a given tumor microenvironment, compared to the rest of the body. This question is probably of lesser significance when dealing with soluble types of malignancies such as leukemias or lymphomas, although they also infiltrate lymphoid tissues where they possibly create tumorous micromilieus of their own. Regarding solid tumors, nothing is known about whether extracellular Ca^{2+} concentrations differ significantly from healthy tissues or plasma levels. The answer to this question could be of major importance considering that Ca^{2+} ion concentrations can have a great influence on the way CTLs eliminate tumor cells. Judging from all presented data, if there was a way to pharmacologically influence NK cell killing behavior, limiting necrosis potential would seem beneficial for two reasons: Firstly, killer cells with high lysis potential kill a few target cells very fast but less cells altogether. Secondly, the growth-promoting effects of tumor cell necrosis appear to surmount those of apoptosis. Hence, lowering Ca^{2+} influx into active NK cells might lead to a more economic, more healthy immune response against some tumors. This hypothesis is backed up by recent results from our research group which show that siRNA knockdown of ORAI1 in NK cells improves global killing efficiency (manuscript in preparation). Possible agents for the blockade of ORAI are well established [159], [160], [161], [162], [163]. If these substances were to be administered to cancer patients, previous thorough dosage titration would be required since too strong blockade would likely dampen global cellular immune function. Be it that an optimal dosage can be found, this approach might prove doubly effective since CRAC proteins have been identified as passenger genes in many tumors [164], possibly accelerating growth. Hence, pharmacological weakening of ORAI activity in both killer and tumor cells might, in the long run, prove as a suitable supportive immunotherapy for the treatment of malignancies.

Appendix

References

[1] Swann JB and Smyth MJ. Immune surveillance of tumors. *J Clin Invest*, 117:1137–1146, 2007.

[2] Hanahan D and Weinberg RA. Hallmarks of cancer: the next generation. *Cell*, 144:646–674, 2011.

[3] Vinay DS, Aguilano K, Amin A, et al. Immune evasion in cancer: Mechanistic basis and therapeutic strategies. *Semin Cancer Biol*, 35:185–198, 2015.

[4] Seliger B. Strategies of tumor immune evasion. *BioDrugs*, 19:347–354, 2005.

[5] Kaerre K, Ljunggren HG, Pointek G, et al. Selective rejection of H-2-deficient lymphoma variants suggests alternative immune defence strategy. *J Immunol*, 319:675–678, 2005.

[6] Neefjes J, Bakke O, Jongsma ML, et al. Towards a systems understanding of MHC class I and MHC class II antigen presentation. *Nat Rev Immunol*, 11:823–836, 2011.

[7] Talmadge JE, Meyers KM, Prieur DJ, et al. Role of NK cells in tumour growth and metastasis in beige mice. *Nature*, 284:622–624, 1980.

[8] Imai K, Matsuyama S, Miyaka S, et al. Natural cytotoxic activity of peripheral-blood lymphocytes and cancer incidence: an 11-year follow-up study of a general population. *Lancet*, 356:1795–1799, 2000.

[9] Cooper MA, Caligiuri MA, Carson WE, et al. Human natural killer cells: a unique innate immunoregulatory role for the CD56(bright) subset. *Blood*, 97:3146–3151, 2001.

[10] Béziat V, Debré P, Decocq J, et al. CD56brightCD16+ NK cells: a functional intermediate stage of NK cell differentiation. *J Immunol*, 186:6753–6761, 2011.

[11] Perussia B. Fc receptors on natural killer cells. *Curr Top Microbiol Immunol*, 230:63–88, 1998.

[12] Melsen JE, Lankerster AC, Lugthart G, et al. Human Circulating and Tissue-Resident CD56(bright) Natural Killer Cell Populations. *Front Immunol*, 7:262, 2016.

[13] Jacobs R, Beul K, Behrens G, et al. Cd56bright cells differ in their KIR repertoire and cytotoxic features from CD56dim NK cells. *Eur J Immunol*, 31:3121–3127, 2001.

[14] Bryceson YT, Björkström NK, Fauriat C, et al. Functional analysis of human NK cells by flow cytometry. *Methods Mol Biol*, 612:335–352, 2010.

[15] Romagnani C, Carrega P, Conte R, et al. CD56brightCD16- killer Ig-like receptor- NK cells display longer telomeres and acquire features of CD56dim NK cells upon activation. *The Journal of Immunology*, 178:4947–4955, 2007.

[16] Vivier E, Caligiuri MA, Lanier LL, et al. Innate or adaptive immunity? The example of natural killer cells. *Science*, 331:44–49, 2011.

[17] Chester C, Fritsch K, and Kohrt HE. Natural Killer Cell Immunomodulation: Targeting Activating, Inhibitory, and Co-stimulatory Receptor Signaling for Cancer Immunotherapy. *Front Immunol*, 6;601:1–9, 2015.

[18] Hoorweg K, Aparicio-Domingo P, Cornelissen F, et al. Functional Differences between Human NKp44(-) and NKp44(+) RORC(+) Innate Lymphoid Cells. *Front Immunol*, 3:72, 2012.

[19] Murphy K. *Janeway's Immunobiology*. Immunobiology: The Immune System (Janeway). Garland Science, 8th edition, 2011.

[20] Lucas M, Aichele P, Diefenbach A, et al. Dendritic cells prime natural killer cells by trans-presenting interleukin 15. *Immunity*, 4:503–517, 2007.

[21] Caliguiri MA. Human natural killer cells. *Blood*, 112:461–469, 2008.

[22] Becknell B and Caligiuri MA. Interleukin-2, interleukin-15, and their roles in human natural killer cells. *Adv Immunol*, 86:209–239, 2005.

[23] S Guia, Al Jumaah S, Al-Hajjar S, et al. A role for Interleukin-12/23 in the maturation of human natural killer and CD56+ T cells in vivo. *Blood*, 111:5008–5016, 2008.

[24] Humphrey MB, Lanier LL, and Nakamura MC. Role of ITAM-containing adapter proteins and their receptors in the immune system and bone. *Immunol Rev*, 208:50–65, 2005.

[25] Chiesa S, Fuseri N, Malissen B, et al. Multiplicity and plasticity of natural killer cell signaling pathways. *Blood*, 107:2364–2372, 2006.

[26] Imamura N, Abe K, Dohy H, et al. Aggressive natural killer cell leukaemia/lymphoma: report of four cases and review of literature. possible existence of a new clinical entity originating from the third lineage of lymphoid cells. *Br J Haematol*, 75:49–59, 1990.

[27] Gelb AB, Cleary ML, Cornbleet JP, et al. Epstein-Barr virus-associated natural killer-large granular lymphocyte leukemia. *Hum Pathol*, 9:953–960, 1994.

[28] Mandelboim O, Arnon TI, Bushkin Y, et al. Recognition of haemagglutinins on virus-infected cells by NKp46 activates lysis by human NK cells. *Nature*, 409:1055–1060, 2001.

[29] Kruse PH, Matta J, Ugolini S, et al. Natural cytotoxicity receptors and their ligands. *Immunol Cell Biol*, 92:221–229, 2014.

[30] Sutherland CL, Chalupny NJ, and Cosman D. The UL16-binding proteins, a novel family of MHC class I-related ligands for NKG2D, activate natural killer cell functions. *Immunol Rev*, 181:185–192, 2001.

[31] Bottino C, Castriconi R, Moretta L, et al. Cellular ligands of activating NK receptors. *Trends Immunol*, 26:221–226, 2005.

[32] Bryceson YT, March ME, Ljunggren HG, et al. Synergy among receptors on resting NK cells for the activation of natural cytotoxicity and cytokine secretion. *Blood*, 107:159–166, 2006.

[33] Lanier LL. NK cell recognition. *Annuv Rev Immunol*, 23:225–274, 2005.

[34] Tomasello E and Vivier E. KARAP/DAP12/TYROBP: three names and a multiplicity of biological functions. *Eur J Immunol*, 35(6):1670–1677, 2005.

[35] Gilfillan S, Cella M, Colonna M, et al. NKG2D recruits two distinct adapters to trigger NK cell activation and costimulation. *Nat Immunol*, 3:1150–1155, 2002.

[36] Colucci F, Di Santo JP, Ortaldo JR, et al. Natural cytotoxicity uncoupled from the Syk and ZAP-70 intracellular kinases. *Nat Immunol*, 3:288–294, 2002.

[37] Upshaw JL, Billadeau DD, Dick CJ, et al. The isoforms of phopholipase C-gamma are differentially used by distinct human NK activating receptors. *J Immunol*, 175:213–218, 2005.

[38] Brandman O, Liou J, Meyer T, et al. STIM2 is a feedback regulator that stabilizes basal cytosolic and endoplasmic reticulum Ca2+ levels. *Cell*, 131:1327–1339, 2007.

[39] Lang S, Zimmermann R, Cavalié A, et al. Sec61 complexes form ubiquitous ER Ca2+ leak channels. *Channels(Austin)*, 5:228–235, 2011.

[40] Erdmann F, Zimmermann R, Ahmad M, et al. Interaction of calmodulin with Sec61α limits Ca2+ leakage from the endoplasmic reticulum. *EMBO J*, 30:17–31, 2011.

[41] Thastrup O, Cullen PJ, Dawson AP, et al. Thapsigargin, a tumor promoter, discharges intracellular Ca2+ stores by specific inhibition of the endoplasmic reticulum Ca2(+)-ATPase. *Proc Natl Acad Sci U S A*, 87:2466–2470, 1990.

[42] Davidson GA and Varhol RJ. Kinetics of thapsigargin-Ca(2+)-ATPase (sarcoplasmic reticulum) interaction reveals a two-step binding mechanism and picomolar inhibition. *J Biol Chem*, 270:11731–11734, 1995.

[43] Hogan PG, Lewis RS, and Rao A. Molecular basis of calcium signaling in lymphocytes: STIM and ORAI. *Annu Rev Immunol*, 28:491–533, 2010.

[44] Liou J, Ferrell JE Jr, Heo WD, et al. STIM is a Ca2+ sensor essential for Ca2+-store-depletion-triggered Ca2+ influx. *Curr Biol*, 15:1235–1241, 2005.

[45] Zhang SL, Cahalan MD, Penna A, et al. Genome-wide RNAi screen of Ca(2+) influx identifies genes that regulate Ca(2+) release-activated Ca(2+) channel activity. *Proc Natl Acad Sci U S A*, 103:9357–9362, 2006.

[46] Feske S, Daly M, Gwack Y, et al. A mutation in Orai1 causes immune deficiency by abrogating CRAC channel function. *Nature*, 441:179–185, 2006.

[47] Shaw PJ, Feske S, Hoth M, et al. Molecular regulation of CRAC channels and their role in lymphocyte function. *Cell Mol Life Sci*, 70:2637–2656, 2013.

[48] Roos J, Calahan MD, DiGregorio PJ, et al. STIM1, an essential and conserved component of store-operated Ca2+ channel function. *J Cell Biol*, 169:435–445, 2005.

[49] Vig M, Beck A, Fleig A, et al. CRACM1 is a plasma membrane protein essential for store-operated Ca2+ entry. *Science*, 312:1220–1223, 2006.

[50] Feske S, Fischer A, and Picard C. Immunodeficiency due to mutations in ORAI1 and STIM1. *Clin Immunol*, 135:169–182, 2010.

[51] Savignac M, Mellström B, and Naranjo JR. Calcium-dependent transcription of cytokine genes in T lymphocytes. *Pflugers Arch*, 454:523–533, 2007.

[52] Dolmetsch RE, Goodnow CC, Healy JI, et al. Differential activation of transcription factors induced by Ca2+ response amplitude and duration. *Nature*, 386:855–858, 1997.

[53] Kupfer A and Kupfer H. Imaging immune cell interactions and functions: SMACs and the Immunological Synapse. *Semin Immunol*, 15:295–300, 2003.

[54] Dustin ML. The immunological synapse. *Cancer Immunol Res*, 2:1023–1033, 2014.

[55] Quitana A, Becherer U, Hoth M, et al. T cell activation requires mitochondrial translocation to the immunological synapse. *Proc Natl Acad Sci U S A*, 104:14418–14423, 2007.

[56] Schwindling C, Hoth M, Krause E, et al. Mitochondria positioning controls local calcium influx in T Cells. *J Immunol*, 184:184–190, 2010.

[57] Quintana A, Hoth M, Kaestner L, et al. Sustained activity of calcium release-activated calcium channels requires translocation of mitochondria to the plasma membrane. *J Biol Chem*, 281:40302–40309, 2006.

[58] Dustin ML and Long EO. Cytotoxic immunological synapses. *Immunol Rev*, 235:24–34, 2010.

[59] Wang X and Schwartz TL. The mechanism of Ca2+ -dependent regulation of kinesin-mediated mitochondrial motility. *Cell*, 136:163–174, 2009.

[60] Saftig P and Klumperman J. Lysosome biogenesis and lysosomal membrane proteins: trafficking meets function. *Nat Rev Mol Cell Biol*, 10:623–635, 2009.

[61] Krzewski K, Coligan JE, Gil-Krzewska A, et al. LAMP1/CD107a is required for efficient perforin delivery to lytic granules and NK-cell cytotoxicity. *Blood*, 121:4672–4683, 2013.

[62] Feldmann J, Bacq D, Blanche S, et al. Munc13-4 is essential for cytolytic granules fusion and is mutated in a form of familial hemophagocytic lymphohistiocytosis (FHL3). *Cell*, 115:461–473, 2003.

[63] zur Stadt U, Beutel K, Diler AS, et al. Linkage of familial hemophagocytic lymphohistiocytosis (FHL) type-4 to chromosome 6q24 and identification of mutations in syntaxin 11. *Hum Mol Genet*, 14:827–834, 2005.

[64] Bryceson YT, Bechensteen AG, Boelens JJ, et al. Defective cytotoxic lymphocyte degranulation in syntaxin-11 deficient familial hemophagocytic lymphohistiocytosis 4 (FHL4) patients. *Blood*, 110:1906–1915, 2007.

[65] zur Stadt U, Becker C, Beutel K, et al. Familial hemophagocytic lymphohistiocytosis type 5 (FHL-5) is caused by mutations in Munc18-2 and impaired binding to syntaxin 11. *Am J Hum Genet*, 85:482–492, 2009.

[66] Pattu V, Becherer U, Hoth M, et al. Syntaxin7 Is required for lytic granule release from cytotoxic T lymphocytes. *Traffic*, 12:890–901, 2011.

[67] Halimani M, Becherer U, Chang HF, et al. Syntaxin11 serves as a t-SNARE for the fusion of lytic granules in human cytotoxic T lymphocytes. *Eur J Immunol*, 44:573–584, 2014.

[68] Marshall MR, Becherer U, Bryceson YT, et al. VAMP8-dependent fusion of recycling endosomes with the plasma membrane facilitates T lymphocyte cytotoxicity. *J Cell Biol*, 210:135–151, 2015.

[69] Colvin RA, Abrazinski T, Andrews NW, et al. Synaptotagmin-mediated vesicle fusion regulates cell migration. *Nat Immunol*, 11:495–502, 2010.

[70] de Saint Basile G, Fischer A, and Ménasché G. Molecular mechanisms of biogenesis and exocytosis of cytotoxic granules. *Nat Rev Immunol*, 10:568–579, 2010.

[71] Stepp SE, Bennett M, Bhawan S, et al. Perforin gene defects in familial hemophago-cytic lymphohistiocytosis. *Science*, 286:1957–1959, 1999.

[72] Feldmann J, Alexander S, Blanche S, et al. Functional consequences of perforin gene mutations in 22 patients with familial haemophagocytic lymphohistiocytosis. *Br J Haematol*, 117:965–972, 2002.

[73] Martínez-Lostao L, Anel A, and Pardo J. How Do Cytotoxic Lymphocytes Kill Cancer Cells? *Clin Cancer Res*, 21:5047–5056, 2015.

[74] Law RH, Baran K, Bird PI, et al. The structural basis for membrane binding and pore formation by lymphocyte perforin. *Nature*, 468:447–451, 2010.

[75] Lopez JA, Bird CH, Bird PI, et al. Perforin forms transient pores on the target cell plasma membrane to facilitate rapid access of granzymes during killer cell attack. *Blood*, 121:2659–2668, 2013.

[76] Liu CC, Walsh CM, and Young JD. Perforin: structure and function. *Immunol Today*, 16:194–201, 1995.

[77] Keefe D, Feske S, Kirchhausen T, et al. Perforin triggers a plasma membrane-repair response that facilitates CTL induction of apoptosis. *Immunity*, 23:249–262, 2005.

[78] Thiery J, Boucrot E, Keefe D, et al. Perforin activates clathrin- and dynamin-dependent endocytosis, which is required for plasma membrane repair and delivery of granzyme B for granzyme-mediated apoptosis. *Blood*, 115:1582–1593, 2010.

[79] Smyth MJ, Cretney E, Degli-Esposti MA, et al. Activation of NK cell cytotoxicity. *Mol Immunol*, 42:501–510, 2005.

[80] Screpanti V, Grandien A, Ljunggren HG, et al. Impact of FASL-induced apoptosis in the elimination of tumor cells by NK cells. *Mol Immunol*, 42:495–499, 2005.

[81] Takeda K, Hayakawa Y, Iwakura Y, et al. Involvement of tumor necrosis factor-related apoptosis-inducing ligand in surveillance of tumor metastasis by liver natural killer cells. *Nat Med*, 7:94–100, 2001.

[82] Zhu Y, Huang B, and Shi J. Fas ligand and lytic granule differentially control cytotoxic dynamics of natural killer cell against cancer target. *Oncotarget*, 7:47163–47172, 2016.

[83] Rosenberg SA. Interleukin-2 and the development of immunotherapy for the treatment of patients with cancer. *Cancer J Sci Am*, 6:2–7, 2000.

[84] Ruggeri L, Aversa F, Capanni M, et al. Effectiveness of donor natural killer cell alloreactivity in mismatched hematopoietic transplants. *Science*, 295:2097–2100, 2002.

[85] Cheng M, Chen Y, Jiang W, et al. Natural killer cell lines in tumor immunotherapy. *Front Med*, 6:56–66, 2012.

[86] Klingemann H, Boissel L, and Toneguzzo F. Natural Killer Cells for Immunotherapy - Advantages of the NK-92 Cell Line over Blood NK cells. *Front Immunol*, 7:91, 2016.

[87] Andersson LC, Gahmberg CG, and Nilsson K. K562 - a Human erythroleukemic cell line. *Int J Cancer*, 23(2):143–147, 1979.

[88] Fujisaki H, Campana D, Eldridge P, et al. Expansion of highly cytotoxic human natural killer cells for cancer cell therapy. *Cancer Res*, 69:4010–4017, 2009.

[89] Kummerow C, Bufe B, Hoth M, et al. A simple, economic, time-resolved killing assay. *Eur J Immunol*, 44:1870–1872, 2014.

[90] Grynkiewicz G, Poenie M, and Tsien RY. A new generation of Ca2+ indicators with greatly improved fluorescence properties. *J Biol Chem*, 260:3440–3450, 1985.

[91] Ellis-Davies GC and Kaplan JH. Nitrophenyl-EGTA, a photolabile chelator that selectively binds Ca2+ with high affinity and releases it rapidly upon photolysis. *Proc Natl Acad Sci U S A*, 91:187–191, 1994.

[92] Shcherbo D, Chepurnykh TV, Chudakov DM, et al. Practical and reliable FRET/FLIM pair of fluorescent proteins. *BMC Biotechnol*, 9:24, 2009.

[93] Backes C. Untersuchung zytotoxischer Mechanismen in human natürlichen Killerzellen. doctoral thesis, Universität des Saarlandes, medical faculty F2, FR 2.5 Biophysics, Prof. Dr. Markus Hoth, 2016.

[94] Nigam SK, Ahn SY, Bhatnagar V, et al. The organic anion transporter (OAT) family: a systems biology perspective. *Physiol Rev*, 95:83–123, 2015.

[95] Anzai N, Chairoungdua A, Endou H, et al. The multivalent PDZ domain-containing protein PDZK1 regulates transport activity of renal urate-anion exchanger URAT1 via its C terminus. *J Biol Chem*, 279:45942–45950, 2004.

[96] Steinberg TH, Newman AS, Silverstein SC, et al. Macrophages possess probenecid-inhibitable organic anion transporters that remove fluorescent dyes from the cytoplasmic matrix. *J Cell Biol*, 105:2695–2702, 1987.

[97] Cunningham RF, Dayton PG, and Israili ZH. Clinical pharmacokinetics of probenecid. *Clin Pharmacokinet*, 6:135–151, 1981.

[98] Di Virgilio F, Silverstein SC, Steinberg TH, et al. Fura-2 secretion and sequestration in macrophages. A blocker of organic anion transport reveals that these processes occur via a membrane transport system of organic anions. *J Immunol*, 140:915–920, 1988.

[99] Hotchkiss RS, McDunn JE, Strasser A, et al. Cell death. *N Engl J Med*, 361:1570–1583, 2009.

[100] Atencia R, Asumendi A, and García-Sanz M. Role of cytoskeleton in apoptosis. *Vitam Horm*, 58:267–297, 2000.

[101] Koopman G, Keehnen RM, Kuijten GA, et al. Annexin V for flow cytometric detection of phosphatidylserine expression on B cells undergoing apoptosis. *Blood*, 84:1415–1420, 1994.

[102] Vermes I, Haanen C, Reutelingsperger C, et al. A novel assay for apoptosis. Flow cytometric detection of phosphatidylserine expression on early apoptotic cells using fluorescein labelled Annexin V. *J Immunol Methods*, 184:39–51, 1995.

[103] Sawai H and Domae N. Discrimination between primary necrosis and apoptosis by necrostatin-1 in Annexin V-positive/propidium iodide-negative cells. *Biochem Biophys Res Commun*, 411:569–573, 2011.

[104] Honda Y and Miyazaki S. Distinct Ca2+ response patterns in human natural killer cells during induction of necrosis or apoptosis of target cells. *Cell Calcium*, 19:297–306, 1996.

[105] Fleet A, Bolsover S, and Ellis-Davies G. Calcium buffering capacity of neuronal cell cytosol measured by flash photolysis of calcium buffer NP-EGTA. *Biochem Biophys Res Commun*, 250:786–790, 1998.

[106] Srienc AI, Burian MA, Kornfield TE, et al. Assessment of glial function in the in vivo retina. *Methods Mol Biol*, 814:499–514, 2012.

[107] Almassy J and Yule DI. Analyzing Ca(2+) dynamics in intact epithelial cells using spatially limited flash photolysis. *Cold Spring Harb Protoc*, 1, 2013.

[108] Bao R, Bellvé K, Fogarty KE, et al. A close association of RyRs with highly dense clusters of Ca2+-activated Cl- channels underlies the activation of STICs by Ca2+ sparks in mouse airway smooth muscle. *J Gen Physiol*, 132:145–160, 2008.

[109] Martin H, Barsotti RJ, Bell MG, et al. Activation kinetics of skinned cardiac muscle by laser photolysis of nitrophenyl-EGTA. *Biophys J*, 86:978–990, 2004.

[110] Patel JR, McDonald KS, Moss RL, et al. Ca2+ binding to troponin C in skinned skeletal muscle fibers assessed with caged Ca2+ and a Ca2+ fluorophore. Invariance of Ca2+ binding as a function of sarcomere length. *J Biol Chem*, 272:6018–6027, 1997.

[111] Michelangeli F and East JM. A diversity of SERCA Ca2+ pump inhibitors. *Biochem Soc Trans*, 39:789–797, 2011.

[112] Quitana A and Hoth M. Apparent cytosolic calcium gradients in T-lymphocytes due to fura-2 accumulation in mitochondria. *Cell Calcium*, 36:99–109, 2004.

[113] Quitana A, Pasche M, Junker C, et al. Calcium microdomains at the immunological synapse: how orai cchannel, mitochondria and calcium pumps generate local calcium signals for efficient t-cell activation. *The EMBO Journal*, 30:3895–3912, 2011.

[114] Petersen OH, Criddle DN, and Sutton R. Failure of calcium microdomain generation and pathological consequences. *Cell Calcium*, 40:593–600, 2006.

[115] Blumenthal R, Henkart MP, Henkart PA, et al. Liposomes as targets for granule cytolysin from cytotoxic large granular lymphocyte tumors. *Proc Natl Acad Sci U S A*, 81:5551–5555, 1984.

[116] Tschopp J, Heusser C, Masson D, et al. Phosphorylcholine acts as a Ca2+-dependent receptor molecule for lymphocyte perforin. *Nature*, 337:272–274, 1989.

[117] Young JD, Cohn ZA, Damiano A, et al. Dissociation of membrane binding and lytic activities of the lymphocyte pore-forming protein (perforin). *J Exp Med*, 165:1371–1382, 1987.

[118] Voskoboinik I, Browne K, Ciccone A, et al. Calcium-dependent plasma membrane binding and cell lysis by perforin are mediated through its C2 domain: A critical role for asparate residues 429, 435, 483, and 485 but not 491. *J Biol Chem*, 280(9):8426–8434, 2005.

[119] Llinás R, Silver RB, and Sugimori M. Microdomains of high calcium concentration in a presynaptic terminal. *Science*, 256:677–679, 1992.

[120] Wang LY and Augustine GJ. Presynaptic nanodomains: a tale of two synapses. *Front Cell Neurosci*, 8:455, 2015.

[121] Sin JI, Celis E, Choe J, et al. Intratumoral electroporation of IL-12 cDNA eradicates established melanomas by Trp2(180-188)-specific CD8+ CTLs in a perforin/granzyme-mediated and IFN-γ-dependent manner: application of Trp2(180-188) peptides. *Cancer Immunol Immunother*, 61:1671–1682, 2012.

[122] Song K, Chang Y, and Prud'homme GJ. IL-12 plasmid-enhanced DNA vaccination against carcinoembryonic antigen (CEA) studied in immune-gene knockout mice. *Gene Ther*, 7:1527–1535, 2000.

[123] Schultz J, Moelling K, Nawrath M, et al. Long-lasting anti-metastatic efficiency of interleukin 12-encoding plasmid DNA. *Hum Gene Ther*, 10:407–417, 1999.

[124] Kodama T, Atsuta M, Hayakawa Y, et al. Perforin-dependent NK cell cytotoxicity is sufficient for anti-metastatic effect of IL-12. *Eur J Immunol*, 29:1390–1396, 1999.

[125] Allard B, Pommey S, Smyth MJ, et al. Targeting CD73 enhances the antitumor activity of anti-PD-1 and anti-CTLA-4 mAbs. *Clin Cancer Res*, 19:5626–5635, 2013.

[126] Morales-Kastresana A, Anel A, Azpilikueta A, et al. Essential complicity of perforin-granzyme and FAS-L mechanisms of achieve tumor rejection following treatment with anti-CD137 mAb. *J Immunother Cancer*, 1:3, 2013.

[127] Omilusik K, Bech-Hansen NT, Chen X, et al. The Ca(v)1.4 calcium channel is a critical regulator of T cell receptor signaling and naive T cell homeostasis. *Immunity*, 35:349–360, 2011.

[128] Zheng J. Molecular mechanism of TRP channels. *Compr Physiol*, 3:221–242, 2013.

[129] Wenning AS, Hoth M, Neblung K, et al. TRP expression pattern and the functional importance of TRPC3 in primary human T-cells. *Biochim Biophys Acta*, 1813:412–423, 2011.

[130] Schwarz EC, Hoth M, and Qu B. Calcium, cancer and killing: The role of calcium in killing cancer cells by cytotoxic T lymphocytes and natural killer cells. *Biochim Biophys Acta*, 1833:1603–1611, 2013.

[131] Qu B, Al-Ansary D, Hoth M, et al. ORAI-mediated calcium influx in T cell proliferation, apoptosis and tolerance. *Cell Calcium*, 50:261–269, 2011.

[132] Zweifach A. Target-cell contact activates a highly selective capacitative calcium entry pathway in cytotoxic T lymphocytes. *J cell Biol*, 148:603–614, 2000.

[133] Maul-Pavicic A, Bass T, Bryceson YT, et al. ORAI1-mediated calcium influx is required for human cytotoxic lymphocyte degranulation and target cell lysis. *Proc Natl Acad Sci U S A*, 108:3324–3329, 2011.

[134] Samanta K, Douglas S, and Parekh AB. Mitochondrial calcium uniporter MCU supports cytoplasmic Ca2+ oscillations, store-operated Ca2+ entry and Ca2+-dependent gene expression in response to receptor stimulation. *PLoS One*, 9, 2014.

[135] Rizzuto R, De Stefani D, Mammucari C, et al. Mitochondria as sensors and regulators of calcium signalling. *Nat Rev Mol Cell Biol*, 13:566–578, 2012.

[136] Fonteriz R, Alvarez J, Alvarez-Illera P, et al. Modulation of Calcium Entry by Mitochondria. *Adv Exp Med Biol*, 898:405–421, 2016.

[137] Parekh AB. Mitochondrial regulation of intracellular Ca2+ signaling: more than just simple Ca2+ buffers. *News Physiol Sci*, 18:252–256, 2003.

[138] Di Capite J, Ng SW, and Parekh AB. Decoding of cytoplasmic Ca(2+) oscillations through the spatial signature drives gene expression. *Curr Biol*, 19:853–858, 2009.

[139] Sripetchwandee J, Chattipakorn N, Chattipakorn SC, et al. Mitochondrial calcium uniporter effectively prevents brain mitochondrial dysfunction caused by iron overload. *Life Sci*, 92:298–304, 2013.

[140] Sanganahalli BG, Herman P, Hyder F, et al. Mitochondrial calcium uptake capacity modulates neocortical excitability. *J Cereb Blood Flow Metab*, 33:1115–1126, 2013.

[141] Manhas N and Pardasani KR. Modelling mechanism of calcium oscillations in pancreatic acinar cells. *J Bioenerg Biomembr*, 46:403–420, 2014.

[142] Schmidt H, Gelhaus C, Janssen O, et al. Effector granules in human T lymphocytes: proteomic evidence for two distinct species of cytotoxic effector vesicles. *J Proteome Res*, 10:1603–1620, 2011.

[143] Peter PJ, Borst J, Fukuda M, et al. Cytotoxic T lymphocyte granules are secretory lysosomes, containing both perforin and granzymes. *J Exp Med*, 173:1099–1109, 1991.

[144] Goldner W. Cancer-Related Hypercalcemia. *J Oncol Pract*, 12:426–32, 2016.

[145] Schattner A, Dubin I, Gelber M, et al. Hypocalcaemia of malignancy. *Neth J Med*, 74:231–239, 2016.

[146] Bittenbring JT, Achenbach M, Altmann B, et al. Vitamin D deficiency impairs rituximab-mediated cellular cytotoxicity and outcome of patients with diffuse large B-cell lymphoma treated with but not without rituximab. *J Clin Oncol*, 32:3242–3248, 2014.

[147] Egeblad M, Nakasone ES, and Werb Z. Tumors as organs: complex tissues that interface with the entire organism. *Dev Cell*, 18:884–901, 2010.

[148] Lin WW and Karin M. A cytokine-mediated link between innate immunity, inflammation, and cancer. *J Clin Invest*, 117:1175–1183, 2007.

[149] Grivennikov SI, Greten FR, and Karin M. Immunity, inflammation, and cancer. *Cell*, 140:883–899, 2010.

[150] Yu H, Kortylewski M, and Pardoll D. Crosstalk between cancer and immune cells: role of STAT3 in the tumour microenvironment. *Nat Rev Immunol*, 7:41–51, 2007.

[151] Karin M. Nuclear factor-kappaB in cancer development and progression. *Nature*, 441:431–436, 2006.

[152] Levy DE and Darnell JE Jr. Stats: transcriptional control and biological impact. *Nat Rev Mol Cell Biol*, 3:651–662, 2002.

[153] Zitvogel L, Chaput N, Kepp O, et al. Immunogenic tumor cell death for optimal anticancer therapy: the calreticulin exposure pathway. *Clin Cancer Res*, 16, 2010.

[154] von Karstedt S, Anderson KI, Annewanter F, et al. Cancer cell-autonomous TRAIL-R Signaling promotes KRAS-driven cancer progression, invasion, and metastasis. *Cancer Cell*, 27:561–573, 2015.

[155] Barnhart BC, Bubici C, Franzoso G, et al. CD95 ligand induces motility and invasiveness of apoptosis-resistant tumor cells. *The EMBO Journal*, 23:3175–3185, 2004.

[156] Hiebert PR and Granville DJ. Granzyme B in injury, inflammation, and repair. *Trends Mol Med*, 18:732–741, 2012.

[157] Parkinson LG, Brown K, Granville DJ, et al. Granzyme B mediates both direct and indirect cleavage of extracellular matrix in skin after chronic low-dose ultraviolet light irradiation. *Aging Cell*, 14:67–77, 2015.

[158] Wensink AC, Bovenschen N, and Hack CE. Granzymes regulate proinflammatory cytokine responses. *J Immunol*, 194:491–497, 2015.

[159] Derler I, Begg M, Fritsch R, et al. The action of selective CRAC channel blockers if affected by the Orai pore geometry. *Cell Calcium*, 53:139–151, 2013.

[160] Fischer BS, Kim K, McDonald TV, et al. Capsaicin inhibits Jurkat T-cell activation by blocking calcium entry current I(CRAC). *J Pharmacol Exp Ther*, 299:238–246, 2001.

[161] Gericke M, Droogmans G, Nilius B, et al. Inhibition of capacitative Ca2+ entry by a Cl- channel blocker in human endothelial cells. *Eur J Pharmacol*, 269:381–384, 1994.

[162] Li JH, Christian EP, and Dargis PG. Properties of Ca(2+) release-activated (Ca2+) channel block by 5-nitro-2-(3-phenylpropylamino)-benzoic acid in Jurkat cells. *Eur J Pharmacol*, 394:171–179, 2000.

[163] Ishikawa J, Ichikawa A, Kubota H, et al. A pyrazole derivative, YM-58483, potently inhibits store-operated sustained Ca2+ influx and IL-2 production in T lymphocytes. *J Immunol*, 170:4441–4449, 2003.

[164] Hoth M. CRAC channels, calcium, and cancer in light of the driver and passenger concept. *Biochim Biophys Acta*, 1863:1408–1417, 2016.

Publications

[1] Mang S, Backes CS, ... , Hoth M*, Kummerow C*. Different Ca^{2+} signals in NK cells are linked to apoptosis and necrosis induction in tumour targets. Manuscript in preparation.

[2] Backes CS, Mang S, ... , Hoth M, Kummerow C. NK cells induce apoptosis, necrosis and mixed forms of target cell death. Manuscript in preparation.

[3] Zhou X, ... , Mang S, ... , Qu B, Kummerow C, Schwarz EC, Hoth M. Efficient target cell killing by human CTL and NK cells at their respective calcium optimum. Manuscript in preparation.

Acknowledgement

Firstly, I would like to express my gratitude towards Prof. Dr. Markus Hoth, head of the biophysics department, who was willing to incorporate me into his research group and entrusted me with this fascinating doctoral thesis. Its completion would not have been possible without his tireless support throughout the project. Secondly, I want to thank Carsten Kummerow for his excellent guidance and advice during my time in the lab. After spending many hours at work together, he has become not only a much-valued colleague but also a dear friend.

I am very grateful for the warm welcome into our group which I received from every single lab colleague. It is also thanks to your expertise and patience that I succeeded in completing this thesis. My special gratitude goes to Carmen Hässig, Cora Hoxha and Gertrud Schwär for their excellent cell culture work on which I relied from the very beginning. Thank you, Christian Backes, for your kind and patient tutorial in fluorescence microscopy and the functionality of our microscopes.

I want to thank all colleagues who were involved in conducting the calcium electrode measurements, especially Eva Schwarz and Kim Friedmann.

Aside from my colleagues at the biophysics department, I also want to express my gratitude towards the numerous blood donors as well as the department of hemostaseology for providing their samples.

A lot of the presented experimental work was conducted at the BioImager microscope in the group of Prof. Dr. Frank Zufall from the department of physiology. My gratitude goes to Prof. Dr. Zufall for letting me use the imaging setup and to Dr. Bernd Bufe for providing a thorough introduction.

I want to commemorate my former colleague Yan Zhou. You were an exceptional researcher, an even more exceptional person and you will be greatly missed.

Finally, I want to thank my family and friends for their continuous support.

Evaluation by the local ethics committee

Experiments presented in this thesis were conducted using isolated peripheral blood mononuclear cells (PBMCs) from healthy donors at the department of hemostaseology at Saarland University. The methods and materials used for isolation were evaluated by the Local Ethics Commitee of Saarland in April 2015 and adjudged ethically uncritical (identification number 84/15, signed by Prof. Dr. G. Rettig- Stürmer, head of the Ethics Committee of the Ärztekammer des Saarlandes)

Im Zuge der vorliegenden Dissertation wurden Arbeiten mit Zellen durchgeführt, die aus Vollblutspenden oder Thrombozytenapheresen gesunder Spender stammten. Die hierzu verwendeten Verfahren und Materialien wurden von der Ethikkommission des Saarlandes geprüft und am 16.04.2015 als berufsrechtlich und ethisch unbedenklich eingestuft (Kennnummer 84/15, gez. Prof. Dr. G. Rettig-Stürmer, Vorsitzender der Ethikkommission der Ärztekammer des Saarlandes)

Declaration of authorship

I hereby declare that this thesis is my own unaided work. All concepts and data which are not my own intellectual property are marked as references and no references except those listed in this thesis were used in its making.

I did not receive help from any person who was not specifically mentioned. In particular, I did not receive help from anyone based on financial or other material compensation.

I am aware that a digital form of this thesis can be examined for the use of unauthorized aid and in order to determine whether the thesis as a whole or parts incorporated in it may be deemed as plagiarism. For the comparison of my work with existing sources, I agree that it shall be entered into a database where it shall also remain after examination to enable comparison with future theses. Further rights of reproduction and usage, however, are hereby not granted.

I declare that these statements were made truthfully and that nothing was left out.

Hiermit erkläre ich an Eides statt, dass ich die vorliegende Arbeit selbständig und ohne unzulässige Hilfe Dritter angefertigt habe. Gedanken und Konzepte, die von anderen Autoren stammen, wurden vollständig unter Angabe ihrer Quellen angegeben. Andere als die hier aufgeführten Quellen und Hilfsmittel wurden nicht verwendet.

Außer den hier angegebenen waren keine weiteren Personen an der inhaltlichen und materiellen Erstellung dieser Arbeit beteiligt. Insbesondere hat niemand von mir finanzielle oder andere Leistungen erhalten, um an der Erstellung der Arbeit mitzuwirken.

Mir ist bekannt, dass die vorliegende Arbeit in eine Datenbank integriert und auf Inhalte anderer Quellen überprüft werden kann. Diese Dissertation darf einer solchen Überprüfung unterzogen werden und zum Vergleich mit zukünftig veröffentlichten Arbeiten in einer entsprechenden Datenbank verbleiben. Darüber hinausgehende Vervielfältigungsrechte werden hiermit nicht eingeräumt.

Ich versichere an Eides statt, dass ich die oben genannten Angaben wahrheitsgemäß getroffen habe und nichts ausgelassen habe.

Homburg, February, 2017